Design, characterization and optimization of an atmospheric pressure hybrid dielectric barrier discharge reactor and application on a pharmaceutical compound

By

Joelle Jureidini

Under the supervision of Professor Sylvain Coulombe

Department of Chemical Engineering

McGill University, Montréal

December 2006

A thesis submitted to McGill University in partial fulfillment of the requirements of the degree of Master of Engineering

© Joelle Jureidini, 2006

Library and Archives Canada

Published Heritage Branch

395 Wellington Street
Ottawa ON K1A 0N4
Canada

Bibliothèque et Archives Canada

Direction du Patrimoine de l'édition

395, rue Wellington
Ottawa ON K1A 0N4
Canada

Your file Votre référence
ISBN: 978-0-494-32599-5
Our file Notre référence
ISBN: 978-0-494-32599-5

NOTICE:
The author has granted a non-exclusive license allowing Library and Archives Canada to reproduce, publish, archive, preserve, conserve, communicate to the public by telecommunication or on the Internet, loan, distribute and sell theses worldwide, for commercial or non-commercial purposes, in microform, paper, electronic and/or any other formats.

The author retains copyright ownership and moral rights in this thesis. Neither the thesis nor substantial extracts from it may be printed or otherwise reproduced without the author's permission.

AVIS:
L'auteur a accordé une licence non exclusive permettant à la Bibliothèque et Archives Canada de reproduire, publier, archiver, sauvegarder, conserver, transmettre au public par télécommunication ou par l'Internet, prêter, distribuer et vendre des thèses partout dans le monde, à des fins commerciales ou autres, sur support microforme, papier, électronique et/ou autres formats.

L'auteur conserve la propriété du droit d'auteur et des droits moraux qui protège cette thèse. Ni la thèse ni des extraits substantiels de celle-ci ne doivent être imprimés ou autrement reproduits sans son autorisation.

In compliance with the Canadian Privacy Act some supporting forms may have been removed from this thesis.

While these forms may be included in the document page count, their removal does not represent any loss of content from the thesis.

Conformément à la loi canadienne sur la protection de la vie privée, quelques formulaires secondaires ont été enlevés de cette thèse.

Bien que ces formulaires aient inclus dans la pagination, il n'y aura aucun contenu manquant.

Canada

Abstract

The main objectives of this project were to design, characterize and optimize a gas-liquid atmospheric pressure dielectric barrier discharge (DBD) reactor and to investigate its potential to degrade an aqueous pharmaceutical compound. The liquid was sandwiched inside a parallel plate semi-batch DBD reactor and thus, directly exposed to the plasma-forming region. The application of 10 kV (17.5 kHz) at low peak current (55 mA) between the high-voltage electrode, resting on an alumina plate, and the solution induced microdischarges in the gas phase and agitated the solution. The dissipated power (55 W on average) was monitored from the measure of Lissajous figures on a customized LabVIEW™ interface. Atomic oxygen was detected by optical emission spectroscopy when oxygen was used as the feed gas. An optimization of the operating conditions was performed by monitoring the absorbance at 600 nm (UV-visible) of blue solutions composed of an indigo dye. The effects of solution volume (42-55 mL) or discharge gap, gas flow rate (15-70 cc/min), treatment time (3-9 minutes), and gas type (pure oxygen or air) were investigated. Some of the optimum values for the operating parameters, which led to a discoloration efficiency of the indigo solution of 99 %, were used to degrade an antibiotic, sulfamethoxazole (SMX) diluted in water.

Résumé

Les objectifs principaux de cette thèse étaient de concevoir, caractériser et optimiser un réacteur à plasma hybride utilisant une configuration de barrière diélectrique et d'étudier la dégradation directe d'un composé pharmaceutique présent dans l'eau. Le liquide à traiter était déposé sur une électrode mise à la masse et se trouvait directement en contact avec la phase gazeuse. L'électrode active était séparée de la surface du liquide et du gaz plasmagène par un isolant électrique (alumine). Les décharges électriques ont été produites par l'application d'impulsions de haute tension (10 kV, 55 mA, 17.5 kHz) aux bornes des électrodes. La solution s'agitait sous l'action des microdécharges. La puissance utilisée (55 W en moyenne) a été mesurée avec l'aide de la technique des figures de Lissajous, ainsi que d'un programme d'acquisition et de traitement des données écrit dans l'environnement LabVIEW™. La mesure du spectre d'émission de la phase gazeuse dans le domaine du visible a permis de détecter de l'oxygène atomique lorsque de l'oxygène (O_2) pur fut utilisé comme gaz plasmagène. Une solution aqueuse bleue dont la coloration est due au composé chimique indigo a été utilisée pour l'optimisation des paramètres d'opération du réacteur. La diminution de l'absorbance de cette solution a été caractérisée par la spectrométrie d'absorption UV-VIS à 600 nm. Différentes valeurs pour le volume de la solution (42-55 mL) ou de la distance inter-électrodes, le débit de gaz plasmagène (15-70 cc/min), le temps de traitement (3-9 min) et le type de gaz plasmagène (oxygène ou air) ont été considérés dans une étude paramétrique visant l'optimisation de la quantité d'espèces oxydantes produites. Quelques-uns des paramètres optimaux pour lesquels la décoloration de la solution indigo était de 99% ont été utilisés pour dégrader un antibiotique modèle, le sulfamethoxazole.

Acknowledgments

I wish to express my gratitude and thankfulness to Dr. Sylvain Coulombe, my supervisor, for his continuous support, edifying guidance and availability throughout the project and for allowing it to be achieved.

I would like to thank my mother Josiane, my father Halim and my brother Gabriel for their love, their moral support and their thoughtful advices. I would also like to thank Helen, Tania, Sandra and Roudy for their friendship and support.

I am pleased to have collaborated, for the pharmaceutical degradation part of the project, with Dr. Viviane Yargeau and Master Student Christine Leclair. I would like to thank them for their help, availability and enriching discussions. I would also like to thank Angela Rodayan for the GC analysis and results.

Many thanks to the staff that helped carrying out my research activities. Mr. Csaba Szalacsi for his advices and for machining the plasma DBD reactor. Mr. Frank Caporuscio, Luciano Cusmish and Alain Gagnon for their technical support. Mrs. Melanie C. Gorman for her help at the departmental store. I would also like to acknowledge Mr. Edward Siliauskas for his help with the indigo method, IC and ICP results. Mr. Ranjan Roy for his continuous help and valuable discussions, as well as for the GC-MS analyses and results.

Many thanks to all my friends and colleagues of the plasma group. I would like to acknowledge Thomas Fleisch for taking the CCD pictures and writing the MATLAB® programs. Special thanks to Rao Lakshminarayana for his help in various occasions and for the pleasant office mate he has been. To Valérie Léveillé for her valuable help. To Jason Tavares for his assistance with the power supply setup and LabVIEW™ voltage control interface. I would also like to thank the chemical engineering administrative and secretarial staff for their helpful work.

Finally, I would like to acknowledge the financial support provided by the Natural Sciences and Engineering Research council of Canada (NSERC), the Eugenie Ulmer Lamothe Funds, les Fonds québéquois de la recherche sur la nature et les technologies (FQRNT).

Table of contents

List of figures

List of tables

Chapter 1. Introduction and objectives

1.1. Introduction

A plasma consists of a collection of free electrons, ionized and neutral atoms, and molecules. Electric discharges in gases are the most widely used methods to create and maintain a plasma. A plasma can be thermal or non-thermal. Thermal plasmas operate at high power densities and generally, at high operating pressures. Non-thermal plasmas feature electron temperatures much greater than the heavy particles and much lower power densities [1]. Non-thermal plasmas tend to be chemically selective and more energy efficient since no or modest cooling is needed. Recently, the operation of non-thermal plasmas at atmospheric pressure has been demonstrated in a variety of geometries. The operation at atmospheric pressure represents a major advantage since the use of costly vacuum chambers is no longer required [2]. Dielectric barrier discharges (DBD) are one example.

DBDs are characterized by the presence of at least one dielectric layer electrically insulating the electrode(s) from the plasma. An important property of this plasma source is that it distributes microdischarges evenly over the entire surface of the dielectric by limiting the amount of charge and energy deposited on each. DBDs allow the generation of non-equilibrium plasma conditions at relatively high pressures, including atmospheric. The production of ozone, an extremely powerful oxidizing agent, is one of the most important applications for this type of plasma source [3]. Ozone formation is optimized in DBDs because the suitable energy range is achieved with the electrons, there is a reduction of energy losses to ionic species and the recombination of atomic oxygen to diatomic oxygen is minimized [4].

Ozone is widely used in potable water and wastewater treatment, disinfection, deodorization, and for the treatment of industrial wastes [5]. In the presence of hydroxyl ions, ozone partly decomposes into OH radicals that have greater oxidative properties than ozone. Their formation is always favored in water treatment and for the degradation of organic molecules. Indeed processes involving the generation of OH radicals with O_3/OH^-, O_3/H_2O_2 or Fe^{2+}/ H_2O_2, as well as photochemical and photocatalytic reactions have been considered in order to remove pharmaceutical contaminants that have been found in surface water [6].

Hybrid gas-liquid plasma reactors are units in which the electrical discharges and the liquid to be treated are in contact with each other. They are also being investigated because water treatment by direct-contact electrical discharges provides a mean to utilize chemical species that are stronger oxidizers than ozone, but could not be used otherwise due to their instability. Those hybrid plasma units are also simpler since they eliminate the need for a separate reactor for ozone generation, ozone transfer lines, contactors, and addition of other chemicals or components in the case of advanced oxidation technologies (AOT).

Different types of hybrid reactors are being investigated. Studies have been performed for both electrical discharges in water and at the surface of the water. Electrical discharges above the water require less energy than electrical discharges in water. They produce ozone and many other chemically reactive species (H_2O_2, $^{\bullet}OH$, $H^{\bullet}$, $O^{\bullet}$) in the close proximity of the aqueous solution. Some of these reactive species dissolve directly into the solution. A simultaneous generation of hydrogen peroxide in the liquid phase has also been proved [7].

DBDs were determined appropriate for treatment of aqueous waste and are inexpensive. Indeed, they can easily be formed and sustained over a large area at atmospheric pressure and near room temperature [8]. In addition, the AC voltage

applied on the electrodes generates conical protrusions from the water surface, also known as Taylor cones. The presence of Taylor cones implies a larger surface area for active species dissolution and a greater agitation of the water surface. The ejection of droplets from the Taylor cones, at the frequency of 60 Hz, becomes a problem. When droplets are suspended on the dielectric plate, the efficiency of ozone production is reduced because it is believed that the droplets become sites for more energetic discharges [9]. Following these results, special considerations have to be taken when choosing the operating frequency of a parallel hybrid DBD.

Sulfonamides are a class of antibiotic inhibiting bacterial growth and have been found in wastewaters. The potential use of a mid-frequency DBD hybrid reactor for the degradation of such compounds has seldom been investigated.

1.2. Objectives of the project

The advantages reported for a parallel plate hybrid DBD reactor are of great interest. This type of reactor needs to be further investigated and characterized, especially at a mid-frequency, where it might hinder the formation of sharp Taylor cones observed at low frequency, but would still promote water turbulence. Such configuration could lead to a potential application for pharmaceutical degradation. Therefore, the objectives of this project were the following:

a. To design and fabricate a parallel hybrid gas-liquid atmospheric pressure DBD reactor, operating at a mid-frequency.

b. To characterize by electrical, chemical and optical means the DBD reactor.

c. To optimize the processing conditions by developing a method that would allow for the investigation of the influence of various parameters, and for the selection of the most efficient ones for operating the DBD reactor.

d. To make preliminary investigations on a novel method for degrading sulfamethoxazole (SMX) using the hybrid gas-liquid atmospheric pressure DBD reactor.

The thesis is divided into eight chapters and four appendices.

This first chapter presented a condensed background and an overview of the project objectives. Chapter 2 consists of a thorough background presentation and literature review relevant to the project. It is followed by Chapter 3, which presents the details of the experimental setup and the materials and methods used throughout the project. The results are presented and discussed in Chapter 4, followed by a case study on SMX degradation in Chapter 5, and the visualization of microdischarges in Chapter 6. Chapters 7 and 8 present the conclusions and recommendations for future work.

The appendices list the problems encountered and which resulted in modifications of the reactor optimization procedure. Also included are rotameter calibration curves and further images of the microdischarges.

Chapter 2. Literature review

2.1. Some concepts on non-thermal plasmas

2.1.1 Plasma definition

Plasma is also referred to as the fourth state of matter (after solid, liquid and gas). It consists of a collection of free electrons, ionized and neutral atoms and molecules that exhibit collective behavior due to the long-range Coulomb forces [10]. Plasmas are produced either by raising the temperature of a substance until high fractional ionization is obtained or by ionization processes that raise the degree of ionization much above its thermal equilibrium value. The plasma, depending on how it is produced, may have high or low temperature and density, may be steady or transient, and stable or unstable [10].

Electric discharges in gases are the most widely used methods to create and maintain plasmas. The electric field applied to the gas volume sustains the acceleration of the electrons, which transfer a fraction of their kinetic energy to the heavy neutral particles through elastic and inelastic collisions, causing the excitation and ionization of the neutrals [1]. Due to the poor efficiency of the electron-heavy particle energy transfers, electron and heavy particle gases may coexist at different temperatures: a non-thermal plasma state prevails. Higher pressures increase the collision frequency, thus favoring the "thermalization" of the two gas streams. When such condition prevails, the plasma is said to be "thermal" [11]. Thermal plasmas operate at high power densities and generally, at high operating pressures, and provide a high-temperature (5000 to 30000 K) and non-chemically selective medium suitable for several applications. Non-thermal plasmas feature electron temperatures much greater than for the heavy particles (a few eV's, one eV being equivalent to 11600 K, compared to room temperature)

and much lower power densities [1]. They tend to be chemically selective and more energy efficient since no or modest cooling is needed [11]. In this category, low-pressure plasmas are being used in material processing applications such as the manufacture of semiconductor devices and the modification and coating of temperature-sensitive surfaces. Recently, the operation of non-thermal plasmas at atmospheric pressure has been demonstrated in a variety of geometries and a limited set of plasma-forming gases. The operation at atmospheric pressure represents a major advantage since the use of costly vacuum chambers in no longer required [2].

2.1.2 Non-thermal plasma formation

In order to ignite and sustain a non-thermal plasma in a gas, the breakdown-voltage of the gas must be exceeded. As a result of the breakdown, different kinds of plasma are generated [11]. Although different plasma sustaining mechanisms exist, all of them start with an electron avalanche, which is the multiplication of primary electrons in a cascade ionization. Figure 2.1 illustrates the so-called Townsend breakdown, which can be explained by the formation of some primary electrons near the cathode providing a low initial current [11]. Then, each primary electron creates an avalanche by drifting to the anode and ionizing the gas at the same time. The primary electrons generated near the cathode produce positive ions in the gap. These positive ions move back to the cathode, and altogether knock out electrons from the cathode in the process of secondary electron emission. The mechanism of ignition of a self-sustained discharge in a gap, controlled by secondary electron emission from the cathode, is known as the Townsend breakdown mechanism [11].

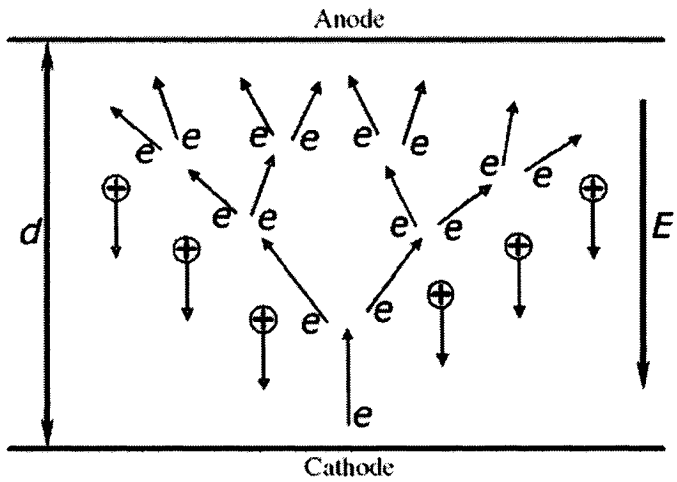

Figure 2.1 Illustration of the Townsend breakdown gap [11]

The Paschen curves of Figure 2.2 show how the breakdown voltage varies with the parameter pd, where d in cm is the inter-electrode spacing, and p in Torr, is the chamber pressure, for the plane-parallel electrodes configuration and in different gases [2]. A minimum is observed on each Paschen curve corresponding to a different gas. Plasma devices are sometimes designed to operate near this minimum to reduce the voltage requirements. In addition, very small discharge gaps are required at the minimum breakdown voltages at atmospheric pressure (760 Torr).

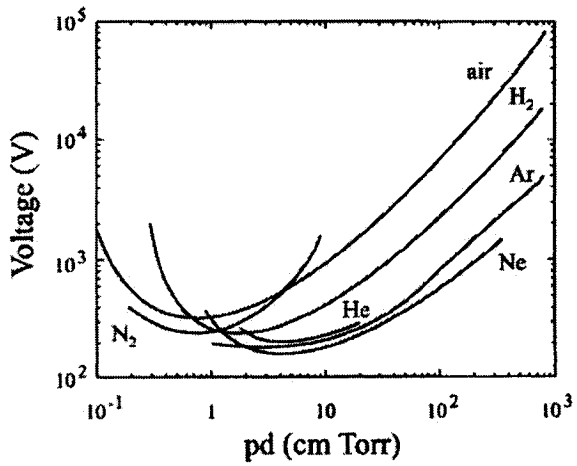

Figure 2.2 Paschen curve for various gases [2]

2.1.3 Dielectric barrier discharge (DBD)

DBDs, also referred to as silent discharges, are characterized by the presence of at least one dielectric layer electrically insulating the electrode(s) from the plasma (an alumina plate for example). They allow the generation of non-equilibrium plasma conditions at relatively high pressures, including atmospheric. They cannot be operated with DC voltages because of the capacitive coupling of the dielectric, which necessitates an AC electric field to drive a displacement current [12]. Typical geometries use plane-parallel and concentric cylindrical electrodes as schematized in Figure 2.3 [11].

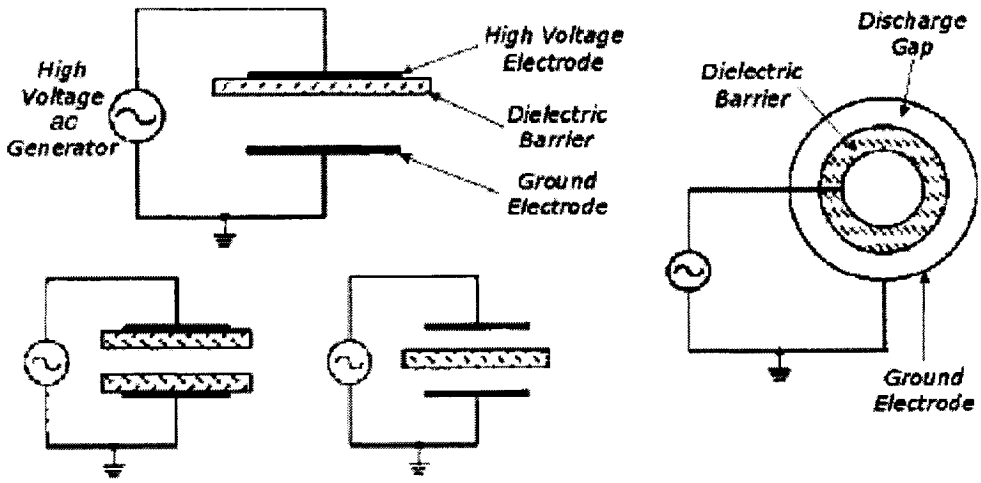

Figure 2.3 Some common dielectric barrier discharge electrode configurations [11]

Different discharge modes are observed with DBDs. The principal factors influencing the modes are the nature of the plasma gas, the properties of the dielectric layer and the excitation conditions. Filamentary, diffuse, glow or patterned discharge modes can exist [13]. For most of the industrial applications, the dielectric barrier discharges operate in the filamentary mode, which is of interest for this project. In this mode, a large number of tiny breakdown channels, short-lived current filaments or microdischarges can be observed. It is to be noted

that the term "streamer" is mostly employed when referring to the direction of propagation of a conducting channel of weakly ionized plasma [11]. For example, an electron can start from some point next to the cathode and develop an electron avalanche as it travels towards the anode. If the avalanche is large enough, a cathode-directed streamer is initiated. The term "microdischarge" could be employed to define the group of local processes in a discharge gap initiated by an electron avalanche and developed until electron current termination [11]. These two terms are often used interchangeably. They will both be used in this thesis, especially in this literature review section, where the ideas are retrieved from references in which authors used the two different terms. Table 2.1 summarizes the microdischarges properties in air at atmospheric pressure.

Table 2.1 Microdischarges properties in air at atmospheric pressure [12]

Duration:	10^{-9}-10^{-8} seconds
Filament radius:	About 10^{-4} m
Peak current:	0.1 A
Current density:	10^{6}-10^{7} Am^{-2}
Total charge:	10^{-10} - 10^{-9} C
Mean electron energy:	1-10 eV

The microdischarge channels spread out on the dielectric surface, covering a much larger surface area than the ones covered by the current-carrying channels in the gap. These weakly ionized filaments start when the breakdown field is reached locally and extinguish when the field is reduced to the extent where electron attachment and recombination dominate over ionization [12]. An important property of the dielectric barrier discharge is that the microdischarges are evenly distributed over the entire surface by limiting the amount of charge and energy deposited in each. An important feature of the dielectric used in DBDs is the charge accumulation on its surface exposed to the streamers. Such charge

build-up counteracts the applied voltage, thus reducing the local electric field. A given microdischarge extinguishes when the local charge build-up becomes important enough to bring the electric field strength under the breakdown threshold. Due to this charge build-up, additional microdischarges can only be initiated when the external voltage is rising. Once the voltage polarity is reversed, the microdischarges reform at the old positions [12]. Ozone generation is one of the most important applications for this type of plasma source [3]. A novel type of dielectric barrier discharge reactors (hybrid gas-liquid DBD reactors) is being investigated for ozone generation and water treatment and will be further discussed in section 2.3.2 [12, 14].

Next, corona and pulsed corona discharges are introduced since they are also used in wastewater treatment applications and will be further mentioned in this chapter.

2.1.4 Corona and pulsed corona discharges

Corona appears as a weakly luminous discharge in atmospheric air. It is localized near sharp points or point tips where the electric field is sufficiently large and non-uniform [2, 11]. Figure 2.4 illustrates a point-to-plane corona discharge system [2]. The apparatus, which consists of a sharp metal tip placed in proximity of a plane electrode, generates a plasma in the shaded area located slightly below the metal tip. The plasma typically ignites with a voltage of 2 to 5 kV DC (which value depends strongly on the inter-electrode spacing and the shape of the electrode tip) and operates at a very small current. Above a threshold current value, of the order of 10^{-5} A, microdischarges or streamers are generated between the electrodes due to the rapid voltage increase with current [2]. There is a maximum current, in the order of 10^{-4} A, above which the device begins to arc.

Such continuous current corona discharge produces active species at a low rate due to the relatively low power and limited size of the discharge.

Intermittent corona discharge sources using periodic voltage pulsations have been developed in order to increase the voltage and power level without spark formation (arcing). With this type of discharges, it is important to use pulsed power supplies generating short voltage pulses with steep front and very short rise times [11]. With duration of generated pulses ranging from 100 to 300 ns, streamers are sustained and the power is transferred into the plasma without sparking [1, 11]. Multi-point electrode corona sources, which use the liquid to be treated as the second electrode, are being studied for the treatment of potable and industrial water [15]. Some pulsed corona reactors were designed to produce electrical discharges directly in the liquid [16] or with a combination of electrical discharge generation directly in the liquid and the gaseous medium located above the water [17, 18]. In these cases, ozone, hydrogen peroxide and hydroxyl radicals are generated in-situ, and synergistically act to degrade organic compounds present in the solution.

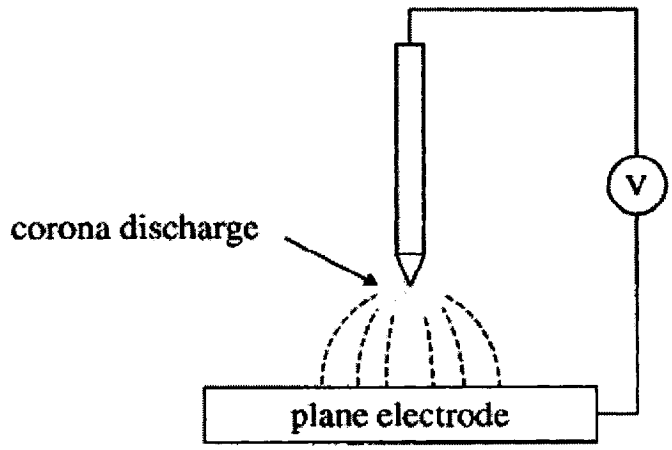

Figure 2.4 Illustration of a corona discharge apparatus [2]

2.2. Ozone

2.2.1 Industrial ozone generation with DBD

In 1840, Schönbein identified ozone (O_3) as a new compound. In 1857, Siemens successfully produced ozone from electrical discharges in molecular oxygen. He built a device composed of an annular discharge gap with an axial gas flow between two coaxial cylindrical glass tubes equipped with two coaxial external electrodes [3]. The design of today's silent ozonizers is based on this concept. Ozone, which is an extremely powerful oxidizing agent, is typically used in bleaching processes, in the semiconductor industry and for chemical synthesis. It is also used in potable water and wastewater treatment, disinfection, deodorization, and for the treatment of industrial wastes and the treatment of flue gases [5].

The ozone concentration and production yield depend on many parameters including excitation frequency, input energy density, gaseous gap spacing and reactor length, flow rate and type of gas, as well as the type of dielectric material used [5]. It was found that the ozone concentration increases by increasing the gap space, the length of the discharge tube and the applied voltage, and that it decreases with increasing pressure and dielectric layer thickness [19]. Industrial ozone generation is typically performed in cylindrical tubes of diameter ranging from 20 to 50 mm and length ranging from 1 to 3 m [12]. Borosilicate glass tubes have been widely used as the dielectric material. They form annular gaps of approximately 1 mm width and are mounted inside stainless steel tubes. The high voltage electrodes are metal coatings inside the glass tubes. The dielectric layer prevents the formation of arc discharges and promotes instead, the development of streamers [5]. Hundreds of discharge tubes are packed inside big steel tanks to produce the required ozone levels. Since ozone destruction by decomposition

increases as the gas temperature increases, water flows counter-currently to provide the required cooling [20]. These generators can give up to 200 g O_3 kWh^{-1} (up to 6% wt) based on an oxygen feed, and around 90 g O_3 kWh^{-1} (0.5 to 2% wt) based on an air feed [21]. Pulsed corona discharges have also been found to produce 240 g O_3 kWh^{-1} and are being used. Most ozonizers operate at the low frequency of 50-60 Hz with typical voltages of 12-20 kV. However, modern ozonizers operate at medium frequency (of about 1000 Hz) and feature greater ozone yields using smaller electrode surface areas and lower power consumption per kg of ozone produced [20].

2.2.2 Ozone production and destruction mechanisms

Ozone cannot be stored and must always be generated at the point of use. It is an unstable molecule, which decays into molecular oxygen (O_2) with a time constant depending on the temperature and the presence of oxidable compounds [22]. Ozone generation starts with the electron-impact dissociation of O_2 that frees up atomic oxygen (O), which upon recombination with O_2, forms the O_3 molecule. Parallel reactions lead to the loss of ozone. Such reaction paths are summarized below. Reactions (R1) to (R4), where M is a third body or the wall of the discharge cell, were first proposed by Devins for ozone generation from oxygen [23].

$$e^- + O_2 \rightarrow O^\bullet + O^\bullet + e^- \qquad \text{(R1)}$$

$$O^\bullet + O_2 + M \rightarrow O_3 + M \qquad \text{(R2)}$$

$$O^\bullet + O_3 \rightarrow O_2 + O_2 \qquad \text{(R3)}$$

$$e^- + O_3 \rightarrow O^\bullet + O_2 + e^- \qquad \text{(R4)}$$

Other reactions have been adopted to describe the chemical processes in air [24]. Some of the main reactions are:

$$e^- + H_2O \rightarrow {}^{\bullet}OH + H^{\bullet} + e^- \quad \text{(R5)}$$

$$e^- + N_2 \rightarrow N^{\bullet} + N^{\bullet} + e^- \quad \text{(R6)}$$

$$N^{\bullet} + O_2 \rightarrow NO^{\bullet} + O^{\bullet} \quad \text{(R7)}$$

$$N^{\bullet} + O_3 \rightarrow NO^{\bullet} + O_2 \quad \text{(R8)}$$

$$NO^{\bullet} + O_3 \rightarrow NO_2 + O_2 \quad \text{(R9)}$$

$$NO_2 + O_3 + e^- \rightarrow NO_3^- + O_2 \quad \text{(R10)}$$

2.2.3 Water disinfection with ozone

Ozone is the strongest commercially available oxidizing agent. Because ozone is very reactive in aqueous environments, it can oxidize material 10 to 1000 times faster then most other oxidants [20]. For example, on a comparison of oxidation strengths of standard oxidants versus hydrogen, ozone is 2.07 volts while chlorine and chlorine dioxide are 1.36 and 1.5 volts, respectively [20]. Ozone processes are being used more frequently than chlorination in water treatment plants due to their stronger efficiency in killing bacteria and viruses, and because there is no need to store and handle toxic chemicals. Furthermore, ozone by-products do not have any known adverse effects on health and the environment. Finally, ozone can destroy a broad range of organic contaminants and helps in the removal of color and odor [21].

Ozone reacts in water or in an aqueous solution either directly or indirectly. Directly, molecular ozone will attack via three mechanisms; cyclo addition on unsaturated bonds, electrophilic addition on molecular sites with strong electronic density or nucleophilic addition on molecular sites with an electronic deficit, usually on carbons carrying electron-withdrawing groups. Indirectly, ozone will form radicals while decomposing in water. Such radicals are hydroxyl radicals, hydroperoxide radicals, superoxide radical ions, and ozonide radical ions. The

formation of these radicals is specific to the exact composition of the water being treated and is dependent on many factors [25]. The direct reaction of ozone predominates in strong acidic solutions and the indirect reaction predominates at pH's above 7 [20]. In effect, the half-life of ozone increases with decreasing pH and decreasing temperature. In the presence of hydroxyl ions, ozone partly decomposes into OH radicals as shown in reactions (R11) and (R12). As shown in Table 2.2, the OH radicals have greater oxidative properties than ozone and their formation is always favored in water treatment and for the degradation of organic molecules.

$$O_3 + OH^- \rightarrow HO_2^- + O_2 \qquad \text{(R11)}$$

$$O_3 + HO_2^- \rightarrow {}^{\bullet}OH + O_2^{\bullet-} + O_2 \qquad \text{(R12)}$$

Hydrogen peroxide (H_2O_2) and UV radiation are factors that may also induce ozone degradation, allowing an advanced oxidation process to occur [26]. Indeed, H_2O_2 is a weak acid that partially dissociates into a hydroperoxide anion (HO_2^-) when combined with water as following:

$$H_2O_2 + H_2O \rightarrow HO_2^- + H_3O^+ \qquad \text{(R13)}$$

As described with mechanism (R12), ozone decomposes in the presence of HO_2^-. In fact, it is now known that the rate constant for the decomposition of ozone, with mechanism (R12), is largely superior than the one for mechanism (R11) [7, 26]. The H_2O_2 molecule reacts very slowly with ozone but again, since the concentration of HO_2^- increases with increasing pH, H_2O_2/ HO_2^- being the ion acid-base pair, ozone will decompose more quickly in a more basic solution [7,26]. On the other hand, ozone standard samples at a pH of 2, made under ideal conditions and with ozone-demand-free water could be stored for a few hours [26]. At 25 °C, the half-life of ozone in water, with a pH of 7, is 15 minutes. It is of approximately 3 days in air [27]. It has also been found that the presence of

carbonate ions in the groundwater can provide stabilization and double the half life of dissolved ozone at a pH of 8 [28]. This is explained by the fact that bicarbonate and carbonate ions are inhibitors of free-radical reaction, which means that they are compounds capable of consuming hydroxyl radicals without regenerating superoxide anion [26]. In the treatment context, water can be effectively disinfected within five minutes, at a maximum concentration of 1.5 mg O_3/L, because no pathogen is known to survive at this concentration [25].

2.3. Hybrid gas-liquid plasma reactors

2.3.1 Electrical discharges in and above water

Studies have been performed for both electrical discharges in water and at the surface of water. These water treatment units are simpler since they eliminate the need for a separate reactor for ozone generation, ozone transfer lines and contactors.

It has been suggested that the conclusions obtained for electrical discharges in water are valid for electrical discharges formed above the water, as far as the mechanism of pollutant oxidation is concerned. For example, phenol is oxidized by OH radicals through the hydroxylation of the benzene ring in both cases [21]. Electrical discharges in water produce the chemically active species in-situ and thus, favor the direct attack of the chemical(s) to be treated (i.e. no need for mass transport across the gas-liquid interface) [21]. Electrical discharges above the water require less energy than electrical discharges in water. They produce ozone and many other chemically reactive species in the close proximity of aqueous solution (H_2O_2, $^{\bullet}OH$, $H^{\bullet}$, $O^{\bullet}$). Some of these reactive species dissolve directly into the solution.

Water treatment by direct-contact electrical discharges provides means to utilize chemical species that are stronger oxidizers than ozone, but could not be used otherwise due to their instability. All free radicals, especially O and OH radicals in the case of air and OH radicals in water, play a significant role in the destruction of pollutants. In the case of electrical discharges in water, and by extrapolation when the electrical discharges are produced at the gas-water interface, the following free radical production and termination reactions can take place [21]:

$$H_2O \rightarrow {}^{\bullet}OH + H^{\bullet} \quad \text{(R14)}$$

$$H^{\bullet} + O_2 \rightarrow HO_2^{\bullet} \quad \text{(R15)}$$

$$H^{\bullet} + HO_2^{\bullet} \rightarrow H_2O_2 \quad \text{(R16)}$$

$$2H^{\bullet} \rightarrow H_2 \quad \text{(R17)}$$

$$HO_2^{\bullet} + {}^{\bullet}OH \rightarrow H_2O + O_2 \quad \text{(R18)}$$

$$2H_2O \rightarrow H_3O^{+} + e^{-} + {}^{\bullet}OH \quad \text{(R19)}$$

$$H_3O^{+} + {}^{-}OH \rightarrow 2H_2O \quad \text{(R20)}$$

$$H^{\bullet} + {}^{\bullet}OH \rightarrow H_2O \quad \text{(R21)}$$

$$e^{-} + {}^{\bullet}OH \rightarrow {}^{-}OH \quad \text{(R22)}$$

$$e^{-} + H^{\bullet} + H_2O \rightarrow {}^{-}OH + H_2 \quad \text{(R23)}$$

$$e^{-} + H_2O_2 \rightarrow {}^{-}OH + {}^{\bullet}OH \quad \text{(R24)}$$

$$H^{\bullet} + H_2O_2 \rightarrow H_2O + {}^{\bullet}OH \quad \text{(R25)}$$

$${}^{\bullet}OH + H_2O_2 \rightarrow H_2O + HO_2^{\bullet} \quad \text{(R26)}$$

$$2{}^{\bullet}OH \rightarrow H_2O_2 \quad \text{(R27)}$$

$$2HO_2^{\bullet} \rightarrow H_2O_2 + O_2 \quad \text{(R28)}$$

$$H_2O \rightarrow \tfrac{1}{2} H_2O_2 + \tfrac{1}{2} H_2 \quad \text{(R29)}$$

Table 2.2 shows the oxidation potentials of some of the species reported above.

Table 2.2 Oxidation potentials of various species [21]

Species	Oxidation Potential (V)
$^{\bullet}OH$	2.8
$O^{\bullet}$	2.42
O_3	2.07
H_2O_2	1.78
$HO_2^{\bullet}$	1.70

As previously mentioned, when produced in the gas phase and dissolved in water, ozone reacts either directly or indirectly. Since OH radicals are primarily responsible for the oxidation of aqueous pollutants, the faster the rate of ozone conversion to OH radicals, the faster the destruction of organic pollutants. When discharges are produced in a hybrid gas-liquid reactor, an appreciable amount of OH radicals will also be produced in the humid air. A simultaneous generation of hydrogen peroxide in the liquid phase has also been proved [7]. For example, one of the initiation reactions (R14) taking place could be followed by the propagation reaction (R15) and the termination reactions (R16) and (R27). The additional hydroperoxide anions formed (R13), promote the indirect attack of ozone, and enhance the degradation by forming OH radicals that have higher oxidative properties than ozone (Table 2.2). It has been shown that H_2O_2 and O_3, under the action of electrical discharges, have a synergistic effect on the destruction of organic compounds by enhancing the overall rate of oxidation of pollutants, because they decompose in free radicals [21].

2.3.2 Parallel hybrid DBD plasma reactors: history and important results

A novel method using a parallel plate discharge geometry featuring the liquid to be treated sandwiched between the electrodes was first described in 1995 in a world patent, with Ion Inculet as the inventor, suggesting the use of this technology for the treatment of municipal and industrial waters [14]. The device

was similar to industrial parallel DBD ozone generator but the difference was that the ground electrode consisted of the water to be treated instead of a metal. The AC voltage applied on the electrodes generated conical protrusions from the water surface, known as Taylor cones (The concept of Taylor cones is detailed in the next paragraph) [14]. This reactor could operate in batch or continuous mode. It was operated at frequencies of 50 or 60 Hz (0.01 to 5000 Hz were also suggested) and water depth of 3.4 cm. Discharge gaps ranging between 6.35 and 19.05 mm have been found satisfactory. The voltage used ranged between 20 and 45 kV (it was suggested that 1 to 200 kV could be used) with an oxygen flow rate of 2.6 L/min. The upper electrode, made of copper or aluminum, rested on a Teflon piece having a thickness ranging between 6.35 mm and 1.27 cm. The latter was used as the dielectric material. It was suggested that a vibrator could be used to increase the turbulence of the water and to complement the action of the electric field. Ozone was monitored in the gas phase in order to obtain preliminary laboratory-scale equipment performance [14]. The ozone production level (in ppm) increased continuously while increasing the output voltage, and the efficiency (amount of ozone generated divided by the input energy, in g/kWh) remained high. The efficiency slightly dropped while increasing the air gap thickness, where the AC voltage had to be increased simultaneously to maintain the maximum efficiency. Furthermore, with a larger thickness for the dielectric layer, an increased applied voltage enhanced the ozone production in the gas phase but reduced the production efficiency. Finally, production efficiency was found to decrease with increasing running water temperature [14].

Conical protrusions from the free surface develop when a gas-liquid interface is exposed to a sufficiently high voltage. These protrusions have been named after Sir Geoffrey Taylor who studied their stability and the conditions under which they exist. Taylor theoretically showed that these cones could exist in

equilibrium in an electric field only when they have a semi-vertical angle of 49.3° [29]. His work was extended by other researchers since his theory was restricted to particular cases and assumptions [30]. Much work has been done since, because these cones represent a great interest in the generation of monodisperse sprays of ultrafine drops for example (i.e. electrospinning process). In this application, a liquid is continuously fed through a sharp nozzle and exposed to a high electric field. When the field is sufficiently strong, the apex of the cone may either pulsate, shed charged drops or emit a thin stationary jet that break into charged drops at some distance downstream of the cone [31]. Studies have been performed looking at the current emitted from Taylor cones as well as the effects of background gas and ion evaporation from its surface [31, 32, 33]. Other studies also investigated the roles of the electrical conductivity and viscosity on the liquid motion inside the Taylor cones and the low and high Reynolds number flows inside them [34, 35]. Most of these studies have investigated a liquid held at the exit of a charged capillary facing a grounded electrode since it was the geometry used in electrostatic atomization.

In parallel hybrid gas-liquid DBD plasma reactors, researchers have used water as the grounded electrode and an electrically insulated electrode as the live electrode due to the practical difficulties associated with the reverse situation [14]. As mentioned in the previous paragraph, Taylor cones were induced in this reactor type [9, 14]. The main interest in these Taylor cones, in this context, is the enhanced mass transfer at the gas-liquid interface associated with the dynamics of the cones. In fact, due to the cyclic change of the live electrode polarity, Taylor cones form intermittently and randomly over the liquid surface leading to a severe agitation of the interface [14].

The first laboratory study of a DBD hybrid gas-liquid reactor was reported

in 1998 [9]. The semi-batch reactor was operated with a frequency of 60 Hz. The discharge gap was varied between 5 and 15 mm. An oxygen flow ranging between 0.73 and 7 L/min was used. The walls were made of an acrylic and the high-voltage brass electrode was enclosed in a chamber filled with insulating silicone transformer oil that prevented unwanted discharging around the electrode [9]. The gas residence or contact times were 7, 25 and 42 seconds. The primary function of such a device was to generate ozone in the gas phase. Data obtained were compared to traditional ozone generators. Ozone was measured in the gas phase using an Orbisphere 3600 sensor. It was found that ozone concentration in the gas phase increased as the gas residence time was increased but that the rate of ozone concentration increase slowed down. This was explained by a possibly warmer discharge gap accelerating the decomposition of ozone molecules, and a higher humidity, which caused a decrease in the net ozone production due to the loss of electrons that would otherwise be used for ozone generation [9]. Ozone concentration and production rates increased with increasing electric field strength but the efficiency, defined as the amount of ozone generated in the gas phase divided by the input energy, declined. Furthermore, it was found that ozone concentration, production rate, and efficiency decreased when the temperature increased. While the concentration and production rate of ozone increased the larger the discharge gap, the efficiency decreased. The use of such parallel plate arrangement with an electrode covered with a layer of water, resulted in an energy efficiency of 110 g/kWh. It was noticed that this value was far under the efficiency levels reported by manufacturers of commercial ozone generators [9].

The quantity of ozone generated in air by the commercial generators is typically 200 g for 1 kWh, but ozone has a short residence time in air and therefore a large quantity of it vanishes before it contacts the water to be

treated [15]. On the other hand, water vapor can hinder net ozone generation by absorbing electronic energy that could otherwise be used in the ozone formation process. Water vapor can also affect the functioning of the surface of the dielectric layer and can cause strong microdischarges [9]. Therefore, in using this type of reactor, the ozone productivity is sacrificed. Ongoing studies continue to investigate whether the unique characteristics of such reactor could lead to efficiencies higher than those obtained using ozonation [36].

From the point of view of a water treatment application, as previously mentioned, the presence of Taylor cones implies a larger surface area for ozone dissolution and a greater agitation of the interface [9]. The apexes of the cones also provide points for electrical discharge pulses, which initiate ozone generation if the electrical stress is high enough. The excitation frequency and the thickness of the liquid film are parameters that affect Taylor cones generation. As mentioned in the Introduction, a repeated problem was the ejection of droplets from the Taylor cones at the frequency of 60 Hz. When droplets were suspended on the dielectric plate, the efficiency of ozone production was reduced because it was believed that the droplets would become sites for more energetic discharges [9].

A range of excitation frequencies was used (20-300 Hz) to study the breakdown of air over a water surface stressed by a perpendicular alternating electric field in the presence of a dielectric barrier [37]. Again, the high-voltage brass electrode was enclosed in transformer oil directly in contact with the dielectric material. The reactor was a batch type and tap water, with a thickness of 25 mm, was separated from the dielectric by an air gap varying between 6 and 12 mm. The results showed that the breakdown voltage depended on the excitation frequency as well as the thickness of the air gap. The breakdown voltage was lower for smaller air gaps and was less than the value expected for air over a metal

electrode. At higher frequencies (between 240 and 300 Hz), the breakdown voltage decreased due to the reduction of the gap thickness associated with the upward bulge of the water surface. At low frequencies (<80 Hz), it was more significantly reduced due to electric field intensification associated with the formation of sharper Taylor cones. Cones were found to be highly predominant at low frequencies [37]. Following these results, special considerations were taken when choosing the operating frequency.

It was also later proved that ozone generation in hybrid DBD was accompanied by a simultaneous production of hydrogen peroxide in the liquid phase. Such mechanism of production of OH radicals is different from what is observed in classical ozonation where the ozone decomposition is the source of production of those radicals [7]. Another factor that was noted was that modest area-to-volume ratio influenced the efficiency of the hybrid ozone generator and limited the gas-liquid transfer of ozone [7].

The flow pattern in the continuous version of the DBD hybrid reactor previously discussed was laminar [36]. To study the effect of high voltage discharge on ozone dissolution, the reactor was replaced by stirred semi-batch reactors. Four-baffle tanks (152.4 mm i.d.) were constructed from an acrylic material. They were placed on magnetic stirrers to allow the agitation of Teflon-coated bar magnets and the mixing of the solution. A bottomless cage, made of a stainless steel plate and a wire mesh, was used as an enclosure for the magnetic bar. The cage prevented a vortex from forming and grounded the water electrode [36]. With a frequency of 60 Hz and a voltage of 25 kV, a 13 mm gap distance had to be used in order to prevent the contact between the liquid surface and the dielectric, due to the protuberances at the surface of the water. An oxygen flow of 0.5 L/min was used and a liquid volume of 2.07 L was processed. The

polished brass, rounded-edge high-voltage electrode, with a diameter of 114 mm, was embedded in a solid RTV-silicone rubber that was attached to a 0.25 mm-thick Teflon membrane that acted as the discharge surface.

Methylene blue (MB) was degraded to allow comparison of the results obtained between three ozone generation setups ((1) dry ex-situ; (2) humid ex-situ; and (3) humid in-situ or "electroozonation") [36]. An initial concentration of 4.44 mg/L of MB was used with a corresponding absorbance reading of 1. The first experimental setup introduced ozone produced externally, in dry oxygen; the second introduced ozone produced externally over water. The third experimental setup generated ozone by discharge directly above the MB solution. It is to be noted that protuberances were constantly arising and collapsing due to the electrostatic forces and that the discharges were mostly concentrated on their apexes. It took approximately 180 minutes for the dry ex-situ experimental setup, 210 minutes for the humid ex-situ experimental setup and 60 minutes for the humid in-situ experimental setup, to decolorize MB completely. The first two experimental setups showed approximately similar results. The third experimental setup showed a three fold faster decomposition of MB in the liquid phase. Several assumptions were suggested in order to explain the faster decomposition rate obtained [36]. First, hydrogen peroxide and its conjugate base both produced in the liquid phase, could have lead to a faster decomposition of ozone, and therefore to a faster generation of secondary OH radicals. Additional generation of OH radicals could have also been produced by the discharge near the gas-liquid interface [36]. Furthermore, the electrostatic forces created protuberances at the surface of the water that increased the mass transfer of ozone by increasing the area of the gas-liquid interface [36]. Another application will be presented next.

Ethylenediaminetetraacetic acid (EDTA) is used as a metal chelating agent in industries including nuclear power plants. It is poorly degraded in wastewater treatment plants and significant amounts of it are released into natural water [8]. Aqueous EDTA chelates the metal electrode when in direct contact with it. A hybrid DBD was used to degrade EDTA since the electrodes were enveloped with dielectric materials. Aqueous EDTA, with concentrations of 2 and 0.2 wt.-%, was used. The corresponding pH of the solutions was about 7 and was controlled using potassium hydroxide. The reactor used was of planar-type with a mid-frequency field (30 kHz) and with voltages ranging between 11 and 14 kV.

The dielectric was made of alumina (Al_2O_3) and the high-voltage electrode was embedded in a PTFE container ($70 \times 70 \times 8$ mm^3), which contained the solution to be treated. This setup prevented the EDTA in solution from reacting with the metal (aluminum) electrode. A mixture of helium, argon, and oxygen was introduced between the Al_2O_3 dielectric and the PTFE container. The total gas flow rate was 2 L/min, at atmospheric pressure and room temperature. The flow rate of oxygen was 0.2-0.8 L/min while the flow rate of argon was the same as that of helium during each degradation process. A gap with a thickness of 3 mm was used between the Al_2O_3 dielectric and the surface of the solution. With this type of mid-frequency discharge (30 kHz), little waves were formed. A volume of 35 mL was used and the discharge area (49 cm^2) was as large as the surface area of the EDTA solution without discharge [8].

Several experimental parameters, including the voltages and the gas compositions, affected the degradation of EDTA. The degradation was faster at higher plasma generation voltages. The assumption was that reactive species (ozone, OH radicals, atomic oxygen) were generated more abundantly the higher the applied voltage [8]. At an applied voltage of 14 kV and an initial concentration of 0.2 wt. %, 50% of EDTA was degraded in 10 minutes and more than 90 % was

degraded in one hour. It was found that the oxygen concentration was saturated below a flow rate 0.2 L/min and its increase up to 0.8 L/min did not affect the degradation of EDTA. However, the plasma density decreased for an oxygen flow rate superior to 0.8 L/min, due to the reduction of helium and argon in the total reaction gas. It was noted, that with such a small volume of water used, the treatment time was longer in comparison to other reports. It was explained by the fact that EDTA concentration was relatively high [8]. In addition, in this case, decomposition was restricted to the water surface. Mass transfer of reactive species in the bulk of the water was more difficult than if the decomposition occurred throughout the entire EDTA solution and if the discharges were generated in the water that was circulated. For an applied voltage of 12 kV, and after a treatment time of 20 minutes, the ratio of TOC to initial TOC was 0.885 for the 0.2 wt. % EDTA solution but remained around 1 for the 2 wt. % EDTA solution. This shows that the degradation kinetics might be dependent on the initial concentration of EDTA.

2.3.3 Other types of hybrid plasma reactors and applications

Advanced oxidation technologies (AOT) are being studied for the degradation of contaminants in water and an increasing number of novel combinations of processes are being thought of. The techniques can be divided in different categories. Chemical, where ozone, hydrogen peroxide, or a combination of ozone and hydrogen peroxide are used. Photochemical and photocatalytic, where combinations of UV, ozone, hydrogen peroxide and TiO_2 are used. Electron beams or ultrasonic irradiations are also being combined. Combinations of the different processes are being thought of to enhance the formation of oxidative species, mainly hydroxyl radicals. Other than hybrid DBDs, other electrical discharges such as corona discharges have been investigated long before and will

be presented in this section, along with other types of discharges.

A non-thermal plasma reactor, leading to the formation of pulsed streamer corona discharges, was first investigated in 1987 as a novel AOT for water processing [38]. Since then, all sort of electrical AOT involving discharges in water and gas-liquid hybrid reactors have been considered. These methods could reveal to be efficient methods for the production of highly active species [39].

Studies have been performed on different types of hybrid-gas liquid apparatuses with the sole objective to make use of them potentially for the degradation of organics and wastewater treatment. As will be seen, degradation of phenol was mostly studied since its properties and its kinetics are well known.

A surface barrier-discharge (SBD) plasma treatment was developed to treat aqueous phenol solutions. The liquid was deposited on the dielectric and was separated, by the flowing gas, from a planar metal electrode [40]. The degradation products appeared less toxic than the starting compounds. A coaxial DBD arrangement of the electrodes was also designed. The fed solution arrived directly on a porous hydrophilic material covering the noninsulated electrode [41]. The flowing water was separated from the dielectric and the other electrode by a discharge gap where the plasma formed. This configuration resulted in a higher effective rate constant for phenol degradation. This phenomenon was studied in more details thereafter by the same group [42, 43, 44]. The configuration was also studied for the removal of organic pollutants in sewage water [45].

Pulsed barrier discharge (PBD) was applied in a system where a water-air medium, consisting of water droplets and air streams, was uniformly distributed over the cross-section of the electrode system [46]. When the mixture moved through the interelectrode spacing, streamers appeared in the gas and on the

liquid-gas boundaries. Trichloroethylene and phenol were degraded. The oxidation of phenol by PBD was compared to various electric discharge methods: corona in water, corona in air over water and conventional ozone treatment. PBD was found to be highly more efficient than the first two corona discharge methods and could even be more preferable than the conventional ozonation method [46].

Other apparatuses have been investigated for the direct ozonation of liquids. The effects of changing different parameters, with a multi-point corona electrode, on the ozone concentration in the liquid phase were investigated [15]. Of interest were the gap distance between the discharge points and, similar to the treatment with DBDs, the thickness of the liquid layer and the exposure time to the corona discharge. It was found that the ozone concentration in the liquid decreased with an increasing thickness of the liquid layer. It was therefore suggested that ozonation was more effective for thinner liquid layers. Again, as was also the case with DBD hybrid reactors, the quantity of ozone produced was found to be proportional to the discharge duration and the applied voltage level [15]. The apparatus was then upgraded to treat thin films of water. The new configuration consisted of a multiple-needle electrode facing an inclined-grounded tray at the surface on which flowed the water films to be treated [47]. Multi-point corona discharge was also studied to degrade azocarmine B. The degradation of this dye detected the creation of chemical radicals useful in water treatment [48]. Phenol removal was also studied in a small batch reactor where pulsed corona discharges were created above the water to be treated. For the same parameters used, increasing the pH values of the solution increased the phenol removal rate. This was explained by the fact that in acidic conditions, ozone reacted directly with phenol but that at higher pH, hydroxyl radicals reacted with phenol. Thus, the decomposition rate was increased [49].

Pulsed plasma discharge systems with electrical discharges generated inside gas bubbles were investigated [50, 51]. The detection of ozone formed inside the bubbles, demonstrated the generation of atomic oxygen that could be used for water purification [50]. Pulsed streamer corona discharge systems, in water, were used to degrade phenol [39, 52]. Furthermore, a pulsed arc discharge system was used to degrade 4-chlorophenol, 3, 4-dichloroaniline, and 2, 4, 6-trinitrotoluene [53].

Reactors where the pulsed corona discharges were produced in the liquid phase only ("reference reactor") or simultaneously in the liquid and the gas phases (two types: "hybrid-series reactor" or "hybrid-parallel reactor") were considered and compared for water treatment [17, 18, 54]. The production of hydroxyl radicals produced by the liquid phase pulsed corona discharge, was quantified in the reactors [55]. The rate of production of the hydroxyl radicals increased linearly with increasing applied voltage. Furthermore, a greater production of hydroxyl radicals was achieved in "hybrid-series reactor" in comparison to the "reference reactor" [55, 56]. In an argon atmosphere, phenol was degraded due to the electrophilic attack of hydroxyl radicals. Hydroxyl radicals were produced by both the discharge in water and the gas phase discharge at the gas–liquid interface [56]. Under an oxygen atmosphere, it was found that the formation of gaseous ozone and its dissolution into the water dominated over the formation of hydroxyl radicals [56]. As previously mentioned for pulsed corona discharges created above the water to be treated, phenol, in this case, was mostly degraded at a high pH (3.5 times larger in alkaline solution compared to acidic solution) under an oxygen atmosphere. In addition to the direct attack of ozone, hydrogen peroxide, produced in the liquid phase, induced the indirect formation of hydroxyl radicals. These were formed by the decomposition of dissolved ozone via a peroxone process [56]. The results for the decomposition of substituted phenols, in the same

reactor, were also reported. The studied compounds were the ortho, meta, and para isomers of hydroxyl-, chloro-, and nitrophenols in water [57].

It is to be noted that the last two paragraphs described types of systems, requiring large voltages ranging between 15 and 200 kV.

2.4. Indigo dye degradation by plasma

Dyes are used as colorants in several industries including textile, food and paper industries. For example, indigo dyes (blue) are predominantly used in the jeans industry. As a result, the colored wastewaters reduce dissolved oxygen in rivers because they prevent sunlight from penetrating to algae at depth. Different methods of degradation are being investigated in order to degrade the dyes dissolved in the effluents of these industries [58]. Advanced oxidation by plasma treatment is one of the techniques being used [59, 60, 61, 62].

The degradation of an indigo dye could be used as a method to optimize a plasma reactor. Indigo trisulfonic acid, which color-producing structure is a cross-conjugated system or H-chromophore with the structure shown in Figure 2.5, is known to react with ozone with a very high reaction rate constant [63]. In general, this compound is mainly used to determine the concentration of ozone dissolved in water using a standard procedure [64].

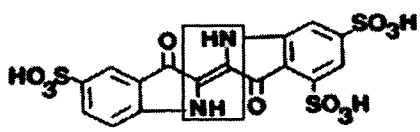

Figure 2.5 Indigo trisulfonic acid structure and reactive C=C [65]

Ozone, as previously explained, is known to react in two ways. Either directly in acidic media, or indirectly in more basic media, where it forms radicals while decomposing in water. Some of these radicals ($^{\bullet}OH$, $O^{\bullet}$) have higher

oxidizing properties than ozone. Acid is used to decrease the pH so that the amino groups of the indigo molecule are protonated and therefore, unreactive [64]. Furthermore, the indigo molecule is much more soluble at low pH. Ozonolysis of the reactive C=C bond produces sulfonated isatin and similar products and eliminates the absorbance at 600 nm [63]. Any active or oxidative species, including ozone, which breaks that reactive bond, can lead to the discoloration of the solution in which the indigo molecule is dissolved. A preliminary optimization of the reactor can easily be performed by monitoring the decrease in absorbance of a specific solution. This will be explained in more detail in the next corresponding sections. Researchers have used this method, with a similar indigo dye, to study the effects of several parameters on the discoloration efficiency of the solution. Others have used it to prove the formation of H_2O_2 and OH radicals in the treated solution. The next two paragraphs further explain these two examples.

Indigo carmine (IC) is another indigo dye. It was degraded using bipolar pulsed dielectric barrier discharge in a mixture composed of air microbubbles and water [66]. IC's structure differs from that of indigo trisulfonic acid by one less sulfonate group. Again, the system is composed of a single C=C double bond substituted by two NH donor groups and two C=O acceptor groups [67]. The central C=C has been found to be very reactive. Any reaction leading to the destruction of the chromophore can lead to the discoloration of the solution. More ozone and hydrogen peroxide were detected when no IC was dissolved in the solution. Therefore, it was deduced that ozone, hydrogen peroxide or their precursors played an important role in the color removal process. For an initial absorbance around 1, 99.9 % color removal efficiency was obtained after 5 minutes [66]. An improvement of the plasma chemistry process was then achieved by loading solid packing into the two-phase water-air mixture discharge

reactor [68].

Water treatment, using discharges inside bubbles, was also proposed to produce ozone, atomic oxygen and other radicals. When the plasma was generated in helium, the discoloration of an indigo (IC) solution reached 67 % after 30 minutes (initial concentration of IC of 20 mg/L and initial absorbance of approximately 1). The generation of H_2O_2 and OH radicals was therefore confirmed [69].

2.5. Wastewater treatment and degradation of pharmaceutics

Pharmaceutical products have been found in surface water, which is a common source of drinking water. After being administered for human or animal medical care, pharmaceutical products are excreted. They then reach the sewage treatment plant, which does not completely remove all the pharmaceuticals in the water [70]. Aquatic and terrestrial pollution is also attributed to emission sources such as direct disposal of surplus in households or effluents of farms. Antibiotics, usually designed to control bacteria in humans and animals, have been found in surface water in concentrations that may rise to μg/L in surface and ng/L in groundwater [6].

Processes involving the generation of OH radicals with O_3/OH^-, O_3/H_2O_2 or Fe^{2+}/ H_2O_2, as well as photochemical and photocatalytic reactions have been considered in order to remove these pharmaceutical contaminants [6]. Promising studies looking at the degradation of pharmaceuticals with ozone have been reported [6, 71, 72, 73]. The removal rates, obtained when using an ozonation process, were much more efficient in a basic solution since both OH radicals and ozone became the oxidizing agents [6]. The mixture of ozone and hydrogen peroxide also increased OH radical formation, which improved the efficiency of

the degradation process [6, 70]. The OH radical is highly reactive but unselective. It was found to degrade all types of sulfonamides [74].

The potential use of a DBD hybrid reactor for sulfonamide decomposition was investigated. It is discussed, in this thesis, as a case study.

Chapter 3. Experimental setup and methods

3.1. Experimental setup

3.1.1 Reactor design

Figure 3.1 shows a schematic diagram of the experimental setup for the parallel hybrid gas-liquid atmospheric pressure dielectric barrier discharge (DBD) reactor and its dimensions. Images of the constructed reactor are presented in Figures 3.2 and 3.3.

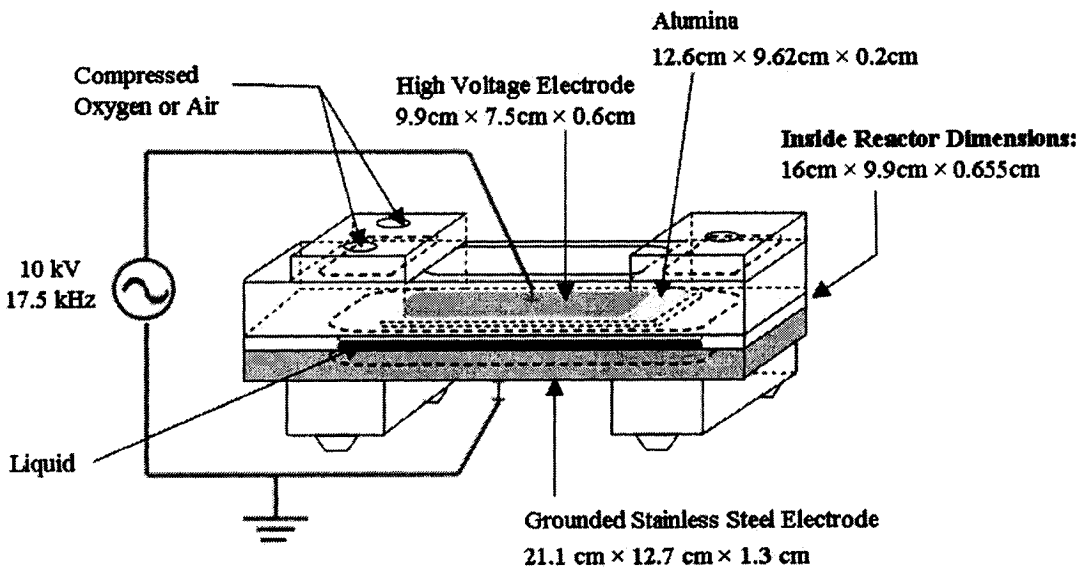

Figure 3.1 Schematic of the parallel hybrid gas-liquid atmospheric pressure dielectric barrier discharge (DBD) reactor

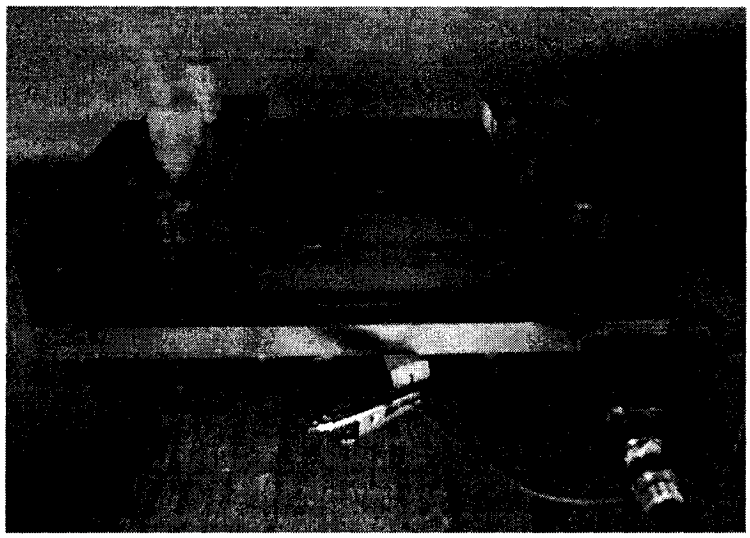

Figure 3.2 Image of the parallel hybrid gas-liquid atmospheric pressure DBD reactor

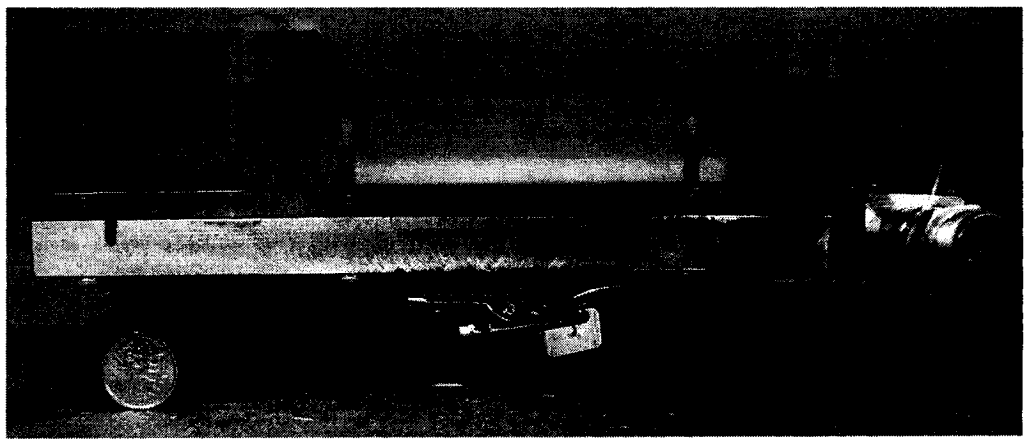

Figure 3.3 Side-view of the parallel hybrid gas-liquid atmospheric pressure DBD reactor

Problems were encountered and design modifications were performed before opting for this final design. The reactor was constructed with symmetrical internal dimensions and was operated as a semi-batch reactor. Two acrylic feet supported the grounded electrode made of stainless steel. The walls of the reactor were made of an acrylic made transparent, after being machined, by polishing (inside dimensions: 16 cm × 9.9 cm × 0.655 cm). The acrylic material was ideal since it is easily machinable, transparent and resistant to ozone [75]. Alumina is a

common material used as a dielectric, due to its excellent dielectric properties and its resistance to ozone [75, 76]. Therefore, an alumina plate, larger and wider than the upper electrode was used as the dielectric material (12.6 cm × 9.62 cm × 0.2 cm, machined "PlasmaPure" alumina plate from Coorstek). The alumina plate was sandwiched, with silicon, inside the upper part of the reactor also made of acrylic. A hole was made on the upper part of the reactor for the high voltage electrode, made of aluminum (metal with the lowest density), to rest on the alumina plate. The high voltage electrode was therefore surrounded by acrylic, which prevented arcing. The borders of the high voltage electrode were rounded to prevent arc formation from its edges. Nylon and stainless steel screws held the reactor parts together. Several nitrile (Buna N) o-rings were used to seal the various joints.

The stainless steel and the aluminum electrodes were connected to the grounded and the high voltage ends, respectively, of a commercial power supply, described in more detail in the next section. Some of the reactor dimensions were designed so that specifications, suggested by the supplier of the power supply, would be met. The voltage of the power supply was controlled by a LabVIEW™ interface (National Instruments version 6.1).

Teflon tubing, connected to two swagelock Teflon fittings, delivered the gas to the reactor at a rate controlled by rotameters (Megs, model: 82B7920, HA1 valve for the low range of flow rates and Matheson 602, HA4 valve for the high range of flow rates). They were calibrated with a gilibrator (GILIAN Gilibrator-2 Calibration System from Sensodyne). The flow rates of both air and oxygen supplies (Compressed air and compressed oxygen from Megs, BOC Gases), which were connected to regulators and stainless steel valves, were calibrated at regulator pressures of 30 psig. The calibration curves, which were obtained for

oxygen and air with both rotameters of different flow rate ranges, are found in Appendix I. Finally, the rotameter with a high range of flow rates was used, with air alone, to purge the reactor.

The gas was introduced from the top of the reactor, in a chamber with a height of 2.4 cm. First, it would flow above the solution, in the gap between the liquid to be treated and the alumina plate. It would then exit from a similar acrylic chamber, and to the fumehood in which the reactor was enclosed. The liquids to be treated were introduced from an inlet, situated in between the gas inlet parts, usually closed with a Teflon plug, or from the gas outlet. A hole was made in the stainless steel and was connected to a brass plug valve, to permit the collection of the treated liquid after each semi-batch experiment. This configuration allowed for the formation of plasma streamers or microdischarges in the gas phase. An image of the complete setup is shown in Figure 3.4.

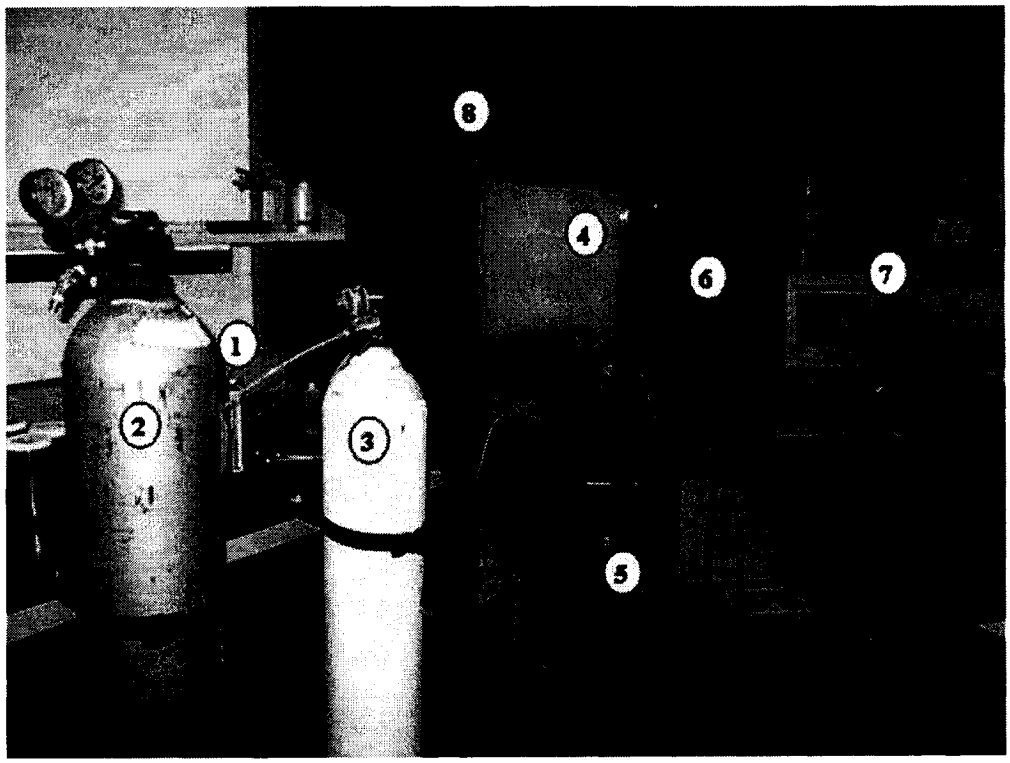

Figure 3.4 Image of the complete setup: 1. Rotameter; 2. Compressed air; 3. Compressed oxygen; 4. Fumehood in which the reactor and power supply were enclosed; 5. Oscilloscope; 6. LabVIEW™ interface customized to calculate power consumed by the DBD reactor; 7. LabVIEW™ interface customized to control the voltage of the power supply; 8. Ozone sensor

3.1.2 Energy dissipation and Lissajous figure

10X voltage (P6139A) and 1000X high voltage (P6015A) Tektronix probes (Figure 3.5) were connected to an oscilloscope (TDS 2024 Tektronix 4 Channels Digital Storage Oscilloscope, 200 MHz, 2 GS/s). The 1000X probe measured the voltage of the DBD reactor and capacitor placed in series (475 nF), while the 10X probe was used to measure the voltage on the capacitor alone. The capacitor was added in order to perform power consumption measurements, with the help of a Lissajous figure. This method is further explained in the next paragraphs. An operating frequency of 17.5 kHz was measured with the oscilloscope when the DBD reactor was connected to a commercial power supply

known to deliver up to 100 Watts (Plasma Technics Inc, PTI Electronic Ozone Transformer, 100 W/ 20 kHz) and shown in Figure 3.5. It is to be noted that all the waveforms and results presented in this section were obtained when an indigo solution was treated and with the optimum parameters that will be discussed in the next sections.

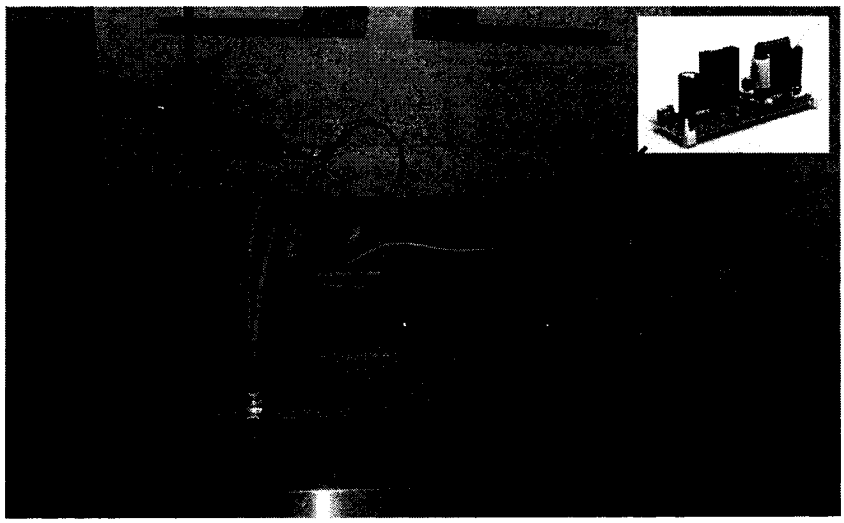

Figure 3.5 Image of the plasma reactor connected to the power supply [77]

The DBD plasma reactor worked at a peak voltage of 10 kV and at a low current with a peak value of 55 mA typically. The current was measured with a Tektronix CT-2 current transformer and a P6041 Probe. The current transformer was inserted in between the DBD reactor and the capacitor. A factor of 1mA/1mV had to be used to convert the voltage readings, obtained from the oscilloscope, to current values. A typical current waveform is shown in Figure 3.6.

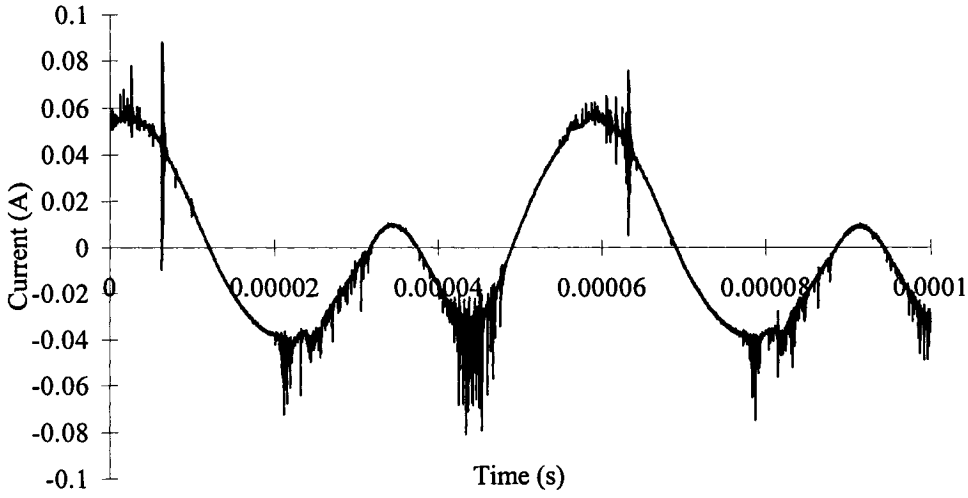

Figure 3.6 Typical current waveform of the DBD reactor

The data was transferred, with the help of a GPIB cable (USB-B National Instruments), to a LabVIEW™ interface (National Instruments version 6.1). Interface tktds1k2k.llb is a VI Library instrument driver for the Tektronix TDS 2024 oscilloscope. The application example provided by Tektronix was first considered. That VI showed how to configure the oscilloscope for a single-channel waveform acquisition, using external triggering. This interface was further modified and customized to transfer the waveforms of two channels, to reduce the noise that is generated by the plasma source, and to obtain the power consumed by the plasma reactor based on one period of the voltage excitation. A single power consumption calculation was obtained after approximately a minute. The LabVIEW™ interface was separated from the LabVIEW™ interface customized to control the voltage of the power supply, which sometimes needed to be turned on and off consecutively to obtain well-distributed microdischarges. Furthermore, the LabVIEW™ diagram customized to calculate power consumed by the DBD reactor contained numerous functions placed in parallel and in series. The highlight execution option had to be always turned on for the interface to work properly. This execution, in addition of showing the movement of data from

one node to the other on the diagram is known to reduce greatly the speed at which the signals are transferred.

The voltage waveforms could be transferred from the LabVIEW™ interface to a MS Excel file. Typical voltage waveforms are shown in Figure 3.7. It is to be noted that the absence of a matching network between the DBD reactor and the power supply might have affected the sinusoidal signals that should have been obtained. Fluctuations were observed on the voltage waveform of the capacitor and were probably due to the noise induced by the streamers during signal transmission. This was not observed on the voltage waveform of the reactor since the Y-axis major units were of 5000 V compared to the Y-axis units of the voltage waveform of the capacitor that were 0.5 V.

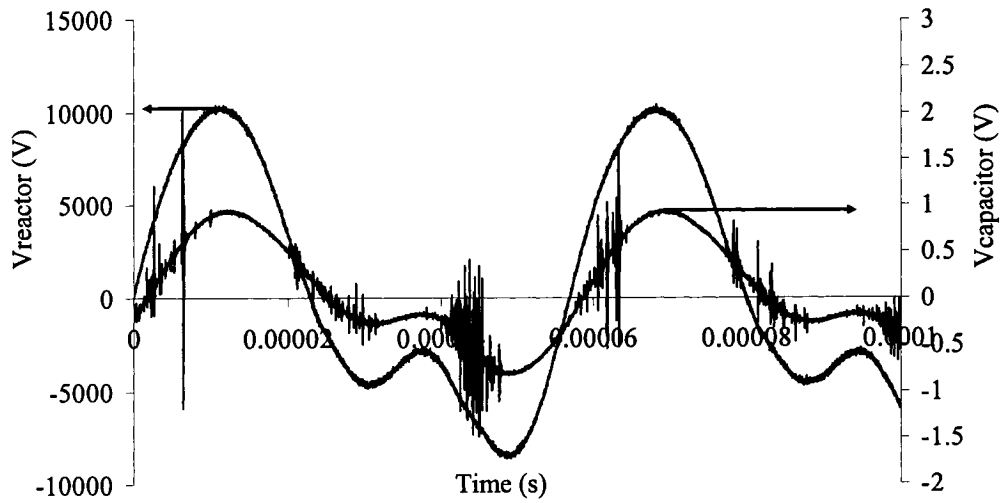

Figure 3.7 Voltage waveforms of the DBD reactor and the capacitor placed in series

As previously mentioned, the average power on a cycle was directly calculated by adding a capacitor in series with the DBD reactor. The voltage was measured on both the capacitor and the plasma reactor. Since there is a phase shift between the two measured voltages, a "Lissajous figure" is obtained on the

oscilloscope with the voltage of the DBD on the Y-axis and the voltage of the capacitor on the X-axis. Therefore, in order to obtain the power consumed by the plasma reactor, the LabVIEW™ interface was customized to first produce a Lissajous figure based on one period. The following formulas, for one period, describe how the power could be calculated from these measurements:

Symbols:

P_A: Average power [W]

$V_r(t)$: Voltage on the DBD reactor [V]

$V_c(t)$: Voltage on the capacitor [V]

$I(t)$: Current [A]

τ: Period [s]

f: Frequency [Hz]

C: Capacitance of the series capacitor [F]

E: Energy consumed [J]

For one period:

$$P_A = Ef = \frac{E}{\tau} \tag{1}$$

And $$E = \int_0^{\tau} V_r(t) i(t) dt \tag{2}$$

Also $$V_c(t) = \frac{1}{C} \int_0^{\tau} i(t) dt \tag{3}$$

From Equation (3):

$$C dV_c(t) = i(t) dt \tag{4}$$

Combining Equations (2) and (4):

$$E = \int_0^{\tau} V_r(t) C dV_c(t) \tag{5}$$

Combining Equations (1) and (5), the average power can be obtained as following

$$P_A = fC\int_0^{\tau} V_r(t)dV_c(t) \qquad (6)$$

With $\int_0^{\tau} V_r(t)dV_c(t)$, the area of the Lissajous figure for one period

The resulting Lissajous figure, transferred from the LabVIEW™ interface to a MS Excel file, is presented in Figure 3.8. The LabVIEW™ diagram was customized to calculate the area of the Lissajous figure by making use of defined arrays and the trapezoidal rule. In this particular example, the average power dissipated in the DBD was 55 W. The power lost (45 W) was probably due to the impedance mismatch resulting from the absence of a matching network between the power supply and the plasma reactor.

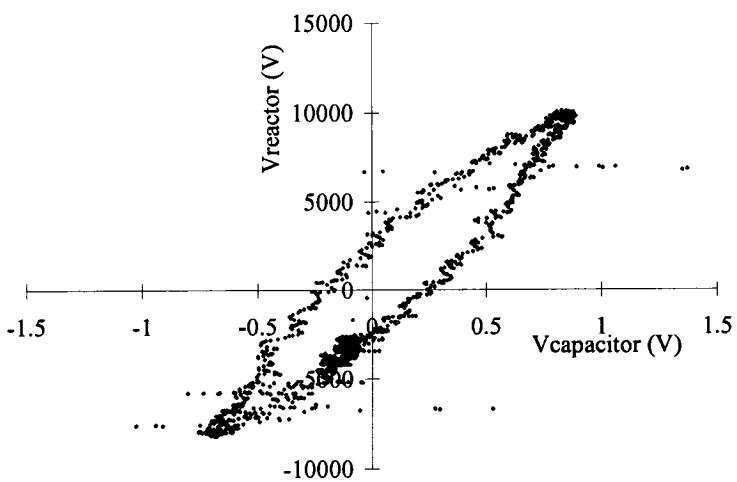

Figure 3.8 A typical Lissajous figure obtained by measuring voltage waveforms of the DBD reactor and the capacitor for one period

The images of the LabVIEW™ interface and diagram, with results obtained on the front panel for one run, are shown in the next figures.

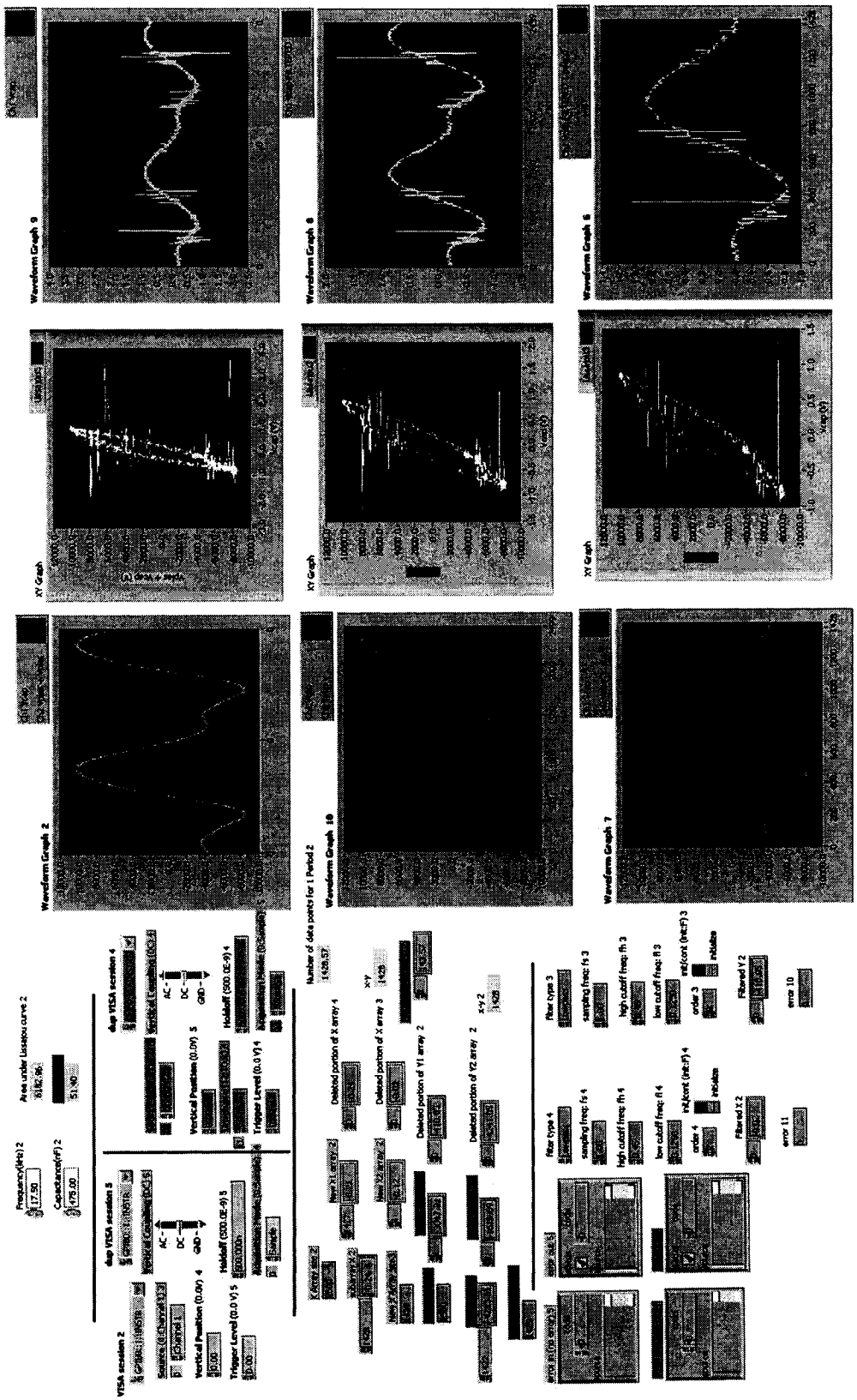

Figure 3.9 Front Panel of the customized LabVIEW™ interface for DBD power consumption

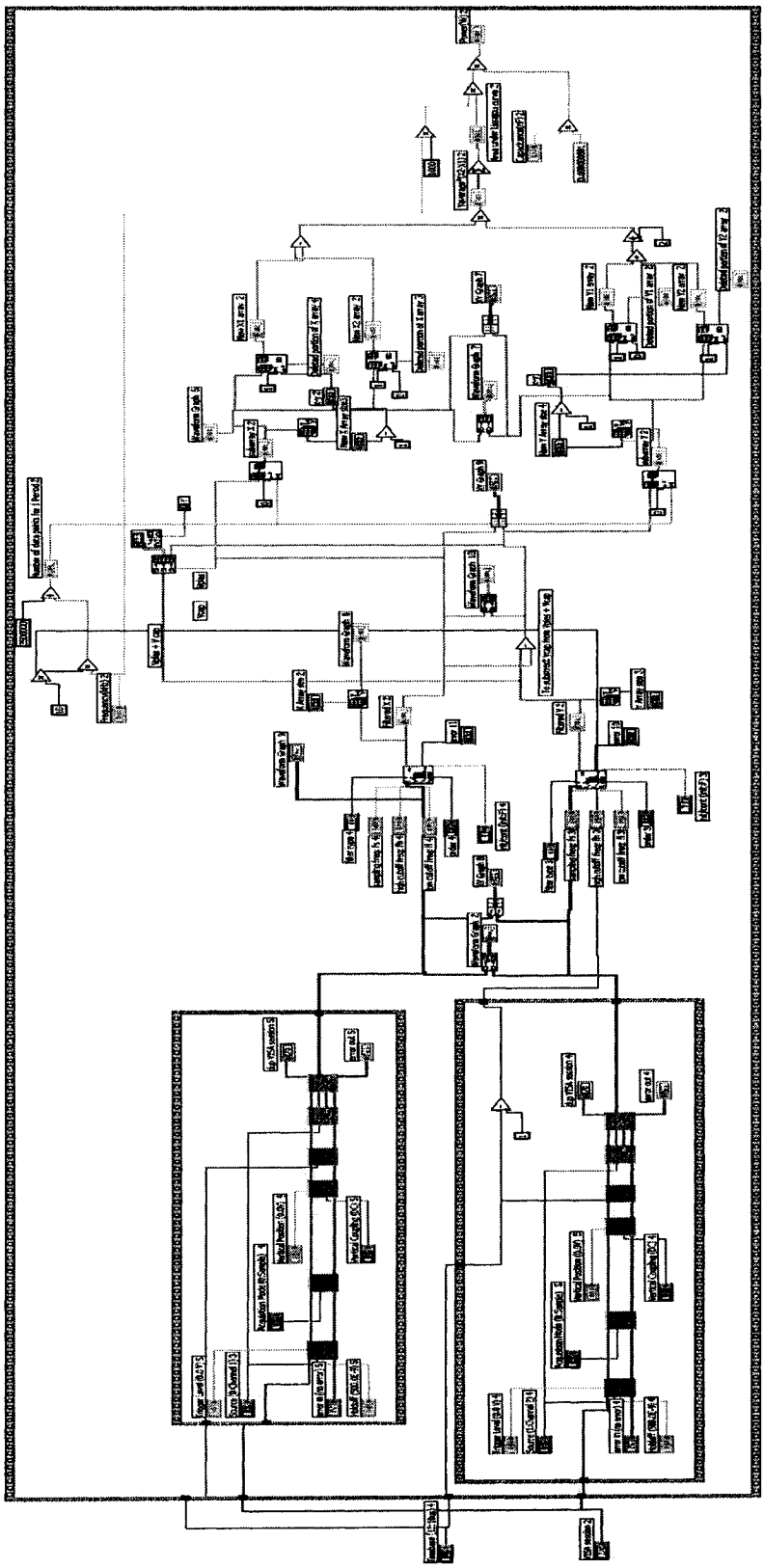

Figure 3.10 Diagram of the customized LabVIEW™ program for DBD power consumption

3.1.3 Safety considerations

Safety issues were considered throughout the project since dangerous chemicals and low current levels were used (55 mA). The safety considerations are enumerated in this section. The final procedure used for each experiment, which will be mentioned in the next section, also includes, the steps performed before and after an experiment to avoid electrical and chemical hazards.

In order to avoid electrical hazards, the power supply was enclosed in a separate metallic box that was grounded. Three on-off security switches were used. The first switch was situated on a power bar on which were plugged all the electrical connections related to the power supply. The second switch was placed on a metallic box containing a fuse and a board that connected the computer's data acquisition card to the power supply. The third switch was placed on the metallic box in which the power supply was enclosed. Before the experiments, warnings were placed on the laboratory doors to indicate potential hazards. After an experiment was performed and after turning off all the switches, both electrodes were electrically joined, starting with the ground electrode, to discharge the capacitor.

In order to avoid chemical hazards, the reactor was always enclosed in a fumehood. An ozone sensor (C-30ZX Ozone sensor, 0.02-0.14 ppm) was used to detect any leaks from the fumehood. Its audio alarm would go on whenever the ozone concentration, in the gas phase outside the fumehood, was above 0.1 ppm (above which there was a health hazard). When this occurred, the emergency button of the fumehood was turned on in order to increase its rate of air uptake. UV protection glasses (Cole Parmer BOUTON Bold professional glasses) were worn during the experiments. An MSA advantage 200 respirator (half mask) and Uvex closed glasses were worn to collect the treated liquids after each experiment.

A fire extinguisher was always nearby and a valve was added to the tubing, in between the reactor and the rotameter, to stop oxygen to flow in case a fire was induced. It was noticed that a flash back arrester should be added to the setup to prevent an eventual fire to get closer, through the tubing, to the oxygen cylinder supply.

3.2. Materials and methods

3.2.1 Chemicals and auxiliary equipment

Potassium indigo trisulfonate (85 % purity grade) and phosphoric acid (85 % wt in water) were obtained from Sigma-Aldrich Canada LTD. A bench pH/Conductivity meter (OAKTON, PC510) was obtained from Cole-Parmer. The probes were calibrated with buffer pH solutions and conductivity calibration solutions obtained from Cole-Parmer.

3.2.2 UV-visible absorption spectroscopy

The optimization of the reactor was performed by monitoring, with a UV-visible spectrophotometer (Varian, Cary 1E UV-visible Spectrophotometer), the absorbance at 600 nm ('Simple Read' option) of an indigo solution. The solution used had a concentration of potassium indigo trisulfonate of 385 ppm and was acidified with 500 ppm v/v of phosphoric acid in distilled water. Acid was used to decrease the pH in order for the indigo molecule to become more soluble and for the amino groups of the molecule to become protonated and therefore, unreactive [64]. The solution had an average pH of 2.6, a conductivity of 1850 μS and an absorbance (relative to air) of 4.6 at 600 nm when measured in quartz vials (Hellma, QS 10.00 mm UV cells, Quartz glass SUPRASIL). Since

the indigo molecule is light sensitive, the aqueous solutions were always stored in the dark.

For all the results obtained in the UV-visible spectrum analysis section (where the 'Scan' option was used), the untreated and treated solutions were diluted, with four times their volumes, in distilled water. The absorbance values, in the spectra obtained for the untreated solutions, would have otherwise been saturated at low wavelengths.

The discoloration efficiency was calculated as the ratio of the difference between the initial absorbance of the solution before treatment and the final absorbance of the treated solution, to the initial absorbance, given as a percentage. All the values were compared at a specific time (15 minutes from the beginning of the experiment) because it was found that absorbance decreased with time. This was probably due to remaining oxidative species having much lower reaction rates.

Two replicates were performed for each experiment. The resulting variances between the replicates are shown on the graphs in the results section. Statistical analysis was used to determine if the changes were significant from one experiment to the other, when one parameter was changed. The "f-test" followed by the "t-test" (standard statistical tests) together can determine if the means of two sets of samples belong to the same population [78]. The "f-test" was first performed on the two sets of data to be compared, to determine if the standard deviations of their populations were equal. According to this result, a type of "t-test" was performed to conclude if the two sets of data belonged to the same population. If they did not, further part of the t-test would conclude which of the values was larger. It could therefore be proved if there were significant changes in

the results when one parameter was changed. The tests were all performed with a confidence interval of 90 %.

It is to be noted that several methods for optimizing the reactor were initially investigated. The problems encountered and the modifications of the method for the reactor optimization are enumerated in Appendix II. The procedure for the experiments using the indigo solution is presented in Appendix III.

3.2.3 Optical emission spectroscopy

A 400-μm optical fiber connected to a UV-visible spectrometer (Ocean Optics USB20000) was used to monitor the optical emission from the discharges across the acrylic material. The fiber was held in contact with the acrylic wall with the help of a positioner (Newport Corporation Fiber Optic Positioner, FPR1-C1A). The positioner was fixed on a machined wood holder as shown in Figure 3.11.

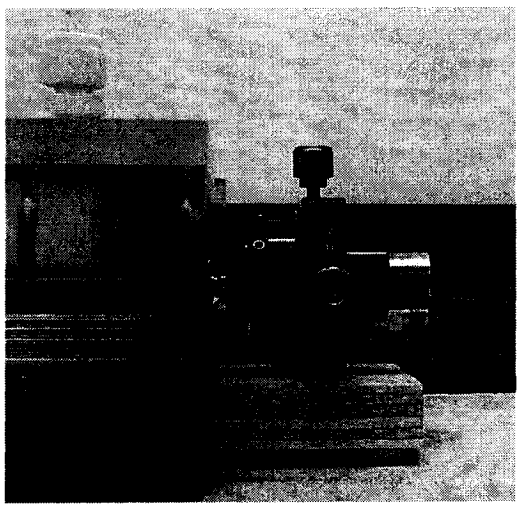

Figure 3.11 Image of the optical fiber setup for optical emission spectroscopy

The OOIBase32 software was used to control the spectrometer, to process the collected data and to save them in a format compatible with MS Excel. The integration time was adjusted to 65000 ms for oxygen and to 16250 ms for air. The emission spectra were collected for two types of solution: indigo solution and tap water. The spectra obtained were identical in both cases. Therefore, the results obtained using the indigo solution only were analyzed.

3.2.4 Visualization of the microdischarges

A PCO 2004, DICAM-PRO charge-coupled device (CCD) camera was used to acquire images of the microdischarges produced in both air and oxygen. The exposure time for the optimum intensity and precision, which are inversely proportional, was of 2 ms. In addition, the exposure time could not be increased to obtain more intensity since the microdischarges are intermittent in nature. Figure 3.12 shows an image of the setup. Band pass optical filters were used in an attempt to map the oxygen (excited atomic oxygen emission at 777 nm, Thor Labs filter) and nitrogen (excited N_2^+ emission at 391 nm, Newport filter) spatial distributions. One of the filters is shown in the picture below. It was located in front of the camera objective, and was fixed on a machined wood holder. The images were collected with the CamWare software and were processed with a MATLAB® program.

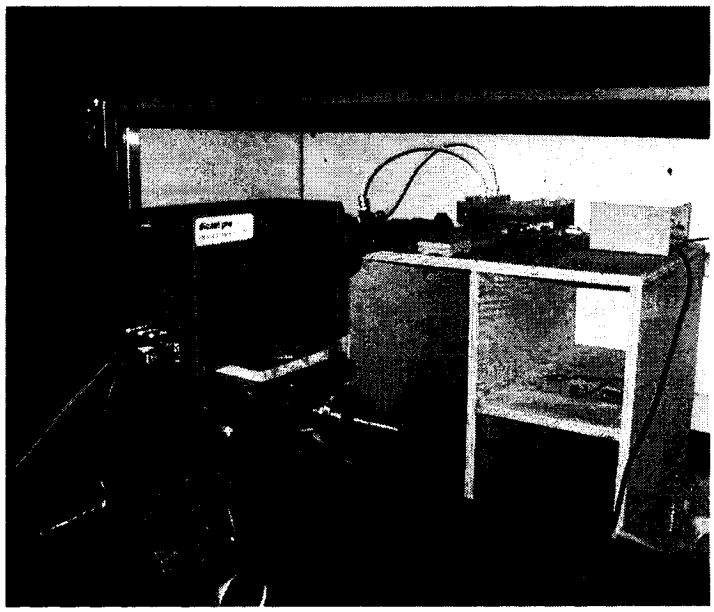

Figure 3.12 Image of the setup used for the visualization of microdischarges

Chapter 4. Results and discussions

4.1. Optimization of the hybrid DBD plasma reactor using UV-visible absorption spectroscopy

Indigo trisulfonic acid dyes water in blue due to its C=C bond. Any active species can break that bond, resulting in the decrease in absorbance of the solution at 600 nm. Details about this molecule were given in the literature review section. The composition of the solution used was given in the materials and methods section. The effects of different parameters on the discoloration efficiency of the dyed solution are examined in this section. The parameters investigated are the solution volume, the gas flow rate, the treatment time and the gas type. A statistical analysis is used to determine if the differences in the results obtained are significant.

4.1.1 Effect of solution volume

The values of the thickness of the liquid layer and discharge gap (gas phase), when there was no discharges, were calculated based on the volume of solution introduced in the reactor and the internal dimensions of the reactor (thickness: 0.655 cm; inside width: 9.9 cm; inside length: 16 cm). With an applied AC voltage of 10 kV, a minimum threshold volume was needed to increase the electric field to its breakdown value, and for the streamers to propagate. When the volume was increased above that minimum value, it would reach a value above which, the upward bulge induced by the streamers would reach the alumina plate. Short-circuiting of the reactor would then be induced.

The effect of the solution volume was investigated while all other

parameters were kept constant (25 cc/min of oxygen flow rate, peak voltage (V_M) of 10 kV, 3 minutes of treatment). It is to be noted that the indigo solution used had been stored for a period of four months. The results obtained were therefore comparable to each other, but were not comparable to the rest of the experiments. After four months of storage, it was found that the solution was much more easily degraded than a fresh solution. When both solutions, with the same initial absorbance, were treated for 3 minutes, the discoloration efficiencies were 58 % and 25 %, respectively for a four months-aged solution and a one week-aged solution. In addition, it was noticed that the treated four months-aged solution would turn yellow after a day while the treated new solution remained blue. Table 4.1 shows the average discoloration efficiency (two replicates) as a function of the solution volume.

Table 4.1 Discoloration efficiency as a function of the solution volume (oxygen flow rate: 25 cc/min, V_M: 10 kV, treatment time: 3 min, 4 months-aged solution)

Solution volume (mL)	Water Thickness (mm)	Discharge Gap (mm)	Discoloration Efficiency (%)
42	2.65	3.90	48.80
45	2.84	3.71	58.00
50	3.15	3.4	53.10

The microdischarges discontinued randomly with a volume of solution of 40 mL introduced in the reactor and the large resulting discharge gap of 4.03 mm. The problem was resolved using volumes equal or larger than 42 mL.

A statistical analysis proved that there was a significant change between the results of discoloration efficiency obtained for volumes of 42 and 45 mL. There was no significant change in the results when using a volume of 50 mL and comparing it to the results obtained with the two other volumes. This was due to

the large variance that was calculated from the discoloration efficiencies obtained for replicates at a volume of 50 mL.

Increasing the volume from 42 to 45 mL decreased the thickness of the discharge gap. This might have allowed for easier streamers propagation. Therefore, a larger number of microdischarges and larger concentrations of oxidative species might have been produced. The agitation at the surface of the solution might have increased slightly, due to a smaller surface tension, resulting in a larger area of contact between the liquid and the gas.

Scattered results (large variance) were obtained using a volume of 50 mL. They were probably due to dead zones promoted in the system when using a bigger volume. The main reason that could explain no further change in discoloration efficiency was that the ratio of the surface in contact with the plasma to the solution volume was decreased [7]. In addition, the production of oxidizing species might have been affected by the smaller gas residence time in the discharge volume when the solution volume was increased.

During experimentation, it was found that it was very difficult to work with a volume of 55 mL, which resulted in a discharge gap of 3.08 mm. The solution, once agitated by the streamers propagation, would reach the alumina dielectric, short-circuiting the reactor.

Finally, a volume of 45 mL was found optimal with this type of solution and was used for the rest of the experiments. It is to be noted that with this volume, the breakdown voltage was 4 kV. The applied voltage used was 10 kV since production of ozone is known to increase, when keeping all the other parameters constant, the larger the voltage [14]. Furthermore, in such type of DBD reactor, the degradation has been found to be faster at larger plasma generation

voltages [8]. The assumption made was that reactive species were generated more abundantly with increasing applied voltages [8].

4.1.2 Effect of gas flow rate

Figure 4.1 illustrates the effect of oxygen flow rate on discoloration efficiency with all other parameters kept constant (volume of solution of 45 mL, V_M of 10 kV, 3 minutes of treatment time, 1 week-aged solution).

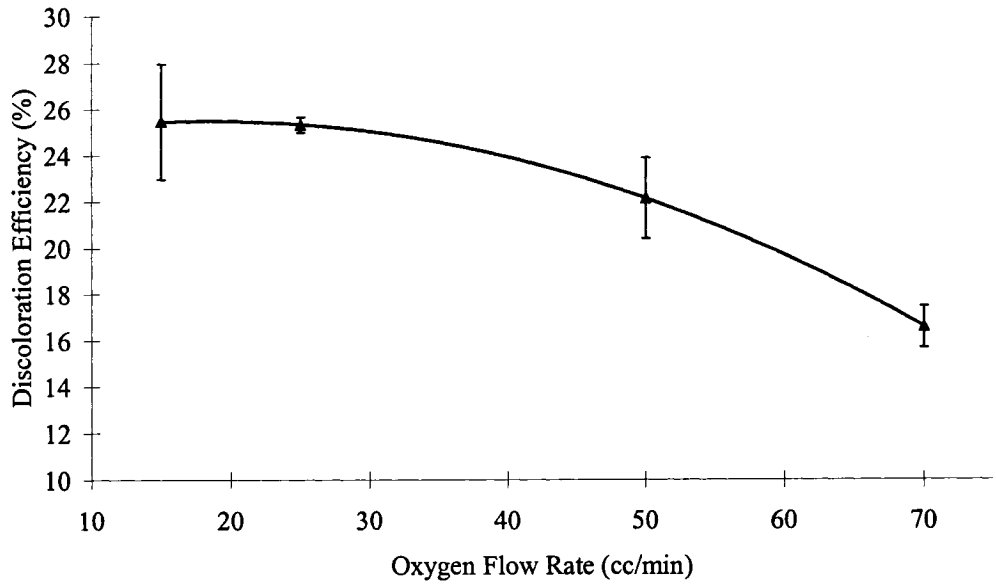

Figure 4.1 Discoloration efficiency as a function of oxygen flow rate (average of 2 replicates)

With an oxygen flow rate of 15 cc/min, brighter and purpler microdischarges were observed. These were probably due to nitrogen infiltration, which was due to the inflow velocity of air into the fumehood where the reactor was enclosed. The values of flow rates tested were therefore not decreased below 15 cc/min. As can be seen in Figure 4.1, scattered results (large variance) were also obtained because nitrogen concentration might have been varying in the reactor from one experiment to another.

However, at the oxygen flow rate 15 cc/min, the gas appeared to be saturated with active species. Statistically, the discoloration efficiency was not significantly different from the one obtained using an oxygen flow rate of 25 cc/min. At this flow rate, nitrogen infiltration was not noticeable and the variance decreased.

The discoloration efficiency decreased significantly when the oxygen flow rate was further increased. It was probably due to the smaller residence time of the gas in the reactor (from 141 seconds at 25 cc/min to 50 seconds at 70 cc/min). The residence time of the gas for a particular experiment was calculated based on the volume of gas present in the reactor, which number is obtained by subtracting the volume of liquid from the internal volume of the entire reactor. Contact time of oxygen with the induced electrostatic field could also be calculated by only taking into account the discharge volume under the alumina plate. This volume was used in the contact time calculations, instead of using the volume under the high voltage electrode, because it was noticed that microdischarges propagated on the whole alumina area, even though the high voltage electrode was smaller. The contact times for flow rates of 25 and 70 cc/min would be, respectively, 104 and 37 seconds. Active and oxidative species, produced in a relatively high oxygen flow rate, probably had fewer chances to be in contact with the solution.

A flow rate of 25 cc/min was therefore used for the rest of the experiments.

4.1.3 Effect of treatment time and gas type

Figure 4.2 illustrates the effect of treatment time on discoloration efficiency, in both oxygen and air, with all other parameters kept constant (volume of solution of 45 mL, gas flow rate of 25 cc/min, V_M of 10 kV, 1 week-aged solution).

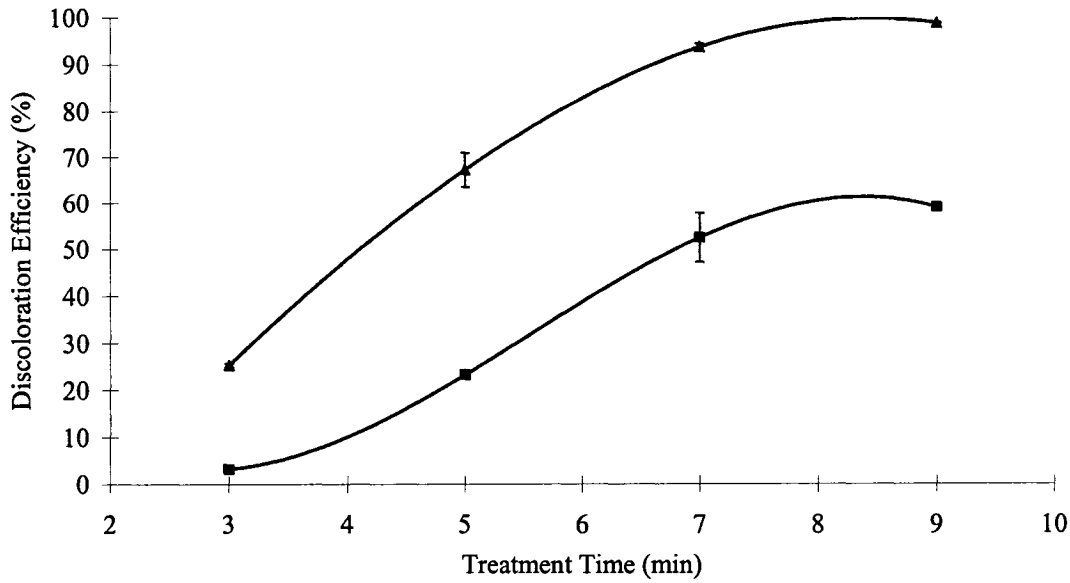

Figure 4.2 Discoloration efficiency as a function of treatment time for oxygen (▲ for average of 2 replicates) and air (■ for average of 2 replicates)

The discoloration efficiency increased with treatment time, both with oxygen and air. This increase was probably due to the greater exposure of the solution to the microdischarges with time, which resulted in higher concentrations of oxidizing species in the solution.

When using oxygen as the feed gas, there were significant statistical differences of discoloration efficiencies at all treatment times. The agitation of the solution induced by the microdischarges, the contact of the solution with high-energy electrons, and the diffusion of active species in the solution resulted, after a treatment time of 9 minutes, in a discoloration efficiency of 99 %. It is to be noted that there was a gradual coloration change that was observed in the reactor with time. The surface exposed to the microdischarges would initially decolorize while the rest of the solution would remain dark blue. The rest of the solution volume would gradually turn yellow, resulting in a green layer between the yellow and the blue regions of the solution. The solution at the bottom of the

reactor (i.e. on the top of the stainless steel electrode) progressively turned green, then yellow. As shown in Figure 4.3, the solution, which was initially dark blue, turned to light yellow after a treatment time of 9 minutes.

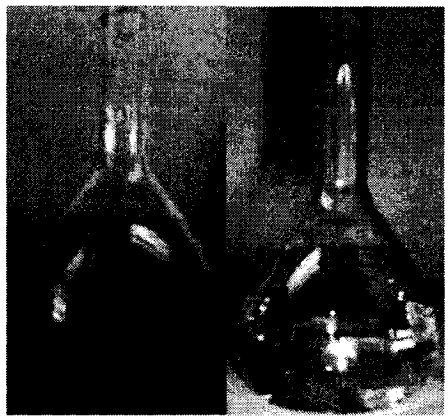

Figure 4.3 Images of an untreated indigo solution and of an indigo solution treated for 9 minutes (volume of solution: 45 mL, oxygen flow rate: 25 cc/min, V_M: 10 kV, 1 week-aged solution)

When air was used, a 59 % discoloration efficiency was observed after 9 minutes, compared to 99 % with oxygen. Furthermore, there were no significant differences in discoloration efficiencies between the treatment times of 7 and 9 minutes. It is known that the ozone generation rate decreases with increasing temperature and humidity [9]. It is possible that the small amount of ozone produced in the air gap, composed of 21 % oxygen, might have been decreased to such an extent that there was no significant change in discoloration efficiency even with two additional minutes of treatment time. It was also suspected that nitrous acid formation reaction might have been competing with the degradation reaction. Indeed, in the presence of N_2, nitrogen monoxide formed in the discharge and led, in the presence of water, to the formation of nitric acid HNO_3 [36]. As shown in reactions (R30) and (R31), oxygen reacts with nitrogen monoxide, formed in the gas phase, to form nitrogen dioxide. The latter reacts with water to form nitrous acid [79]. Nitrous acid, when in solution, is known to

rapidly decompose into nitric acid HNO_3, nitrogen monoxide and water [80].

$2\,NO^{\cdot} + O_2 \rightarrow 2NO_2$ (R30)

$4NO_2 + 2H_2O \rightarrow 4HNO_2 + O_2$ (R31)

In addition, reactions (R6) to (R10), introduced in a previous section, describe in detail nitrate ions formation in the presence of nitrogen, oxygen, and ozone in the gas phase [24]. These ions could contribute to the formation of nitric acid in the solution. Since nitric acid is colorless [81], the absorbance values that were obtained after treating the indigo solution, with air as the feed gas, might have been underestimated. The actual value of the discoloration efficiency obtained was probably less significant than the one obtained with the additional contribution of nitric acid. The solution was treated, with air as the feed gas, for 25 minutes. It turned pale green with brownish traces a few minutes after collection, indicating the presence of NO_2 in the solution [82].

Experiments were performed in the ambient air of the fumehood (without gas flow) with all other parameters kept constant. After a treatment time of 3 minutes, although the residence time was larger, no significant difference in discoloration efficiency was found when compared to the value obtained with a flow rate of air of 25 cc/min.

4.2. Analysis of the UV-visible absorption spectrum

In order to better understand the discoloration process of the indigo solution, absorbance was studied as a function of the wavelength. The optimum parameters were used to treat the solution, with a volume of solution of 45 mL, a peak value for the voltage V_M of 10 kV and an oxygen flow rate of 25 cc/min. As previously mentioned in the Materials and Methods section, the solution initially containing 385 ppm of potassium indigo trisulfonate and 500 ppm v/v of

concentrated phosphoric acid was diluted in distilled water, after treatment, with four times its volume.

Before treatment, the diluted indigo solution had mainly five absorption peaks, respectively at 194 nm, 210 nm, 253 nm, 310 nm, and 600 nm as shown on Figure 4.4. The peak at 600 nm is characteristic of the chromophore in the indigo trisulfonic acid molecule, which structure is shown in Figure 4.4. Any reaction leading to the destruction of this chromophore would lead to the discoloration of the solution.

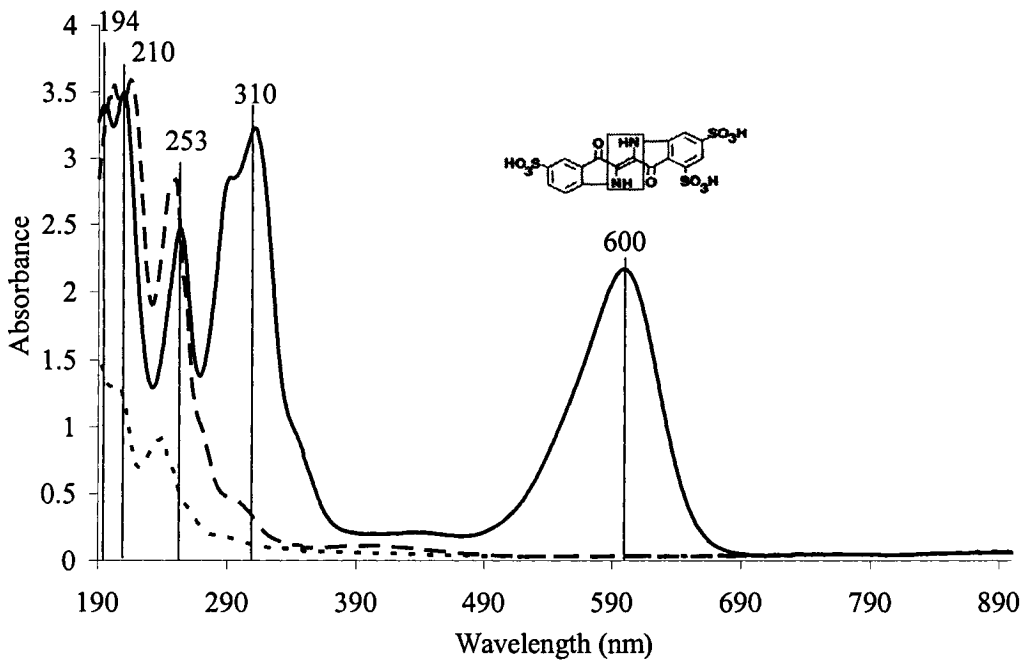

Figure 4.4 UV-visible absorption spectra as a function of treatment time and age of the solution (— before treatment, — — after 9 min of treatment, -- after 9 min of treatment but aged after treatment for 2 days)

The temporal degradation of the indigo molecule is shown in Figure 4.5. The intensity of the characteristic peak of the molecule at 600 nm, along with that of the peak at 310 nm, decreased with treatment time. Starting from very dark blue indigo solutions (absorbance of 4.6 before dilution), the samples turned green and yellow after treatment times of respectively 5 and 9 minutes in oxygen (final

absorbance of 0.046 before dilution). Figure 4.3, showed the difference in coloration between the initial and final solutions.

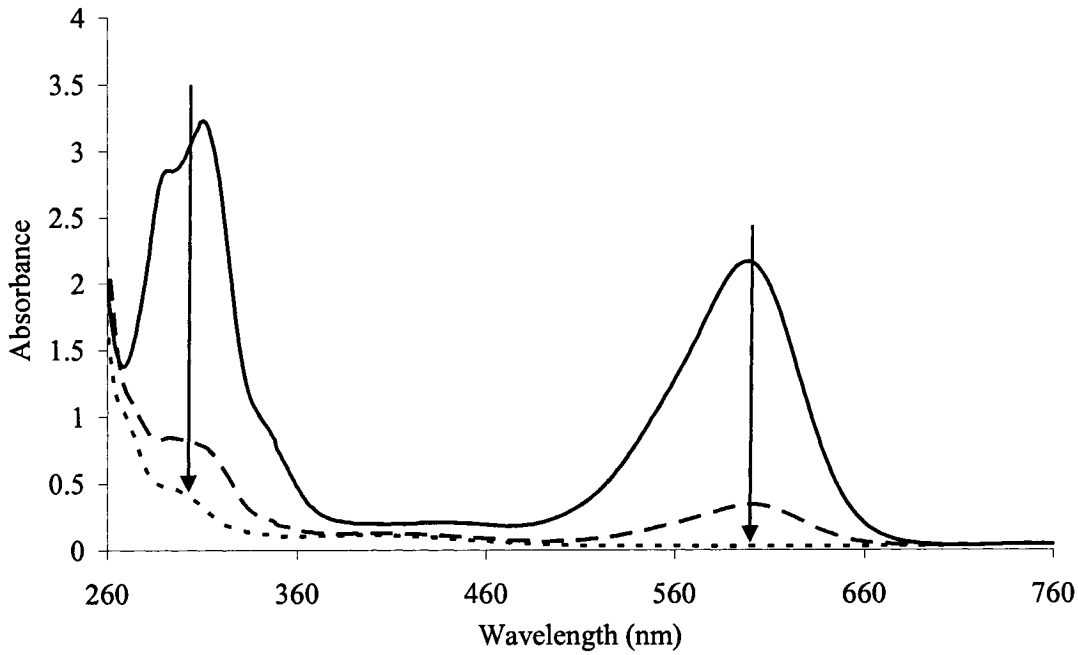

Figure 4.5 UV-visible absorption spectra as a function of treatment time (— before treatment, — — after 5 min of treatment, -- after 9 min of treatment)

If the indigo molecules were being reduced from the oxidized form at 600 nm to the reduced form, a peak would have appeared at 421 nm [83]. Instead, an increase in intensity of the first peaks was observed when comparing, in Figure 4.4, the spectra obtained before and after 9 minutes of treatment. Many reactions leading to the destruction of the central C=C are possible, due to the active species produced in the gas phase and to the contact of the electrical microdischarges with the water surface. For example, it was suggested that the destruction of indigo disulfonate, by ozonolysis, could lead to the production of aldehydes and ketones [84]. Furthermore, ozonolysis of indigo trisulfonic acid molecule at low pH is known to generate two isatin sulfonic acid products shown in Figure 4.6 [65].

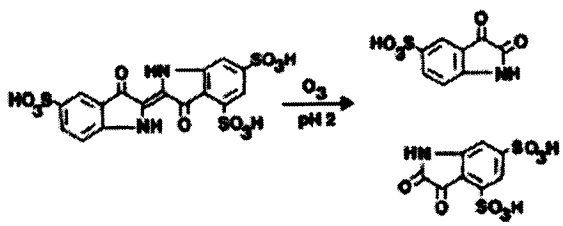

Figure 4.6 Ozonolysis of indigo trisulfonic acid at low pH [65]

The increase in intensity of the first peaks, in Figure 4.4, could be in correlation with the formation of the indigo dye degradation products [66]. The ultraviolet spectrum of isatin-5-sulfonic acid, one of these degradation products, shows a characteristic peak around 248 nm [85]. This may justify the increase in the peak intensity and the hypsochromic shift observed from 253 nm, before treatment, to 250 nm after a treatment time of 9 minutes.

Figure 4.4 shows the spectrum of a sample that was treated for 9 minutes and analyzed after 2 days. The peak assumed to be corresponding to isatin-5-sulfonic acid was drastically reduced. Other oxidative species, with much smaller reaction rates, could have remained in the solution and allowed further degradation.

4.3. Optical emission from the gas phase

Optical emission spectra from the microdischarges were collected. Since the acrylic walls absorb UV radiations, the emission in the UV range could not be characterized. In particular, the exited OH ($A^2\Pi - X^2\Sigma$) transitions at 307 and 309 nm could not be detected [69]. The presence of excited OH radicals is suspected in the gas phase, when using oxygen as the feed gas, since OH radicals can be formed by electronic impact dissociation of the water molecule (mechanism (R5) shown in section 2.2.2) or by reaction of atomic oxygen with a water molecule [21], especially near the gas-liquid interface [36].

Figure 4.7 presents a typical emission spectrum of microdischarges in O_2.

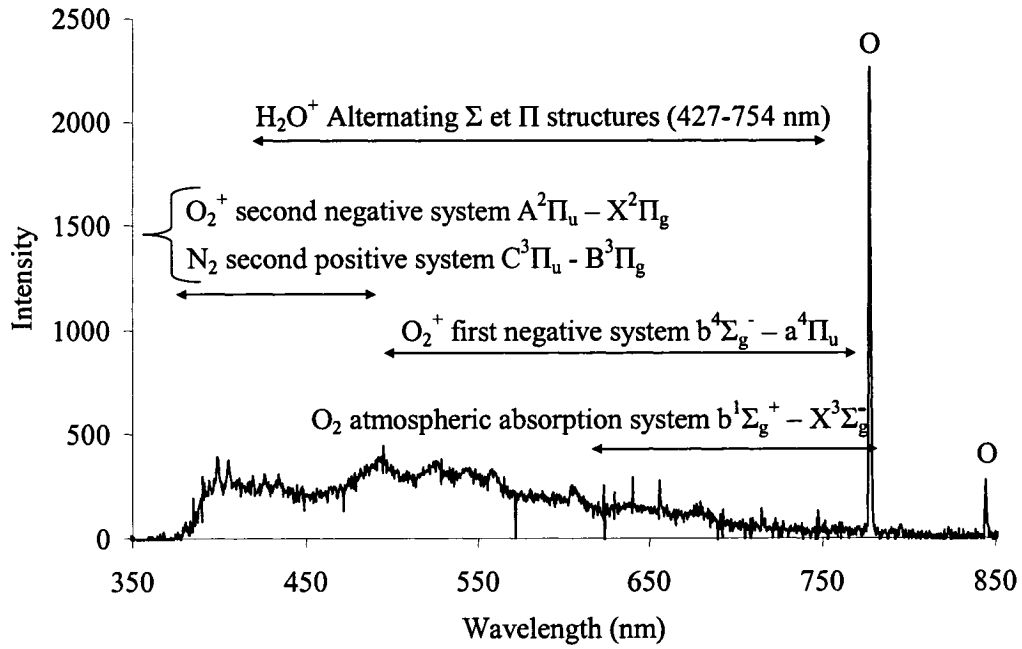

Figure 4.7 Optical emission spectrum of microdischarges in oxygen (volume of solution: 45 mL, oxygen flow rate: 25 cc/min, V_M: 10 kV, 1 week-aged indigo solution, integration time: 65000 ms)

Strong atomic oxygen emission (3^5S-3^5P and 3^3S-3^3P electronic transitions at respectively 777 and 844 nm) is observed in the spectrum [86]. Band systems, with much lower intensities, are also observed. The O_2^+ first and second negative systems ($b^4\Sigma_g^- - a^4\Pi_u$ and $A^2\Pi_u - X^2\Pi_g$ transitions) are observed and are known to occur in high-frequency discharges [87]. The O_2 atmospheric absorption system was suspected ($b^1\Sigma_g^+ - X^3\Pi_g^-$ transition). The alternating Σ and Π structures of exited H_2O^+ were also detected and the N_2 second positive system ($C^3\Pi_u - B^3\Pi_g$ transition) was suspected. The later band system is probably due to air, which could have been infiltrating in the reactor due to the fumehood air uptake. This band is known to occur frequently and is used as an impurity indicator [87].

Figure 4.8 compares the emission spectra obtained in oxygen and air for an integration time of 65000 ms. The same band systems found in oxygen can be

seen except for the almost complete attenuation of the atomic oxygen emission at 777 and 844 nm. Furthermore, studies have been previously conducted to understand why, in similar conditions, molecular nitrogen emission was observed ($C^3\Pi_u$ - $B^3\Pi_g$) while the emission from the oxygen molecule ($b^1\Sigma_g^+ - X^3\Sigma_g^-$) was not, though the excitation energy of the nitrogen molecule is larger than that of the oxygen molecule [88]. The process was simulated (Monte Carlo method) in the same study and it was found that the number of electrons colliding with nitrogen molecule was far more significant than the ones colliding with the oxygen molecule [88].

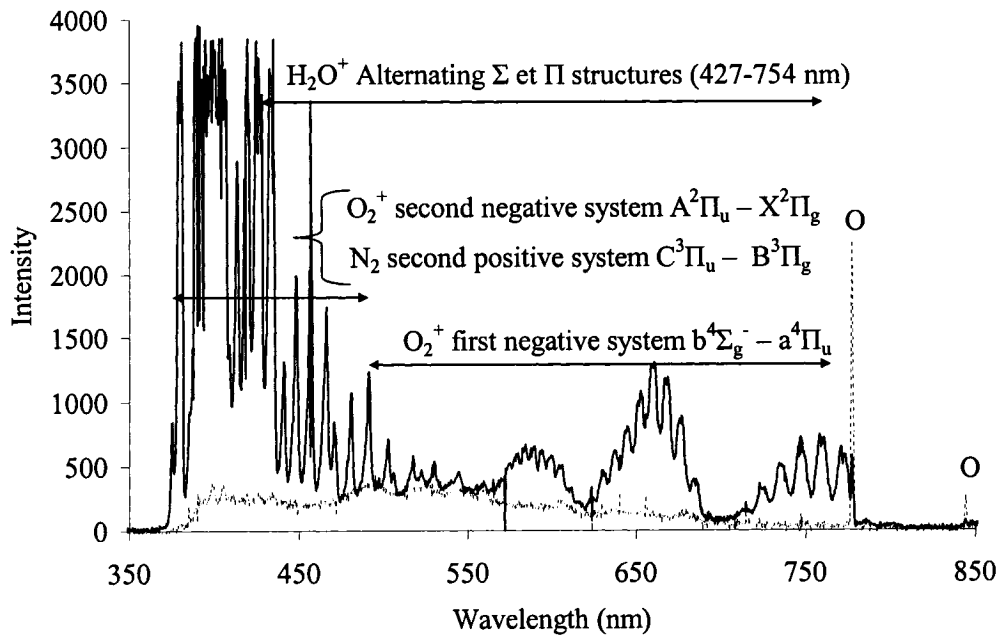

Figure 4.8 Optical emission spectra of the microdischarges in oxygen (---) and air (—) (volume of solution: 45 mL, gas flow rate: 25 cc/min, V_M: 10 kV, 1week-aged indigo solution, integration time: 65000 ms)

An optical emission spectrum of the air microdischarges was obtained with a lower integration time to avoid saturation of the detector. In Figure 4.9, the emission lines observed between the near visible and 500 nm, characterize transitions in the N_2 second positive system ($C^3\Pi_u$ - $B^3\Pi_g$ transition), the N_2

Vegard-Kaplan band ($A^3\Sigma_u^+ - X^1\Sigma_g^+$ transition), and the N_2^+ first negative system ($B^2\Sigma_u^+ - X^2\Sigma_g^+$ transition) [87]. The rest of the spectrum is characterized by bands linked to the N_2 first positive system ($B^3\Pi_g - A^3\Pi_u^+$ transition) [87]. As discussed in the previous section, it was suspected that nitric acid was produced in the liquid phase, because of the probable nitrogen monoxide production in the gas phase. Strong emission lines for exited nitrogen monoxide exist between wavelengths of 200 to 300 nm. Therefore, when using air as the feed gas, these photons could have affected the discoloration efficiencies by breaking chemical bonds by photodissociation [89].

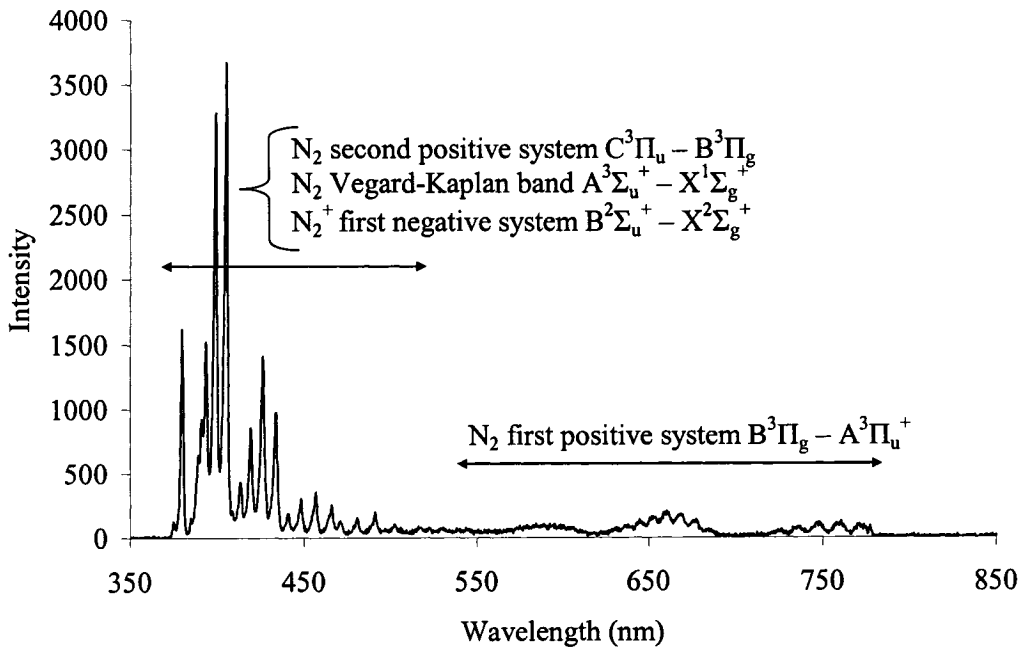

Figure 4.9 Optical emission spectrum of microdischarges in air (volume of solution: 45 mL, air flow rate: 25 cc/min, V_M: 10 kV, 1 week-aged indigo solution, integration time: 16250 ms)

Optical emission spectroscopy mainly showed that atomic oxygen was present in the discharge volume when a feed gas of oxygen was used. Ozone formation could then take place (mechanism (R2) shown in section 2.2.2). Therefore, atomic oxygen, together with ozone and OH radicals, could have

dissolved in the solution, helping in the degradation of the indigo dye. Simultaneously, insignificant amounts of nitrogen might have been infiltrating in the reactor, from the fumehood. Furthermore, the oxygen emission was drastically reduced, in the presence of N_2, when air was used as the feed gas.

Chapter 5. Case study: Sulfamethoxazole (SMX) degradation

5.1. Introduction and literature review

Sulfonamides or sulfa drugs are a class of antibiotics inhibiting bacterial growth. As mentioned in section 2.5, these products have been found in surface water and need to be decomposed before reaching the sewage treatment plant. Figure 5.1 shows the chemical structure of sulfamethoxazole (SMX) or 4-amino-*N*-(5-methyl-3-isoxazolyl), which is a particular type of sulfonamide. As an example, SMX is administered for the treatment of malaria in combination with quinine sulfate and pyrimethamine. It is also used for the treatment of conjunctivitis and, in combination with pyrimethamine, for urinary tract infections.

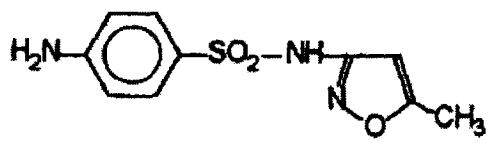

Figure 5.1 Sulfamethoxazole (SMX) structure [90]

It was observed that the main reaction site for oxidation with ozone was the aromatic amino group [71] .Ozone is expected to first attack this site and the other aromatic ramifications, and then perform aromatic breakdown. Research is being conducted on the ozonation of pharmaceutical compounds and their disappearance from the bulk solution after transformation. It was suggested that even if, through oxidation, the pharmaceutical's effects are mainly lost; an analysis of the products obtained should be performed to prove that this was actually the case [72]. It was suggested to analyze the nature of the products obtained after oxidizing pharmaceutical compounds, even if these pharmaceutical compounds are expected to loose their effects [72].

Photochemical decomposition of SMX was performed by irradiating an aqueous solution with a UV lamp [90]. A more elevated degradation rate was obtained for a pH of 3.4 compared to a pH of 7. The degradation products that were found are shown in Figure 5.2 [90].

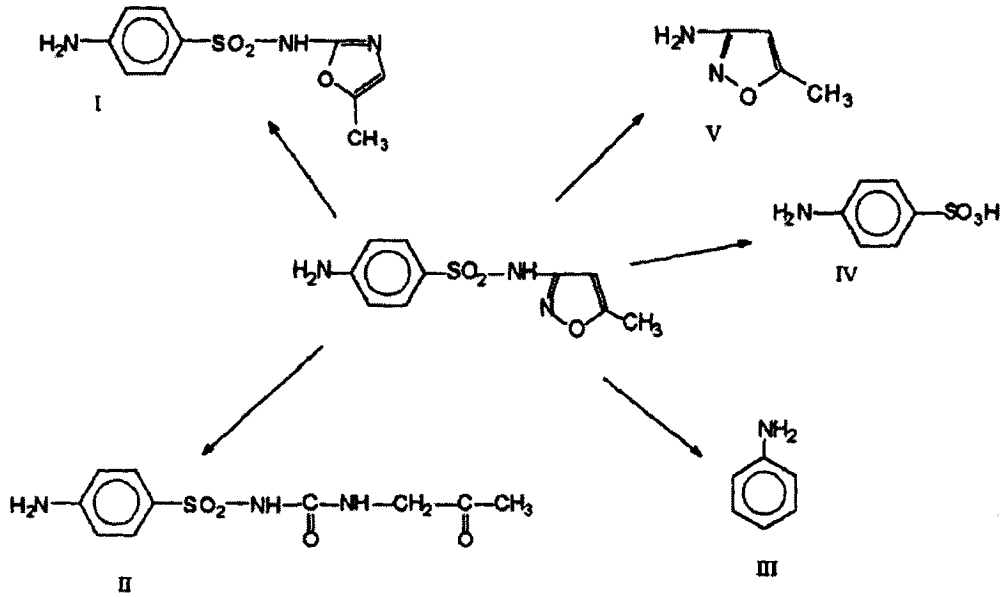

Figure 5.2 Photochemical degradation of SMX [90]

The photoisomerization of SMX led to the structural isomer of SMX, product I (4-amino-n-(5-methyl-2-oxazolyl)benzenesulfonamide) , which was the main degradation product. The cleavage of the $-SO_2$-NH- linkage led to the formation of products IV (sulfanilic acid) and V (3-amino-5-methylisoxazhole). These three products were also identified in a study where SMX was degraded in pure water in a sunlight simulator [91]. The addition of 1 mM H_2O_2 increased the rate of SMX degradation.

Since SMX degraded rapidly by photolysis, degradation was performed with OH radicals generated with a non-photochemical source (dark Fenton reactions) [91]. The degradation products obtained showed that the structural

isomer of SMX (product I) did not form but that the products of sulfonamide bond cleavage were observed (products IV and V) [91]. It was deduced that in addition to direct photolysis, OH radicals might have provided another pathway leading to the production of these compounds. In addition to these products, a hydroxylated analogue to SMX and a hydroxylated version of 3-amino-5-methylisoxazhole, with the OH radical most probably occurring on the isoxazole ring, were identified by mass spectrum analysis [91]. The exact order for the path of formation of these products was not identified.

The aim in this case study was to look at the potential use of the DBD hybrid reactor for SMX degradation. This was performed using a solution, which was being used by collaborators Prof. Viviane Yargeau and Master student Christine Leclair, who decomposed SMX using a conventional ozone degradation process. A pH level of about 8 was used by the collaborators, taking into account that the removal rates of wastewaters, when using an ozonation process, were superior in a basic solution [6]. In such solution, both OH radicals and ozone became the oxidizing agents [6].

5.2. Materials and methods

Aqueous synthetic solutions containing SMX at different concentrations (40 and 80 ppm) were used. SMX (4-Amino-N-(5-methyl-3-isoxazolyl)) was obtained from Sigma-Aldrich Canada, LTD. Potassium phosphate dibasic anhydrous (K_2HPO_4) and sodium acetate trihydrate (SA) were obtained from Fisher Scientific Canada. A buffer solution was needed in order to increase the pH of the SMX aqueous solution. 10 g of potassium phosphate (KH_2PO_4) were diluted in 1 L of deionized water to produce a solution with a pH of 8.9. Finally, the solutions used for the experiments contained sodium acetate (SA) with a

concentration of 3.9892 g/L, a chemical added to enhance the solution's chemical oxygen demand (COD) to 3000 mg/L. COD was increased to simulate contaminated water. KH_2PO_4 buffer solution was added to these solutions to increase the solution's pH to 8. With deionized water, an 80 ppm SMX solution, containing SA and buffer, had a conductivity of 4 mS.

The initial objective was to use HPLC (High Performance Liquid Chromatography) to determine the composition of the plasma-treated solutions. Unexpected malfunctioning of the apparatus delayed the analysis of the samples. Furthermore, it was preferred to measure directly the concentration of SMX remaining after each experiment. That would have been difficult by HPLC, where a group of samples corresponding to several experiments had to be analyzed. A quick and efficient method had to be developed to determine the remaining SMX concentration.

Since the characteristic absorption peak of SMX can be identified by UV spectrometry around 254 nm, a method was developed to obtain SMX concentration as a function of the height of its characteristic peak at the corresponding wavelength. Figure 5.3 presents absorption spectra obtained for solutions containing only SMX, only sodium acetate and buffer, and containing SMX, sodium acetate, and buffer. The peak at 214 nm is related to the SMX molecule since it is observed for a solution containing only SMX. Sodium acetate or buffer also contributes to the increase in intensity of the peak at 214 nm, since the peak is detected even when only the sodium acetate and the buffer are present. In this aqueous mixture, the characteristic peak of SMX is observed at a wavelength of 256 nm.

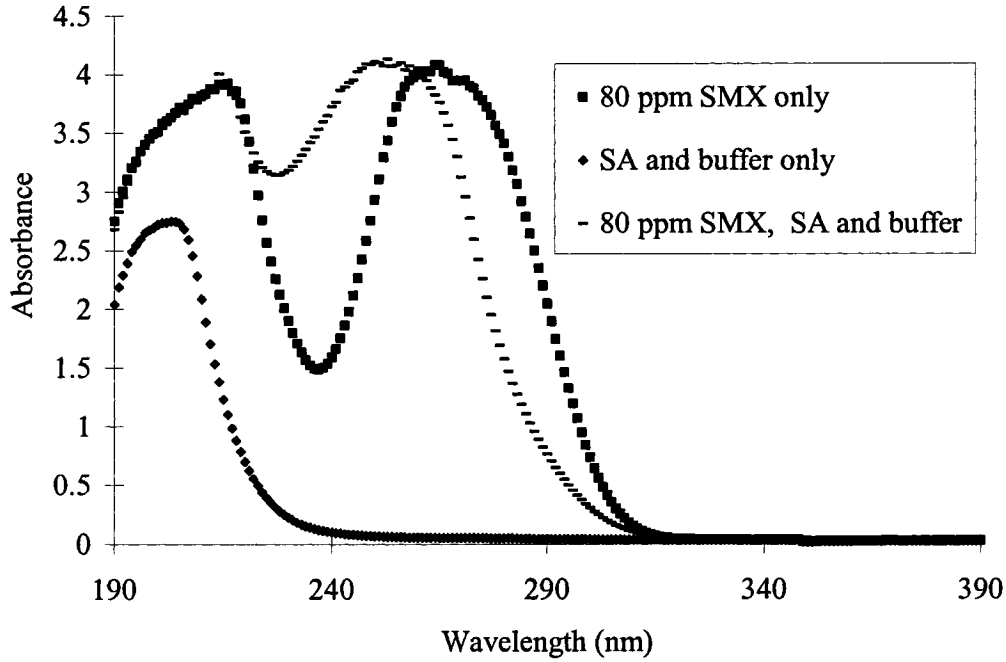

Figure 5.3 UV-visible absorption spectra of solutions containing only SMX, only sodium acetate and buffer, and containing SMX, sodium acetate, and buffer

Solutions with different pH were analyzed (three replicates at each pH) to verify that the peak at 256 nm does not shift due to a change in pH resulting from SMX degradation products. As shown in Figure 5.4, with the same initial sodium acetate and SMX concentrations, varying the buffer concentrations to obtain different pH does not significantly shift the wavelength at which SMX absorption characteristic peak is observed.

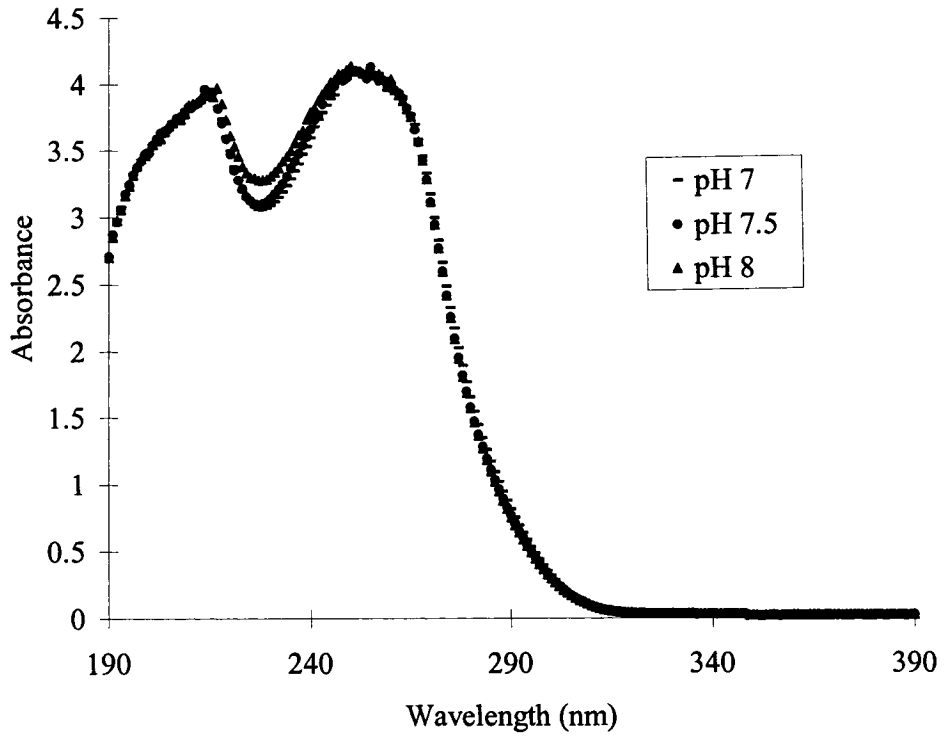

Figure 5.4 UV-visible absorption spectra of solutions at different pH (Initial SMX concentration: 80 ppm, COD of 3000 mg/L)

In order to obtain the calibration curve, solutions with a COD of 3000 mg/L, a pH of 8, and different SMX concentrations were prepared. Figure 5.5 presents the UV-visible absorption spectra of solutions with concentrations of 0, 10, 20, 40, 60 and 80 ppm. As expected, at the wavelength of 256 nm, SMX characteristic peak intensity (absorbance) increases with increased SMX concentration in the solution.

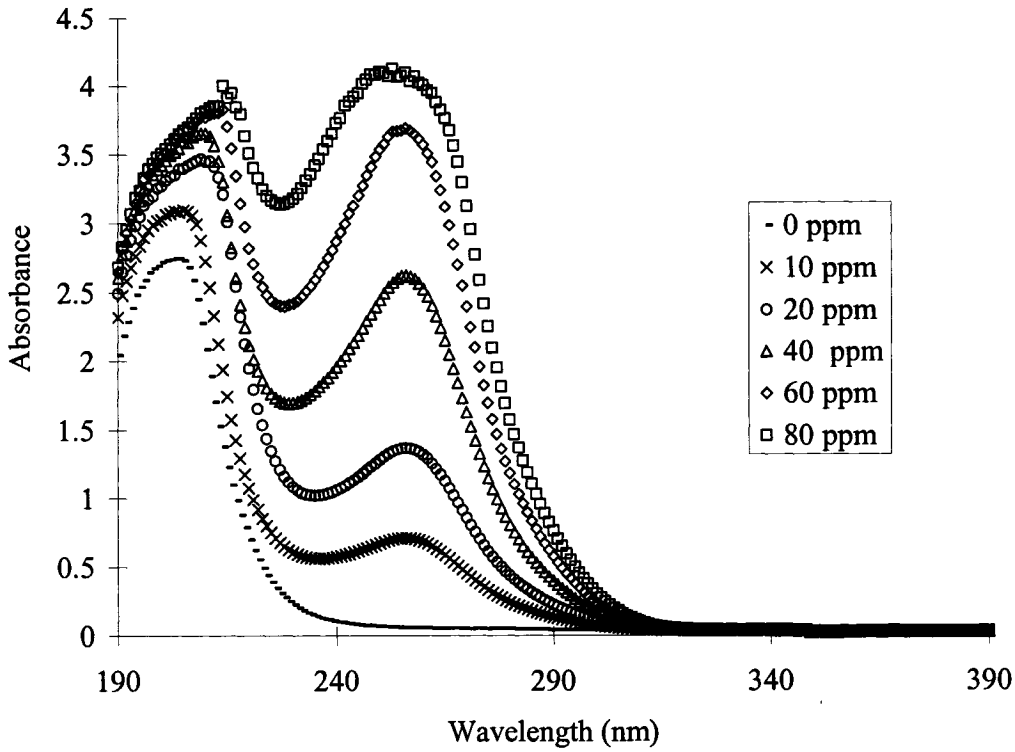

Figure 5.5 UV-visible absorption spectra of SMX solutions of various concentrations (COD of 3000 mg/L and pH of 8)

Figure 5.6 shows the linear fit of the absorbance at 256 nm for SMX for concentrations ranging between 10 ppm and 60 ppm. When the absorbance data point obtained for a concentration of 80 ppm was added to the calibration curve, the fit became non-linear. This was probably because, at such relatively high concentration, the Beer-Lambert law was no longer applicable. This data point was therefore removed.

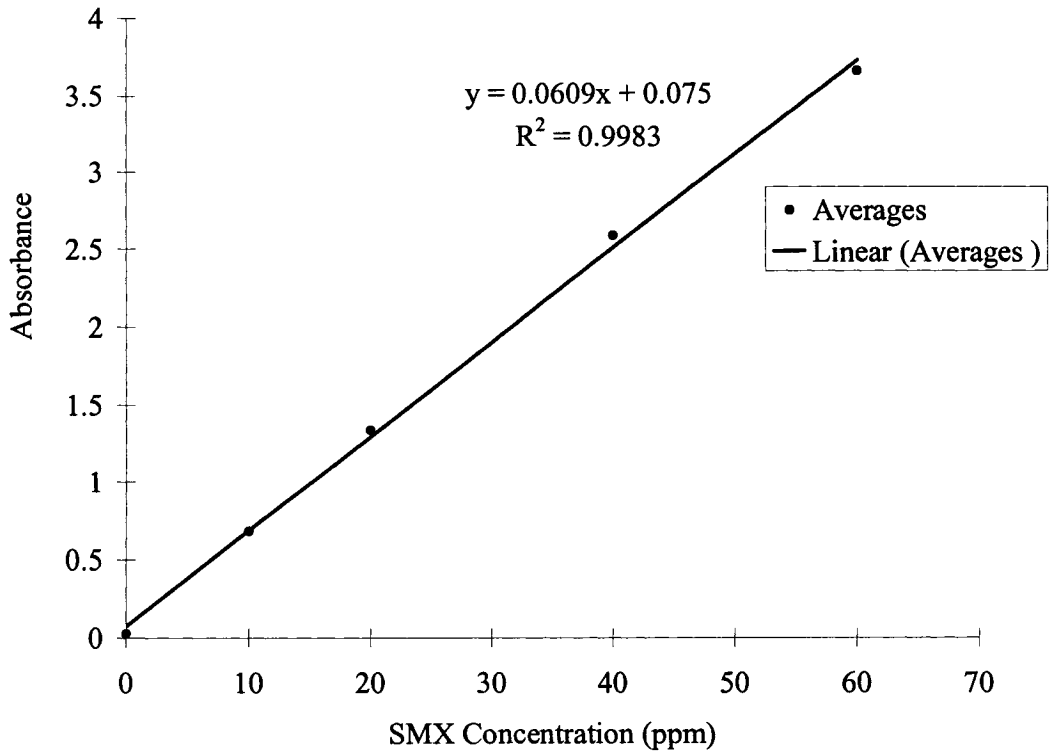

Figure 5.6 Calibration curve of aqueous SMX solutions based on UV absorbance at 256 nm (COD of 3000 mg/L and pH of 8)

A Hewlett Packard 5870 Gas Chromatograph (GC) with an FID detector was used to deduce the boiling point of the compounds present in the solution after treatment. It was also used to detect the presence of methanol, ethanol and phenol by comparing the results obtained to those of tests made on these compounds. The Stabilwax column used was 30 m long with a temperature of 250 °C. The injector was a split/splitless injector suitable for a Hewlett Packard 5890 GC with a split ratio of 10 to 1. The oven temperature was initially 80 °C (for 2 minutes) and was ramped up at a rate of 20 °C/min to 200 °C. A 0.5 μL glass syringe was used with a GC injection port septa with the following properties: 11 mm SOL SEPT 508D-8896 Hewlett Packard. He, Air, and H_2 were used throughout the procedure.

Trace GC 2000 Gas Chromatograph (Thermo) and GCQ/Polaris MS (Thermo) Mass Spectrometer were used to determine the compounds remaining in the solution after treatment. Liquid-liquid extractions in chloroform had to be performed first. The RTX-5MS column used had the following properties: length of 30 m, film thickness of 0.25 μm, and internal diameter of 0.25 mm. A 1 μL glass syringe was used with a Thermolite septa. A constant flow of 1 mL/min was used for the helium carrier gas. First, an oven temperature of 120 °C was maintained for three minutes, and then the temperature was ramped up at a rate of 20 °C/min to 275 °C, at which value it was held for 10 minutes. The temperature was finally ramped up at a rate of 5 °C/min to 300 °C and was maintained at this level for 5 minutes. The X-Calibur software was used to process the data obtained.

The experimental procedure used before every experiment with the SMX solution was similar to the one used with the indigo solutions. In addition, 30 mL of solution was initially introduced in the reactor, which was purged at an air flow rate of 600 cc/min for 2 hours before adding the remaining solution volume. This step was added because when the solution containing SMX was introduced in the reactor, some of it would get in contact with the alumina plate. It was noticed that it did not dry as fast as the indigo solution; some drops hanging on the dielectric would not dry out. Therefore, if the reactor was not purged, drops of SMX solution would remain on the alumina plate and orange microdischarges (flames) would form mainly on those spots. They would then expand and burn the walls of the reactor made of acrylic, inducing a fire that could only be extinguished when the power was shut down and the oxygen supply stopped. The fire was probably due to the fast degradation of SMX, on the surface of the alumina, leading to inflammable products in contact with the plasma. Due to this problem, each data point presented in this case study corresponds to the result obtained with one

experiment.

Each sample was mixed for 1 minute directly after the experiment. The UV-visible absorption spectrum measurements were taken after 15 and 30 minutes. The untreated solutions retained their properties when stored in the dark (i.e. the UV-visible absorption spectra remained the same with time). Furthermore, the SMX concentration did not decrease with time as was observed with the indigo solutions. The values of the absorbance at 256 nm, after treatment, remained stable for several hours. The UV-visible absorption spectra were more or less the same after 3 days.

5.3. Results

As in any type of wastewater treatment unit, the optimal parameters always have to be investigated for the specific type of solution that is processed. The solutions composed of the indigo dye allowed a preliminary study of the reactor optimal parameters. Only oxygen feed gas was used to process SMX aqueous solutions because when degrading indigo dye using air, the efficiency was inferior. Furthermore, nitric acid formed in the liquid phase, with the acidified indigo solution, and when using air as the fed gas. This was probably due to the nitrogen monoxide that was produced in the gas phase. Since it was found that, the experiments with aqueous SMX were dangerous to perform, the optimum flow rate of 25 cc/min of oxygen, used for the degradation of the indigo dye, was also used for the limited number of experiments involving SMX degradation.

Aqueous solutions with initial SMX concentrations of either 40 or 80 ppm were plasma-treated. The optimum volume was again investigated. A volume of 48 mL, corresponding to a discharge gap of 3.52 mm, was necessary for this type of solution to avoid encountering the problems mentioned when working with

small volumes of indigo solution (section 4.1.1). A peak value for the voltage V_M of 10 kV and an oxygen flow rate of 25 cc/min were used for all experiments. Special precautions were considered since the solution containing SMX was more flammable than the one containing the indigo dye.

Figure 5.7 presents the UV-visible absorption spectra obtained when solutions, initially containing a SMX concentration of 80 ppm, were plasma-treated for different treatment times. Table 5.1 summarizes the corresponding concentrations of remaining SMX and percent degradation obtained as a function of the treatment time. The percent degradation was calculated as the ratio of the difference between the initial and final concentrations, over the initial concentration, transformed to a percentage.

Figure 5.7 illustrates how the UV absorbance at 256 nm decreases with increasing treatment time. However, the base of the peak at 256 nm is wider after treatment, probably due to the presence of degradation products. It is important to note that some degradation products might be absorbing light at the same wavelength. Consequently, with the results of absorbance obtained at 256 nm, only the minimum amount of SMX degraded can be determined. After 9 minutes of treatment, and as shown in Table 5.1, at least 68.9 % of the aqueous SMX is degraded and the pH of the solution decreases from 8 to 7.3. As expected, the results seem very specific to the solution being degraded; the aqueous indigo dye, with a much larger initial concentration of 385 ppm, was mostly degraded after 9 minutes of treatment.

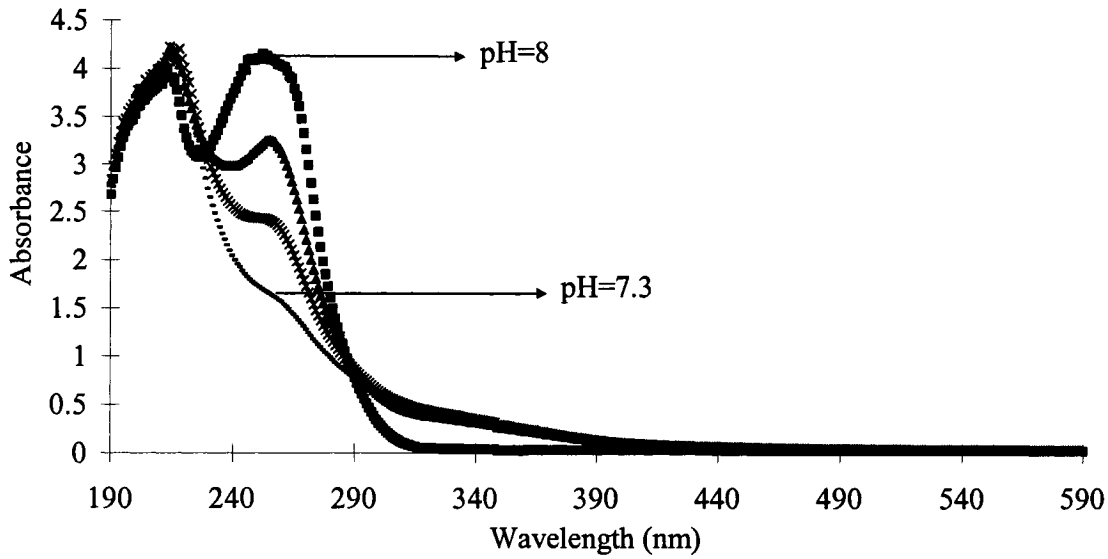

Figure 5.7 UV-visible absorption spectra of plasma-treated SMX solutions for increasing treatment times (■ for 0 min, ▲ for 3 min, x for 5 min, - for 9 min). (Initial SMX concentration: 80 ppm, volume of solution: 48 mL, oxygen flow rate: 25 cc/min, V_M: 10 kV)

Table 5.1 Concentration of remaining SMX and percent degradation as a function of treatment time (Initial SMX concentration: 80 ppm, volume of solution: 48 mL, oxygen flow rate: 25 cc/min, V_M: 10 kV)

Treatment Time (min)	Remaining SMX Concentration (ppm)	% Degradation
0	80	0
3	51.54	35.57
5	37.68	52.89
9	24.91	68.86

Figure 5.8 presents the UV-visible absorption spectra obtained when a solution initially containing a SMX concentration of 40 ppm was plasma-treated for different treatment times. Table 5.2 summarizes the corresponding concentration of remaining SMX, and percent degradation obtained as a function of treatment time. The same conclusions that were deduced from the

observations made for the plasma-treated solutions with initial concentrations of 80 ppm are applicable.

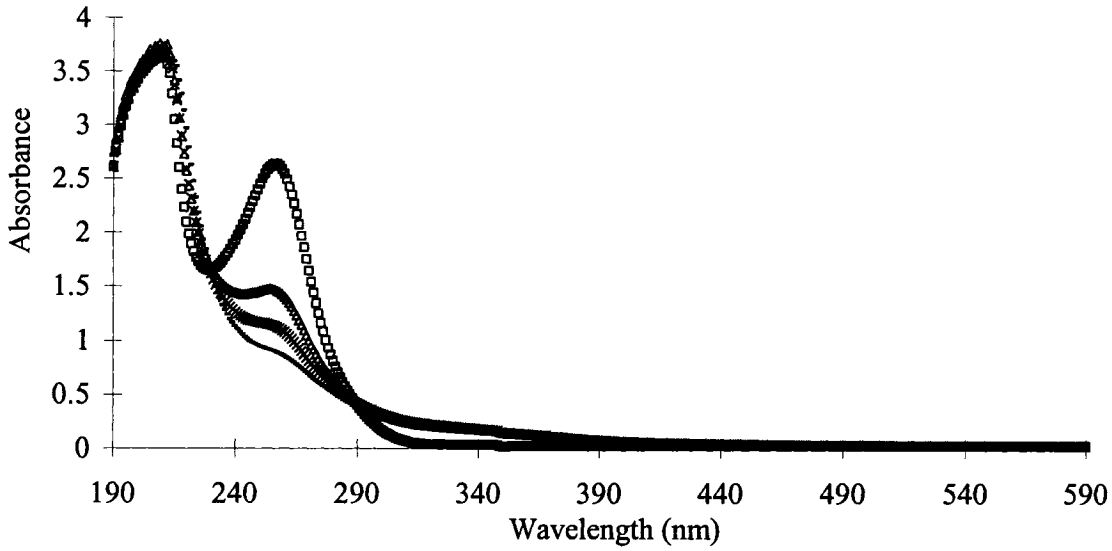

Figure 5.8 UV-visible absorption spectra of plasma-treated SMX solutions for increasing treatment time (□ for 0 min, Δ for 3 min, x for 5 min, - for 7 min). (Initial SMX concentration: 40 ppm, volume of solution: 48 mL, oxygen flow rate: 25 cc/min, V_M: 10 kV)

Table 5.2 Concentration of remaining SMX and percent degradation as a function of treatment time (Initial SMX concentration: 40 ppm, volume of solution: 48 mL, oxygen flow rate: 25 cc/min, V_M: 10 kV)

Treatment Time (min)	Remaining SMX Concentration (ppm)	% Degradation
0	40	0
3	22.35	44.13
5	16.96	57.59
7	13.00	67.49

Figure 5.9 summarizes the results obtained for both initial concentrations. After 7 minutes of treatment time, at least 67 % of the solution, with the initial concentration of SMX of 40 ppm, was degraded. When comparing the results

obtained using the two initial concentrations, it was noticed that this result was similar to the one obtained when the SMX solution with the initial concentration of 80 ppm was treated for 9 minutes. After 3 minutes of treatment, at least 44 % and 35 % degradation were obtained for the solutions of initial SMX concentrations of respectively 40 and 80 ppm. Indeed, at each treatment time, the percent degradation, for the solution with the 40 ppm initial SMX concentration, was superior to that obtained for the solution having an initial SMX concentration of 80 ppm. Kinetic studies are presented in the next section in an attempt to understand which mechanisms might be affecting the degradation results.

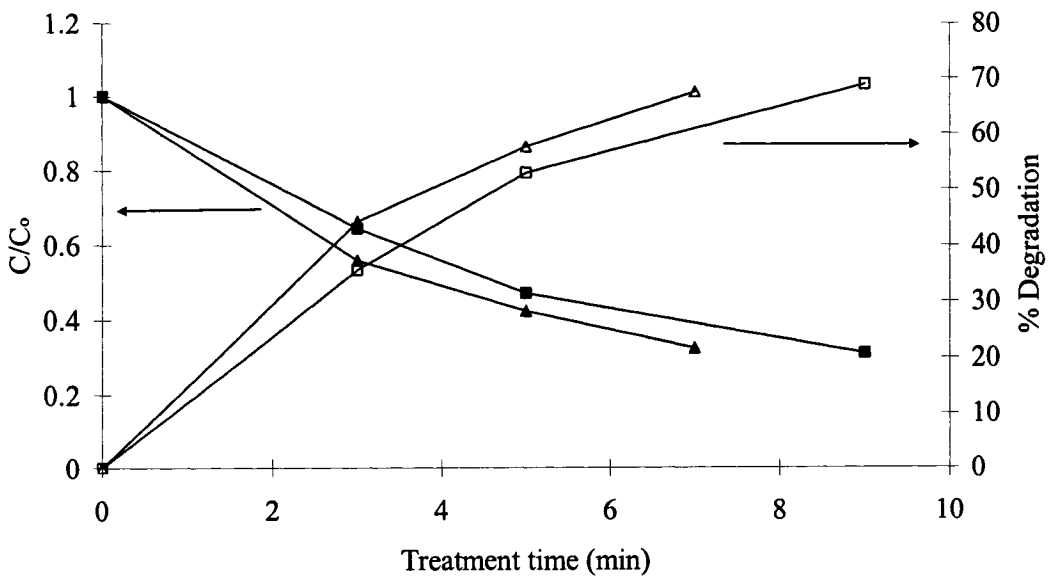

Figure 5.9 Ratio of remaining SMX concentration to initial SMX concentration and percentage degradation as a function of treatment time (Δ and ▲ for initial concentration of 40 ppm, □ and ■ for initial concentration of 80 ppm) (Volume of solution: 48 mL, oxygen flow rate: 25 cc/min, V_M: 10 kV)

5.4. Kinetic study

As previously mentioned, each data point presented in this case study corresponds to the result obtained with one experiment. Some features of this reactor should be changed before generating more replicates, which could lead to

more precise kinetic studies for the decomposition of SMX. These will be discussed in the last section of the thesis. For now, only hypotheses can be made to try to understand the mechanism of SMX degradation with the DBD hybrid reactor.

The responses of first order and second order kinetic models were fitted to the data. If the reaction kinetics is first order, a plot of $\ln(C_{smx}/C_{smx0})$ versus time should give a straight line passing by zero. If the reaction kinetics is second order, a plot of $1/C_{smx}$ versus time should give a straight line with $1/C_{smx0}$ as the intercept (Assuming C_{smx} to be the remaining SMX concentration and C_{smx0}, the initial SMX concentration). With the number of points available and no replicates, both models seemed to fit. When aqueous SMX was degraded by ozonation by collaborators, most of the kinetic models obtained were first order. It was therefore decided to investigate the results at the two different concentrations assuming a pseudo-first order kinetic model, which is explained below [92].

Symbols:

r_{smx} : Rate of consumption of SMX [ppm min^{-1}]

C_{smx}: Concentration of SMX [ppm]

C_{ox}: Concentration of oxidants (O_3, $O^{\bullet}$, $^{\bullet}OH$ ...) [ppm]

t: Time [min]

k: Rate constant [ppm^{-1} min^{-1}]

$$r_{smx} = \frac{dC_{smx}}{dt} = -kC_{ox}C_{smx} \qquad (7)$$

Assuming that the oxidants concentration is constant and is much greater than the concentration of SMX, it can be incorporated in the rate constant as following:

$$k' = kC_{ox} \qquad (8)$$

Combining equations (7) and (8), the following equation is obtained:

$$r_{smx} = \frac{dC_{smx}}{dt} = -k'C_{smx} \qquad (9)$$

With k' is the new rate constant in min^{-1}

Integrating equation (9) as shown below, with C_{smx0} the initial SMX concentration, equation (10) is obtained:

$$\int_{C_{smx0}}^{C_{smx}} \frac{dC_{smx}}{C_{smx}} = -\int_{0}^{t} k'dt$$

$$-\ln(\frac{C_{smx}}{C_{smx0}}) = k't \qquad (10)$$

Figure 5.10 presents the fit of the pseudo first-order plots for SMX kinetics. The first observation that can be made is that the rate constants were not the same for two different initial concentrations of SMX. A smaller rate constant value is observed when using a larger initial concentration. The rate constant values found are 0.1675 min^{-1} and 0.1355 min^{-1}, for initial SMX concentrations of 40 and 80 ppm, respectively. Assuming that this difference is not due to experimental errors, it would mean that the SMX is less quickly degraded when larger initial SMX concentrations are used. This observation was made in the last section when the degradation results for the solutions with the two initial SMX concentrations were compared. At higher initial SMX concentration, the degradation could be slower due to a lack of additional oxidants. Assuming that the entire amount of oxidants, produced in the gas phase and reaching the solution surface, is immediately consumed for both initial concentrations then, if no additional oxidants reached the solution surface to degrade higher concentrations of SMX, the rate constant would decrease. The lack of oxidants in the liquid could occur either because the oxidants are produced at a slower rate than they are consumed or because the limiting step is the diffusion of the oxidative species

from the gas to the liquid phase. A limiting step could also be the slow diffusion of oxidative species inside the solution. It is to be reminded how gradual coloration changes with time were observed in the reactor when the aqueous indigo dye was degraded (section 4.1.3).

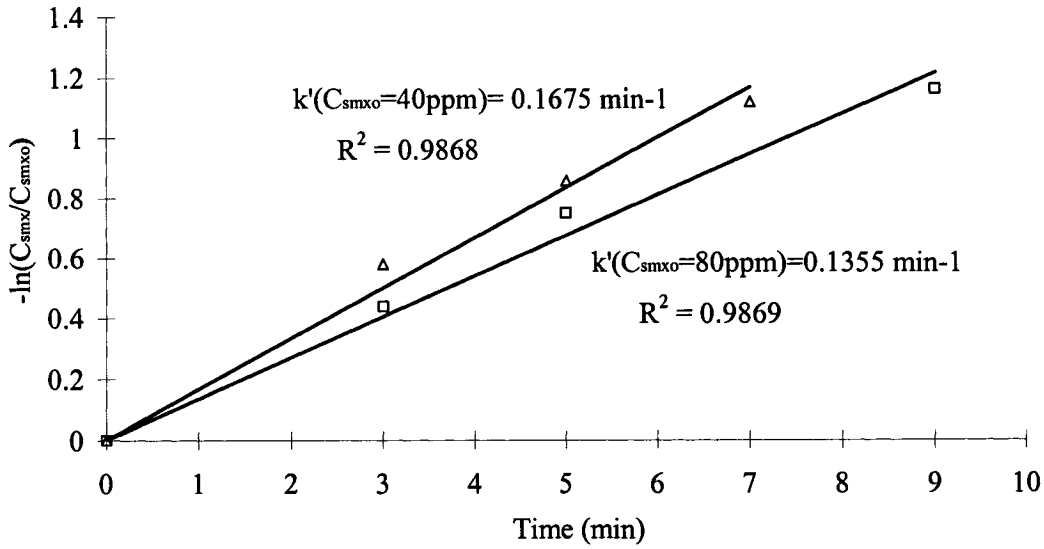

Figure 5.10 Pseudo first-order plots for SMX kinetics (Δ for initial concentration of SMX of 40 ppm, □ for initial concentration of SMX of 80 ppm)

It appears that pseudo-first order kinetics is valid but that the rate constants depend on the initial SMX concentrations. More experiments should be performed at lower SMX concentrations to determine at what point the rate constant becomes dependent on the initial SMX concentration due to a lack of additional oxidants.

Furthermore, it is certain that the concentrations of the different oxidative species did not remain constant since the humidity increases in the DBD reactor with the processing time. In this semi-batch reactor, which is not in equilibrium, ozone production probably decreases with time due to the increase in humidity and temperature. In the presence of the water vapor, the concentrations of H and OH radicals in the gas phase also increase by dissociation of the water molecule by electronic collisions [93]. All the possible oxidative species that can degrade

SMX should be investigated. The concentrations of oxidative species in the gas and liquid phases should be monitored, while degrading SMX. The correct mechanism of degradation of the SMX molecule could then be elaborated. Another kinetic model could therefore be considered, introducing all the different oxidant types and concentrations. The reactor should also have an optical access through a quartz view port so that the UV emission from the microdischarges could be measured in order to determine if photodegradation can be a possible mechanism for degrading SMX. Suggestions will be cited in the conclusion in order to enhance the diffusion of the oxidative species in the solution and obtain a more efficient degradation.

Researchers have investigated the degradation of nitrophenols in aqueous solution by plasma using submersed glow discharge electrolysis [94]. It was found that a pseudo-first order model also fitted the data well. The dependence of the rate constant on the initial concentration of nitrophenols was also noticed. In that case, the rate constant increased with an increase of the initial concentration. The dependence was justified by expressing the degradation rate by Langmuir-Hinshelwood kinetics [94]. Furthermore, different types of nitrophenols disappeared at different rate constants [94].

The degradation pattern observed with the DBD used in this project was similar to the one observed when a similar planar-type reactor with a mid-frequency excitation (30 kHz) and with voltages ranging between 11 and 14 kV was used to degrade EDTA [8]. For an applied voltage of 12 kV, and after a treatment time of 20 minutes, the ratio of TOC to initial TOC was 0.885 for the 0.2 wt. % EDTA solution but remained around 1 for the 2 wt. % EDTA solution. Degradation kinetics might have also been dependent on the initial concentration of EDTA, with a greater degradation at lower concentrations of EDTA. The same

researchers mentioned that their next studies would concentrate on plasma diagnostics and the identification of by-products as organic forms and gas phases to reveal the decomposition kinetics and mechanism of EDTA by DBD [8].

5.5. GC analysis

A gas chromatography (GC) analysis was carried to investigate the nature of the degradation products obtained. With GC, a peak at a retention time of approximately 5 minutes was observed with the treated samples. Usually, peaks are obtained on GC depending on the boiling points of the processed compounds. The heights of the peaks are proportional to the corresponding concentration of each compound. A boiling point around approximately 140 °C was calculated based on the retention time of 5 minutes. When the treated samples were analyzed, the heights of the peak at a retention time of 5 minutes, varied according to the concentration of SMX initially in each sample. The larger the initial SMX concentration, the greater was the height of the peak. Also, for the same initial concentration, the height of the peak was inferior when the sample was treated for lesser time. These observations imply that larger concentrations of this compound were detected when larger amounts of SMX were degraded. It was therefore concluded that this peak was characteristic of a product of degradation of SMX.

Methanol, ethanol and phenol were detected in samples treated by ozone, by Master student Christine Leclair, and quenched with sodium sulfite. The samples that were analyzed did not show the characteristic peak at a retention time of about 5 minutes. Furthermore, none of the characteristic peaks corresponding to methanol, ethanol or phenol was detected in the plasma-treated samples. Therefore, a different mechanism of degradation might have arised with the hybrid DBD plasma reactor. Aniline, with a boiling point of 184 °C, is a

product that is obtained by the photodegradation of SMX [90]. The boiling point deduced for the degradation compound, in the plasma-treated samples, is of 140 °C. If photodegradation contributed to the degradation of SMX in the DBD reactor, it was suspected that a product with a similar structure to that of aniline but with a lower boiling point (affected by the medium), could have been produced.

GC analysis was carried again after one month, on samples left in the dark, in order to determine if the same peaks could still be observed. If it was the case, then further diagnostic of the samples by GC-MS could determine the nature of the degradation compounds. However, after a month, the GC analysis of the samples, which were extracted with chloroform to be processed later by GC-MS, did not show the peak that had been found at a retention time of 5 minutes. This component probably decomposed or recombined with other degradation products. If it recombined, the boiling point would be larger than the temperatures that the GC could detect (up to 200 °C). GC-MS was used to identify the degradation compounds left in the sample that initially had a concentration of 80 ppm of SMX and that had been treated for 5 minutes. The spectrum of relative abundance versus retention time is presented in Figure 5.11.

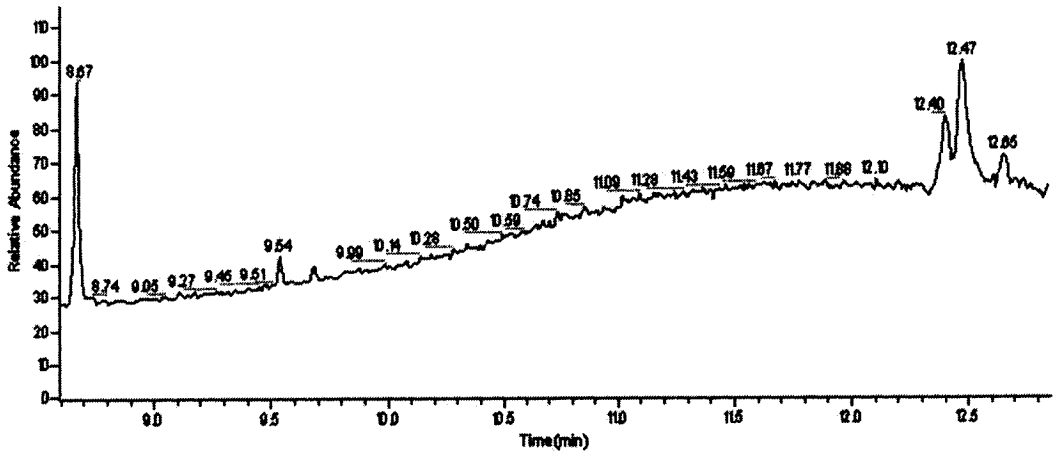

Figure 5.11 GC-MS spectrum of relative abundance versus retention time

Two main compounds were identified, at retention times of 8.67 minutes and 12.4 minutes. The mass-to-charge ratios obtained at the two retention times were compared to the GC-MS spectra library. The most probable structures were N-propyl benzamide at the retention time of 8.67 minutes and 3,5-di-tert-butyl-4-hydroxybenzaldehyde at the retention time of 12.4 minutes. The respective structures of these two compounds are shown in Figure 5.12.

Figure 5.12 Chemical structures of N-propyl benzamide (left) and 3,5-di-tert-butyl-4- hydroxybenzaldehyde (right)

Compounds having similar chemical structures to the benzaldehyde were also suspected because several peaks, close to each other, were detected in the graph of relative abundance versus time (Figure 5.11) near the retention time of 12.4 minutes. After one month, the degraded products of SMX must have degraded even more and/or recombined among each other and with impurities and compounds (especially SA) initially present in the solution to produce such benzamide and benzaldehyde structures.

In conclusion, in a normal situation where it is safer to run more experiments and obtain more replicates, the samples should be analyzed by GC and GC-MS directly after the experiments are performed. GC should first be performed on both the water phase and the chloroform phase because if the liquid-liquid extraction is poor, the products might have stayed in the water phase.

In general, it is very important to note that, even if the degradation of the pharmaceutical compounds is achieved, the toxicity of the degraded products

should be looked at, along with the possible recombined products. These might be more dangerous than the initial products (Aniline for example is cancerigenic and mutagenic [95]). Complete degradation of both the pharmaceutical compounds and their degradation products should be verified, so that no (possibly dangerous) recombination products are allowed to form with time.

5.6. Comparison with ozonation

The collaborators carried ozonation experiments to degrade aqueous SMX. The setup used consisted of a cylindrical container of 6 cm of internal diameter with a height of 60 cm. Ozone was produced by an Ozomax ozone generator (OZO 4 VTT) and was bubbled with a diffusion plate made of porous stainless steel (holes of 2 μm). As previously mentioned, different degradation products were obtained when comparing the peaks obtained by GC for the ozonated solutions and the plasma-treated solutions. Methanol, ethanol and phenol were detected when ozonation was used and a characteristic peak close to a retention time of about 5 minutes was detected when the plasma treatment was used. Furthermore, after 9 minutes of treatment by plasma, at least 68.9 % of the aqueous SMX (initial concentration of 80 ppm) was degraded and the pH of the solution decreased from 8 to 7.3. When completely degraded by ozonation, the pH of the samples would only go down to a pH of 7.5. That could also be explained by the fact that the degradation products obtained by the plasma treatment are different from those obtained by ozonation. These observations suggest different mechanisms of degradation for the two approaches. Further studies should be performed to determine if photodegradation might be one of the additional features that the DBD reactor offers.

Most of the kinetic models obtained with ozonation are pseudo-first order.

For the plasma-treated samples, the rate constants changed as a function of the initial SMX concentration. The maximum power consumed by the ozonator was 550 W, the volume treated was of 500 mL and a maximum of 1 minute of treatment time was needed to degrade most of the SMX initially present in solution. The DBD plasma reactor consumed a maximum of 100 W, the volume treated was of 48 mL and a treatment time of 7 minutes was required to degrade at least 67.5 % of the SMX solution with an initial concentration of 40 ppm. These parameters give an idea of the main differences between the two reactors. The long treatment time in the DBD is explained by the fact that the degradation is mainly restricted to the water surface. Even in the presence of turbulence induced by the electrostatic forces at the surface of the solution, the mass transfer of reactive species from the gas phase to the bulk of the water was more difficult than in the ozonation experiments. When using the ozonator, ozone was bubbled inside the entire solution thus providing efficient mass transfer and contacting. Design suggestions for the DBD reactor will be given in the last section of the thesis in order to improve the mass transfer of oxidative species in the solution.

In order to compare the efficiency of both processes in the future, the degradation results of the plasma-treated samples could be compared to the degradation results obtained when ozone is passed over a solution in the DBD reactor, without discharges and for the same treatment time. Before, an estimation of the ozone production in such reactor should be made by measuring its concentration in the gas phase in the presence of microdischarges, with the same discharge gap, but in a dry reactor. Therefore, the ground electrode and the high voltage electrode covered with the dielectric should have to be positioned closer to each other.

The photochemical oxidation of SMX proved to be more efficient in an

acidic media [90] and the direct photolysis rate constants were found to be highly pH dependent and not consistent among the class of sulfa drugs [74]. As previously explained, the aim of this case study was to look at the potential use of the DBD hybrid reactor for SMX degradation. This was performed using the same solution that is used by collaborators that degrade SMX using the ozonation process and therefore, with a pH of about 8. Further studies should be performed to determine which pH level would be most efficient for SMX degradation in this type of DBD reactor. When using the DBD reactor, the optimal pH could be different from the one used with ozonation.

The experiments were all performed with a sodium acetate (SA) concentration of 3.9892 g/L, added to enhance the solution COD to 3000 mg/L. With the ozonation process, it took more time to degrade solutions with higher COD levels. Therefore, it should also be determined if different SA concentrations would have an impact on the degradation results obtained with plasma-treated samples.

Chapter 6. Visualization of the microdischarges

As mentioned in the materials and methods section, images of the microdischarges were taken with a PCO 2004, DICAM-PRO CCD camera, in both oxygen and air in order to study their shape.

Following the initiation of an experiment, only a limited number of microdischarges would appear. This phenomenon is probably due to the space charges that initially did not support microdischarge formation. When the space charges accumulated within the gap space, the number of microdischarges might have increased until they finally reached a saturation level [96].

Figures 6.1 and 6.2 present images of microdischarges that were taken in air and oxygen with the same focus on a width of 2.55 cm, and that were processed with a MATLAB® program. In order to observe the microdischarges present in the oxygen atmosphere, the images were first processed with the CamWare software to double their intensity. Therefore, to be able to compare the arbitrary intensities between the two pictures, the intensities shown on the graph corresponding to the image taken in the oxygen atmosphere, have to be divided by two.

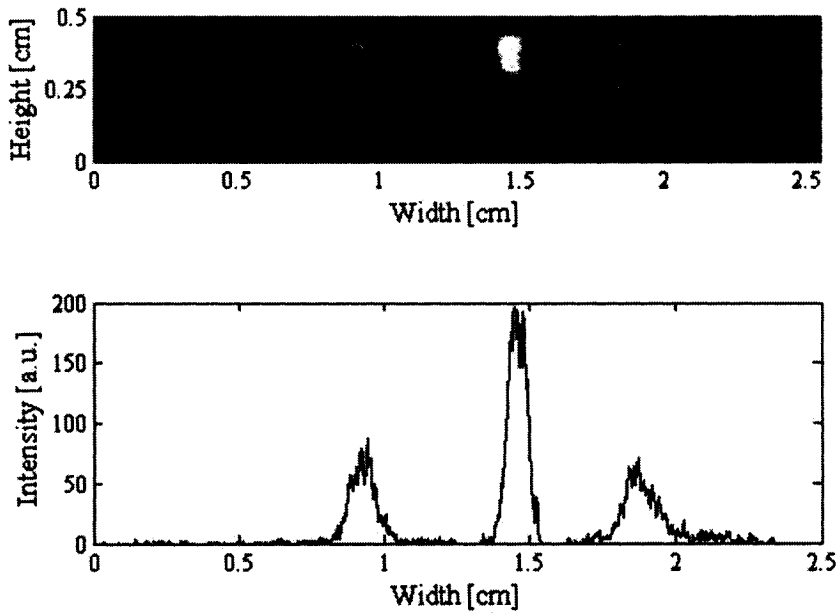

Figure 6.1 Image of microdischarges in air and the corresponding intensity graph chart in arbitrary units (Focus on a width of 2.55 cm, 2 ms exposure time, initial SMX concentration: 40 ppm, volume of solution: 48 mL, air flow rate: 25 cc/min, V_M: 10 kV)

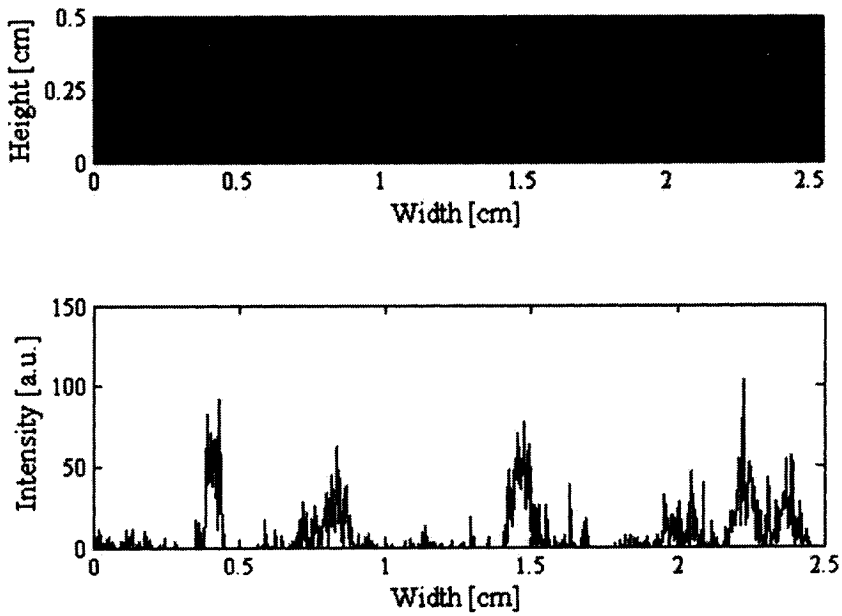

Figure 6.2 Image of microdischarges in O_2 and the corresponding intensity graph chart in arbitrary units (Focus on a width of 2.55 cm, 2 ms exposure time, initial SMX concentration: 40 ppm, volume of solution: 48 mL, O_2 flow rate: 25 cc/min, V_M: 10 kV)

It was noticed that the microdischarges appeared to be thicker in air than in oxygen. This observation is validated with Figures 6.1 and 6.2 by the fact that the bases of the peaks in the intensity graphs are wider in air than in oxygen. Such observation was also reported in a previous study, where both numerical calculations and measurements showed that the radius of the breakdown channel is larger in air than in oxygen [3].

It was also noticed that the optical emission from the microdischarges was more intense when using air as the feed gas. This can also be concluded by comparing the respective intensities of the peaks in Figures 6.1 and 6.2 (taking into account that the intensities should be divided by two for the oxygen graph). This difference is probably due to the emission of exited nitrogen between the wavelengths of 380 and 450 nm in the case of air.

For fixed values for the operating parameters (initial SMX concentration: 40 ppm, volume of solution: 48 mL, gas flow rate: 25 cc/min, V_M: 10 kV), a larger number of microdischarges are generated in oxygen in comparison to air. For a focus on a width of 5.25 cm along one side of the reactor, an average of 6.5 microdischarges was observed in oxygen versus 3.3 in air (average of 150 images each). Twenty representative images taken in oxygen and in air are included in Appendix IV. The overall appearance of the microdischarges was more homogeneous with oxygen than with air. These results are similar to the findings of previous authors, studying microdischarges behavior between metal and glass electrodes, with increasing oxygen content in the gas phase [97]. Because of the electronegative character of oxygen, increasing its content in the gas phase decreases the number of transferred charges per microdischarge and therefore, its intensity. When increasing oxygen content, the electron attachment increases and fewer charges per microdischarge are transferred. Furthermore, the decay time of

the microdischarges decreases but their number increases as well as the total transferred charges per half cycle [97].

In the presence of water vapor, it was found that fewer and more intense discharges occurred because water vapor coated the dielectric, decreasing its surface resistance and increasing the number of transferred charges per microdischarge [97]. In a semi-batch DBD reactor, we can then expect the number of microdischarges to decrease and the individual microdischarges to be more intense with increasing treatment time due to the increase of humidity.

Most of the images showed microdischarges that were more intense close to the alumina dielectric region and less intense close to the grounded water electrode. This can be observed with Figures 6.1 and 6.2 and in the images of Appendix IV. Other researchers explained that, in oxygen or air dielectric barrier discharges, each microdischarge consists of a thin cylindrical channel. It has a constricted electrode spot at the metal electrode (in this case particular case, the water electrode) that spreads into a surface discharge on the dielectric [98]. Figure 6.3 illustrates the formation of microdischarges between a metal electrode and another electrode covered with a dielectric [98]. This shape was explained by the fact that, as soon as a current flow was initiated in a microdischarge, charges start to accumulate in the area where the microdischarges hit the dielectric [98].

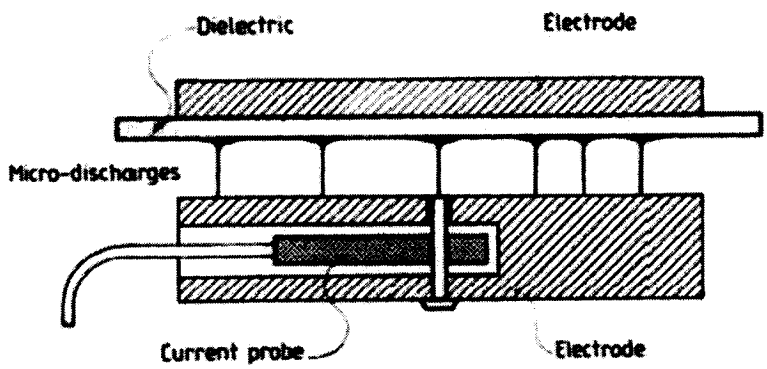

Figure 6.3 Schematic illustration of microdischarges [98]

In the particular case where water vapor is also present at the water-gas interface, the effect seemed intensified. A potential explanation for this behavior is that, since the reactor is not in equilibrium, there is a gradient of concentration of water vapor along the distance separating the water electrode and the alumina dielectric. More water vapor close to the water electrode results in less nitrogen or oxygen excitation and therefore, in a weaker optical emission.

Figure 6.4 presents one of the many images that show diagonal microdischarges. It is to be noted that the horizontal lines perceived are due to the imperfection of the acrylic material of which the wall of the reactor is made. This image was taken with a focus on a width of 2.55 cm along one side of the reactor and in air. The diagonal microdischarge is not due solely to the flow of air at the rate of 25 cc/min because such phenomenon is observed inverse to the flow direction too, as in Figure 6.4. An explanation is that a streamer usually propagates most easily within a gap with the smallest thickness and therefore must form between the dielectric and a protuberance present at the water surface. Extinguishing streamers nearby must create upward bulges due to the electrostatic forces they exert on the water surface, inducing agitation and protuberances at the water surface. This observation indicates that the microdischarges produced at a frequency of 17.5 kHz, promote water turbulence and that the discharge gap cannot be assumed constant, and that it is reduced at some locations.

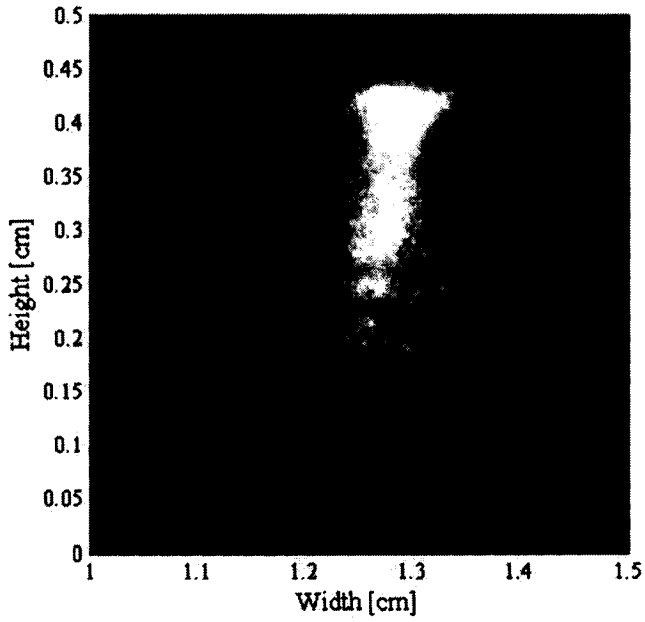

Figure 6.4 Side-view of a microdischarge in air (Focus on a width of 2.55 cm, 2 ms exposure time, initial SMX concentration: 40 ppm, volume of solution: 48 mL, air flow rate: 25 cc/min, V_M: 10 kV)

Figure 6.5 is one of the rare images that showed microdischarges with the base more intense than its upper part. This image is in contradiction with all other images where the microdischarges spreaded onto the dielectric and were more constricted next to the water electrode. A potential explanation to this is that, as in Figure 6.4, the microdischarge in Figure 6.5 was probably in diagonal; but in the transverse direction. Its base must have been nearer than its upper part to the side of the reactor where the objective of the camera was placed. It therefore seemed that its base was more intense than the part close to the dielectric but that was probably not the case.

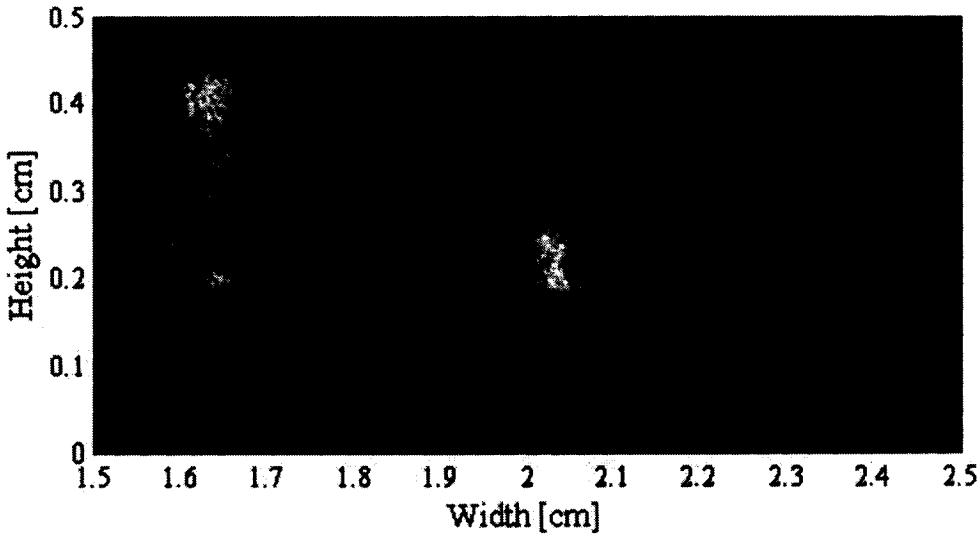

Figure 6.5 Side-view of microdischarges in air (Focus on a width of 2.55 cm, 2 ms exposure time, initial SMX concentration: 40 ppm, volume of solution: 48 mL, air flow rate: 25 cc/min, V_M: 10 kV)

Band pass optical filters were used in an attempt to map the atomic oxygen (O emission at 777 nm) and ionized molecular nitrogen (N_2^+ emission at 391 nm) spatial distributions. These filters cut approximately 40 % of the incoming light. Nothing was visible when the oxygen filter was used with air as the feed gas. Furthermore, ionized molecular nitrogen was observed, at very low intensity, when using the corresponding filter with air. These observations validated the results obtained using optical emission spectroscopy. When using oxygen as the feed gas and using the O filter, the microdischarges were visible but at a much lower intensity. It was therefore impossible to obtain clear images, though they certainly proved that atomic oxygen was indeed present. As expected from the results obtained by optical emission spectroscopy, ionized molecular nitrogen was not detected when oxygen was used as the feed gas.

Chapter 7. Conclusions

A semi-batch parallel hybrid gas-liquid atmospheric pressure DBD reactor was designed, characterized (power consumption, optical emission, shape of microdischarges) and optimized (solution volume, gas flow rate, treatment time and gas type). The degradation of a dye (indigo) and a model pharmaceutical compound (SMX) were studied.

- The semi-batch reactor, mainly made from an acrylic, had inside dimensions of 16 cm × 9.9 cm × 0.655 cm. The liquid to be treated rested on a stainless steel grounded electrode above which was flowing oxygen or air. The aluminum high-voltage electrode rested on the dielectric material (alumina). The voltage output value of the power supply was controlled by a LabVIEW™ interface. The DBD plasma reactor worked at high AC voltage (10 kV) and low peak current (55mA) at a frequency of 17.5 kHz when connected to a commercial power supply known to deliver up to 100 Watts at 20 kHz. The configuration induced the formation of microdischarges in the gas phase.

- A method for power consumption measurements was developed by customizing a LabVIEW™ interface. Based on the Lissajous figures technique, it was determined that the average power dissipated in the DBD was 55 W.

- The optimization of the reactor was performed by monitoring via UV-visible absorption spectroscopy the absorbance of indigo solutions at 600 nm. The effects of different parameters, on the discoloration efficiency of the dyed solution were examined. The parameters investigated were the solution volume, the gas flow rate, the treatment time and the gas type. Statistical analyses were performed in order to determine if the differences in the results obtained were significant.

The discoloration efficiency was found optimal for a solution volume of 45 mL. At the frequency of 17.5 kHz, the discharge gap, which was 3.71 mm without discharge, was reduced by the protuberances formed at the surface of the solution. Promoted water turbulence, was proved by CCD images showing diagonal microdischarges.

Discoloration efficiency decreased when the oxygen flow rate was increased. It was probably due to the smaller residence time of the gas in the reactor (from 141 seconds at 25 cc/min to 50 seconds at 70 cc/min).

Using a volume of 45 mL and a gas flow rate of 25 cc/min, the discoloration efficiency increased with treatment time, when using both oxygen and air. The agitation of the solution induced by the plasma microdischarges, the contact of the solution with high-energy electrons, and the diffusion of active species in the solution, resulted after a treatment time of 9 minutes, in a discoloration efficiency of 99 %. After 9 minutes using air, only a 59 % discoloration was observed. The actual value of discoloration efficiency, obtained in air, was probably even smaller due the formation of nitric acid in the liquid phase. Oxygen, as the feed gas, proved to be much more efficient than air and less toxic.

- The analysis of the UV-visible absorption spectra of the indigo solutions, before and after treatment, showed a temporal decrease in intensity of the peak characteristic of the indigo molecule. The spectra also showed an increase in intensities of the peaks that may be related to the degradation products of the indigo molecule. The analysis of an aged treated solution showed that oxidative species, with much smaller reaction rates, could have remained in the solution, allowing post-treatment degradation.

- The optical emission from atomic oxygen (3^5S-3^5P transition at 777 nm and 3^3S-3^3P transition at 844 nm) was observed in the spectrum of microdischarges produced in oxygen. Alternating Σ and Π structures of exited H_2O^+ were also detected. The atomic oxygen optical emission was insignificant in the spectrum of microdischarges produced in air, where band systems of excited N_2 and N_2^+ mainly were observed. Some of these observations were validated when taking images with a CCD camera and using band pass optical filters in an attempt to map the atomic oxygen and ionized molecular nitrogen spatial distributions.

- The newly developed plasma source was studied as a new approach for the decomposition of the sulfamethoxazole (SMX) antibiotic.

A UV-visible spectrometric method was developed to obtain remaining SMX concentration. At 10 kV and 17.5 kHz, at least 70 % degradation was obtained, for solutions with initial concentrations of SMX of 40 and 80 ppm, treated respectively for 7 and 9 minutes. The liquids formed were inflammable. The fact that flames would form restricted the number of experiments performed.

Pseudo-first order kinetics was assumed and it was found that the rate constant was dependent on the initial SMX concentration in the solution. More replicates and further investigations of the species produced as well as a measure of their concentrations with time would need to be performed in order to determine the exact kinetic model.

The GC analysis showed that, contrary to ozonated samples, methanol, ethanol and phenol were not detected in the plasma-treated solution. Instead, a compound with a boiling point close to 140 °C was detected. These observations suggested that different mechanisms of degradation could exist between the two methods.

The GC-MS analysis of treated samples left in the dark for one month showed the formation of recombined products. This observation led to a very

important conclusion, which is that even if the degradation of the pharmaceutical compound is achieved, the toxicity of the degraded products should be looked at. It is recommended that complete degradation of all the pharmaceutical compounds as well as their degradation products be verified, so that no possible recombination products are allowed to form with time. If the compounds are only partially degraded, the plasma treatment might actually be dangerous to use for SMX degradation. If the compounds structures are close to that of aniline structure, the degraded products could be possible carcinogens and mutagens.

- Images of the microdischarges were taken. Most of the images showed microdischarges that were more intense close to the alumina dielectric and less intense close to the grounded water electrode. It was noticed that the microdischarges appeared to be thicker in air than in oxygen and that the light emitted from the microdischarges was more intense when using air instead of oxygen. Furthermore, a larger number of microdischarges were detected in oxygen in comparison to air. For a focus on a width of 5.25 cm along one side of the reactor, an average of 6.5 microdischarges were observed in oxygen versus 3.3 in air (average of 150 images each).

Finally, this semi-batch parallel hybrid gas-liquid atmospheric pressure DBD reactor proved suitable to degrade both the indigo molecule and the SMX pharmaceutical compound. At the frequency of 17.5 kHz, active species were produced in the gas phase. The diffusion of these species and the contact of the solution with high-energy electrons were both promoted by the waves formed at the surface of the liquid. This novel method for degrading SMX or any pharmaceutical should be further investigated, keeping in mind that an efficient degradation should not only degrade SMX but all of its degradation products that might be more environmentally harmful than SMX itself.

Chapter 8. Recommendations for future work

Suggestions and modifications of the actual DBD design are presented in this section to mitigate the problems encountered and better degrade the pollutants. A safer reactor would permit to obtain more replicates. The proposed modifications will allow a better mixing and probably smaller treatment times.

The modified configuration should allow for better mixing, which in turn would reduce the differences in degradation for different initial concentrations of pollutant and a reduction in the observed coloration change in the reactor with time. The reactor could be cylindrical and placed on a magnetic stirrer to allow the agitation of a Teflon-coated bar magnet and the mixing of the solution, as proposed in a previous study [36].

It is to be noted that the new reactor should be operated at voltages larger than 10 kV to allow larger discharge gaps. This would reduce the chances of having short-circuiting of the electrical circuit. It would also prevent the solution to be treated from touching the dielectric, when introduced in the reactor, and therefore will prevent fire from being induced.

The reactor should be designed in such a way that there will be a larger space between the walls of the reactor and the dielectric placed below the high-voltage electrode. It would therefore prevent microdischarges touching the walls of the reactor when the liquid is agitated.

Further studies should be performed to determine which pH level is most efficient for SMX degradation. It is also suggested that the degradation be optimized to break the bonds of all the cyclic aromatic compounds, thus reducing

the carcinogenic properties of the products.

Finally, an optical access through a quartz view port should be made to allow determining, by UV optical spectroscopy, if slight photodegradation could be involved in SMX degradation when compared to ozonation. It will also allow detecting excited OH radicals produced in the gas phase.

References

[1] Friedman, Alexander, and Lawrence A. Kennedy, *Plasma physics and engineering*, 2004, New York: Taylor and Francis.

[2] Schutze, A., et al., *The atmospheric-pressure plasma jet: a review and comparison to other plasma sources.* IEEE Transactions on Plasma Science, 1998. **26**(6): p. 1685.

[3] Eliasson, B. and U. Kogelschatz, *Modeling and applications of silent discharge plasmas.* IEEE Transactions on Plasma Science, 1991. **19**(2): p.309.

[4] Kogelschatz, U., *Atmospheric-pressure plasma technology.* Plasma Physics and Controlled Fusion, 2004. **46**(12 B): p. 63-75.

[5] Samaranayake, W.J.M., et al., *Pulsed power production of ozone using nonthermal gas discharges.* IEEE Electrical Insulation Magazine, 2001. **17**(4): p. 17.

[6] Balcioglu, I.A. and M. Otker, *Treatment of pharmaceutical wastewater containing antibiotics by O3 and O3 H2O2 processes.* Chemosphere, 2003. **50**(1): p. 85.

[7] Velikonja, J., et al., *Co-generation of ozone and hydrogen peroxide by dielectric barrier AC discharge in humid oxygen.* Ozone: Science and Engineering, 2001. **23**(6): p. 467.

[8] Yoon-Kee, K., et al. *Decomposition of ethylenediaminetetraacetic acid using He-Ar-O_2 dielectric barrier discharge.* 2005. Padua, Italy: Wiley-VCH.

[9] Robinson, J.A., et al. *A new type of ozone generator using Taylor cones on water surfaces.* 1997. New Orleans, LA, USA: IEEE.

[10] Bittencourt J.A., Fundamentals of PLASMA PHYSICS, 3rd edition, 2004, New York: Springer.

[11] Fridman, A., A. Chirokov, and A. Gutsol, *Non-thermal atmospheric pressure discharges.* Journal of Physics D: Applied Physics, 2005. **38**(2): p.1-24.

[12] Kogelschatz, U., *Fundamentals and their applications of dielectric-barrier discharges*, ABB Corporate Research Ltd, 5405 Baden, Switzerland, Ulrich.kogelschatz@ch.abb.com, received 24.05.2000.

[13] Kogelschatz, U., *Filamentary, patterned, and diffuse barrier discharges.* IEEE Transactions on Plasma Science, 2002. **30**(4): p. 1400.

[14] Inculet, Ion I., *Method and apparatus for ozone generation and treatment of water,* PCT Int. Appl. (1995), 24 pp., World Patent written in English. www.espacenet.com Patent number: WO9505340, as of February 2005.

[15] Suarasan, I., et al., *Experimental characterization of multi-point corona discharge devices for direct ozonization of liquids.* Journal of Electrostatics, 2002. **54**(2): p. 207.

[16] Grymonpre, D.R., et al., *Hybrid Gas-Liquid Electrical Discharge Reactors for Organic Compound Degradation.* Industrial and Engineering Chemistry Research, 2004. **43**(9): p. 1975.

[17] Lukes, P., A.T. Appleton, and B.R. Locke, *Hydrogen peroxide and ozone formation in hybrid gas-liquid electrical discharge Reactors.* IEEE Transactions on Industry Applications, 2004. **40**(1): p. 60.

[18] Lukes, P., et al., *Generation of ozone by pulsed corona discharge over water surface in hybrid gas-liquid electrical discharge reactor.* Journal of Physics D: Applied Physics, 2005. **38**(3): p. 409.

[19] Garamoon, A.A., et al., *Experimental study of ozone synthesis.* Plasma Sources, Science and Technology, 2002. **11**(3): p. 254.

[20] Steven Carruthers, *Introduction to ozone generation, Issue 36 Sep/Oct 1997* http://www.hydroponics.com.au/back_issues/issue36.html, as of February 2005.

[21] Malik, M.A., A. Ghaffar, and S.A. Malik, *Water purification by electrical discharges.* Plasma Sources, Science and Technology, 2001. **10**(1): p. 82.

[22] Chalmers, I.D., L. Zanella, and S.J. MacGregor. *Ozone synthesis in oxygen in a dielectric barrier free configuration.* 1995. Albuquerque, NM, USA: IEEE, Piscataway, NJ, USA.

[23] Devins, J. C, *Mechanism of ozone formation in the silent electric discharge*, General Elec. Co., Schenectady, NY, Journal of the Electrochemical Society 1956, 103: p. 460-6.

[24] Yagi, S. and M. Tanaka, *Mechanism of ozone generation in air-fed ozonisers.* Journal of Physics D (Applied Physics), 1979. **12**(9): p. 1509.

[25] Jim Eagleton, *Ozone {O_3} in drinking water,* http://www.hydroserve.com/Ozone%20Documents/ozone_in_drinking_water_treatment.pdf, as of February 2005.

[26] Cooperative research report, *Ozone in water treatment Application and engineering*, American Water Works Association Research Foundation, Second printing, 1991, LEWIS PUBLISHERS, INC.

[27] Lenntech Ozone generation, http://www.lenntech.com/ozone/ozone-generation.htm, as of February 2005.

[28] Staehelin, J. and J. Holgne, *Decomposition of ozone in water in the presence of organic solutes acting as promoters and inhibitors of radical chain reactions.* Environmental Science and Technology, 1985. **19**(12): p.1206.

[29] Latham, J. and I.W. Roxburgh, *Disintegration of pairs of water drops in an electric field.* Proceedings of the Royal Society of London, Series A (Mathematical and Physical Sciences), 1966. **295**(1440): p. 97.

[30] Allen, J.E., *A note on the Taylor cone.* Journal of Physics D (Applied Physics), 1985. **18**(7): p. 59.

[31] Higuera, F.J., *Flow rate and electric current emitted by a Taylor cone.* Journal of Fluid Mechanics, 2003. **484**: p. 303.

[32] Aguirre-de-Carcer, I.; Fernandez de la Mora, J. *Effect of background gas on the current emitted from Taylor cones.* Journal of Colloid and Interface Science (1995), 171(2), 512-17.

[33] Higuera, F.J., *Ion evaporation from the surface of a Taylor cone.* Physical Review E (Statistical, Nonlinear, and Soft Matter Physics), 2003. **68**(1): p.16304.

[34] Barrero, A., et al., *The role of the electrical conductivity and viscosity on the motions inside Taylor cones.* Journal of Electrostatics, 1999. **47**(1-2): p.13.

[35] Barrero, A., et al., *Low and high Reynolds number flows inside Taylor cones.* Physical Review E (Statistical Physics, Plasmas, Fluids, and Related Interdisciplinary Topics), 1998. **58**(6): p. 7309.

[36] Velikonja, J., et al., *Ozone dissolution vs. Aqueous methylene blue degradation in semi-batch reactors with dielectric barrier discharge over the water surface.* Ozone: Science and Engineering, 2002. **24**(3): p. 159.

[37] Robinson, J.A., et al., *Breakdown of air over a water surface stressed by a perpendicular alternating electric field, in the presence of a dielectric barrier.* IEEE Transactions on Industry Applications, 2000. **36**(1): p. 68.

[38] Clements, J.S., M. Sato, and R.H. Davis, *Preliminary investigation of prebreakdown phenomena and chemical reactions using a pulsed high-voltage discharge in water.* IEEE Transactions on Industry Applications, 1987. **IA-23**(2): p. 224.

[39] Sugiarto, A.T. and M. Sato, *Pulsed plasma processing of organic compounds in aqueous solution.* Thin Solid Films, 2001. **386**(2): p. 295.

[40] Grinevich, V.I.B., A. G.; Kuvykin, N. A.; Kostrov, V. V., *Surface barrier-discharge plasma treatment of aqueous phenol solutions.* High energy chemistry, 1999. **33**(2): p. 114.

[41] Bubnov, A.G.G., V. I.; Kuvykin, N. A., *Phenol Degradation Features in Aqueous Solutions upon Dielectric-Barrier Discharge Treatment.* High Energy Chemistry, 2004. **38**(5): p. 338.

[42] Grinevich, V.I., *Kinetics of ozone formation in the gas and liquid phases in a barrier-discharge plasma.* Theoretical Foundations of Chemical Engineering, 2004. **38**(1): p. 56.

[43] Bubnov, A., et al., *Combined Plasma-Induced and Catalytic Decomposition of Phenols.* Russian Journal of Applied Chemistry, 2005. **78**(7): p. 1106.

[44] Bubnov, A.G., et al., *Plasma-catalytic decomposition of phenols in atmospheric pressure dielectric barrier discharge.* Plasma Chemistry and Plasma Processing, 2006. **26**(1): p. 19.

[45] Bubnov, A.G.G., V. I.; Kuvykin, N. A.; Maslova, O. N., *The Kinetics of Plasma-Induced Degradation of Organic Pollutants in Sewage Water.* High Energy Chemistry, 2004. **38**(1): p. 41.

[46] Kornev, J. *Electric discharge treatment of water containing organic substances.* Science and Technology, 2003. Proceedings KORUS 2003. The 7th Korea-Russia International 28 June- 6 July 2003. V1: p.221- 226.

[47] Suarasan, I., et al., *A novel type ozonizer for wastewater treatment.* Journal of Electrostatics, 2005. **63**(6-10): p. 831.

[48] Winkler, J., N. Karpel Vel Leitner, and H. Romat, *An experimental study on the possible use of corona discharge in water treatment,* Inst. Phys. Conf. Ser. N0 163, Paper presented at the 10th Int. Conf., Cambridge, 28-31 March 1999.

[49] Grabowski, L.R., et al., *Corona above water reactor for systematic study of aqueous phenol degradation.* Plasma Chemistry and Plasma Processing, 2006. **26**(1): p. 3.

[50] Ihara, S., et al., *Ozone generation by a discharge in bubbled water.* Japanese Journal of Applied Physics, Part 1: Regular Papers and Short Notes and Review Papers, 1999. **38**(7B): p. 4601.

[51] Espie, S., et al. *Investigation of dissolved ozone production using plasma discharges in liquid.* 2001. Las Vegas, NV, USA: IEEE.

[52] Sun, B., M. Sato, and J.S. Clements, *Use of a pulsed high-voltage discharge for removal of organic compounds in aqueous solution.* Journal of Physics D (Applied Physics), 1999. **32**(15): p. 1908.

[53] Willberg, D.M., et al., *Degradation of 4-chlorophenol, 3,4-dichloroaniline, and 2,4,6-trinitrotoluene in an electrohydraulic discharge reactor.* Environmental Science and Technology, 1996. **30**(8): p. 2526.

[54] Sunka, P., et al., *Generation of chemically active species by electrical discharges in water.* Plasma Sources, Science and Technology, 1999. **8**(2): p. 258.

[55] Mayank Sahni, W.C.F., and Bruce R. Locke. *Quantification of hydroxyl radicals produced in aqueous phase pulsed electrical discharge reactors.* in 17th International Symposium on Plasma Chemistry (ISPC 17). 2005. Toronto, Ontario, Canada.

[56] Lukes, P. and B.R. Locke, *Plasmachemical oxidation processes in a hybrid gas-liquid electrical discharge reactor.* Journal of Physics D (Applied Physics), 2005. **38**(22): p. 4074.

[57] Lukes, P. and B.R. Locke, *Degradation of substituted phenols in a hybrid gas-liquid electrical discharge reactor.* Industrial and Engineering Chemistry Research, 2005. **44**(9): p. 2921.

[58] Adams, C.D. and S. Gorg, *Effect of pH and gas-phase ozone concentration on the decolorization of common textile dyes.* Journal of Environmental Engineering, 2002. **128**(3): p. 293.

[59] Tri Sugiarto, A., T. Ohshima, and M. Sato. *Advanced oxidation processes using pulsed streamer corona discharge in water.* 2002. Tokyo, Japan: Elsevier.

[60] Sugiarto, A.T., et al., *Oxidative decoloration of dyes by pulsed discharge plasma in water.* Journal of Electrostatics, 2003. **58**(1-2): p. 135.

[61] Abdelmalek, F., et al., *Plasmachemical degradation of azo dyes by humid air plasma: Yellow Supranol 4 GL, Scarlet Red Nylosan F3 GL and industrial waste.* Water Research, 2004. **38**(9): p. 2338.

[62] Huijuan, W., L. Jie, and Q. Xie, *Decoloration of azo dye by a multi-needle-to-plate high-voltage pulsed corona discharge system in water.* Journal of Electrostatics, 2006. **64**(6): p. 416.

[63] Bader, H. and J. Hoigne, *Determination of ozone in water by the indigo method.* Water Research, 1981. **15**(4): p. 449.

[64] Bader, H. and J. Hoigne, *Determination of ozone in water by the indigo method; a submitted standard method.* Ozone: Science and Engineering, 1982. **4**(4): p. 169.

[65] Straka, M.R., G. Gordon, and G.E. Pacey, *Residual aqueous ozone determination by gas diffusion flow injection analysis.* Analytical Chemistry, 1985. **57**(9): p. 1799.

[66] Zhang, R.-B., G.-F. Li, and Y. Wu. *Degradation of indigo carmine using bipolar pulsed Dielectric Barrier Discharge (DBD) in the water-air mixture.* 2004. Seattle, WA, United States: Institute of Electrical and Electronics Engineers Inc., Piscataway, NJ 08855-1331, United States

[67] Zhang, R.-B., et al., *Plasma induced degradation of Indigo Carmine by bipolar pulsed dielectric barrier discharge (DBD) in the water-air mixture.* Journal of Environmental Sciences, 2004. **16**(5): p. 808.

[68] Zhang, R.-b., Y. Wu, and G. Li, *Enhancement of the plasma chemistry process in a three-phase discharge reactor.* Plasma Sources, Science and Technology, 2005. **14**(2): p. 308.

[69] Yamabe, C., et al., *Water treatment using discharge on the surface of a bubble in water.* Plasma Processes and Polymers, 2005. **2**(3): p. 246.

[70] Zwiener, C. and F.H. Frimmel, *Oxidative treatment of pharmaceuticals in water.* Water Research, 2000. **34**(6): p. 1881.

[71] Huber, M.M., et al., *Oxidation of pharmaceuticals during ozonation and advanced oxidation processes.* Environ Sci Technol, 2003. **37**(5): p. 1016-24

[72] Ternes, T.A., et al., *Ozonation: a tool for removal of pharmaceuticals, contrast media and musk fragrances from wastewater?* Water Res, 2003. **37**(8): p. 1976-82.

[73] Andreozzi, R., et al., *Ozonation and H2O2/UV treatment of clofibric acid in water: a kinetic investigation.* J Hazard Mater, 2003. **103**(3): p. 233-46.

[74] Boreen, A.L., W.A. Arnold, and K. McNeill, *Photochemical fate of sulfa drugs in then aquatic environment: Sulfa drugs containing five-membered heterocyclic groups.* Environmental Science and Technology, 2004. **38**(14): p. 3933.

[75] Roman Huppee, *Design of a pressurized dielectric discharge water-electrode ozonation system*, Project report for CHEE 695, McGill University, 2003

[76] Scott, S.J., C.C. Figgures, and D.G. Dixon, *Dielectric barrier discharge processing of aerospace materials.* Plasma Sources Science and Technology, 2004. **13**(3): p. 461.

[77] PTI Plasma Technics, Inc. Electronic Ozone Transformer http://www.plasmatechnics.com/ET50-100.html as of September 2006

[78] Douglas C. Montgomery and George C. Runger. *Applied Statistics and probability For Engineers,* Third edition, John Wileys and Sons, Inc

[79] Wikipedia, The Free Encyclopedia, http://en.wikipedia.org/wiki/Nitrogen_monoxide as of September 2006

[80] Wikipedia, The Free Encyclopedia, http://en.wikipedia.org/wiki/Nitrous_acid as of September 2006

[81] Wikipedia, The Free Encyclopedia, http://en.wikipedia.org/wiki/Nitric_acid as of September 2006

[82] Wikipedia, The Free Encyclopedia, http://en.wikipedia.org/wiki/Nitrogen_dioxide as of September 2006

[83] Tratnyek, P.G., et al., *Visualizing Redox Chemistry: Probing Environmental Oxidation–Reduction Reactions with Indicator Dyes.* The Chemical Educator, 2001. **6**(3): p. 172.

[84] Takeuchi, K.I., Takashi, *Quantitative determination of aqueous-phase ozone by chemiluminescence using indigo-5,5'-disulfonate.* Analytical chemistry, 1989. **61** (6): p. 619.

[85] Jones, J.H.H., L.S.; Heine, K.S, JR., *Coal-tar colors. XX. FD & C Blue No. 2.* Journal of The association of Official Agricultural Chemists, 1955. **38**: p.949-77.

[86] NIST National Institute of Standards and Technology, Basic Atomic Spectroscopic Data for Oxygen. http://physics.nist.gov/PhysRefData/Handbook/Tables/oxygentable3.htm as of September 2006

[87] R.W.B Pearse and A.G. Gaydon. *The identification of Molecular Spectra,* Fourth Edition, John Wiley & Sons. Inc, New York

[88] Zhiguo, M., D. Lifang, and R. Junxia. *Spectrum of dielectric barrier discharge in atmosphere.* 2005. Beijing, China: International Society for Optical Engineering, Bellingham, WA 98227-0010, United States.

[89] Wekhof, A., *Treatment of contaminated water, air and soil with UV flashlamps.* Environmental Progress, 1991. **10**(4): p. 241.

[90] Zhou, W. and D.E. Moore, *Photochemical decomposition of sulfamethoxazole.* International Journal of Pharmaceutics, 1994. **110**(1): p.55.

[91] Lam, M.W. and S.A. Mabury, *Photodegradation of the pharmaceuticals atorvastatin, carbamazepine, levofloxacin, and sulfamethoxazole in natural waters.* Aquatic Sciences - Research Across Boundaries, 2005. **67**(2): p.177.

[92] Chamberlain, E. and C. Adams, *Oxidation of sulfonamides, macrolides, and carbadox with free chlorine and monochloramine.* Water Research, 2006. **40**(13): p. 2517.

[93] Peyrous, R., P. Pignolet, and B. Held, *Kinetic simulation of gaseous species created by an electrical discharge in dry or humid oxygen.* Journal of Physics D (Applied Physics), 1989. **22**(11): p. 1658.

[94] Gao, J., et al., *Oxidative degradation of nitrophenols in aqueous solution induced by plasma with submersed glow discharge electrolysis.* Plasma Processes and Polymers, 2004. **1**(2): p. 171.

[95] Physical & Theoretical Chemistry Laboratory, University of Oxford, Aniline MSDS, http://ptcl.chem.ox.ac.uk/MSDS/AN/aniline.html as of September 2006

[96] Alexandre Chirokov, *Self-Organization Of Microdischarges in DBD plasma*, A Thesis submitted to The Faculty of Drexel University in partial fulfillment of the requirements for the degree of Master of Science, November 2003, http://dspace.library.drexel.edu/retrieve/2672/ch3.pdf as of September 2006

[97] Falkenstein, Z. and J.J. Coogan, *Microdischarge behaviour in the silent discharge of nitrogen-oxygen and water-air mixtures.* Journal of Physics D (Applied Physics), 1997. **30**(5): p. 817.

[98] Eliasson, B., M. Hirth, and U. Kogelschatz, *Ozone synthesis from oxygen in dielectric barrier discharges.* Journal of Physics D (Applied Physics), 1987. **20**(11): p. 1421.

[99] Standard method for the examination of water and wastewater, *4500-O_3 Ozone (Residual),* Approved by Standards Methods Committee 1997

[100] Joelle Jureidini, *Determination of Dissolved Ozone Concentrations by the Indigo Colorimetric Method,* Project report for CHEE 690-Research Techniques, McGill University, December 2005

Conference presentations

Jureidini J., Coulombe S., Leclair C and Yargeau V. (2006) "Study of dye degradation for the optimization of an atmospheric pressure direct-contact DBD and application on a pharmaceutical compound," 56th Canadian Chemical Engineering Conference, Université de Sherbrooke, October 15-18.

Jureidini J. and Coulombe S. (2006) "Optimization of an atmospheric pressure direct-contact DBD for the treatment of aqueous pharmaceutical solutions," IEEE Conference Record – Abstract, 33rd International Conference on Plasma Science (ICOPS 2006), Traverse City, Michigan (USA), June 4-8.

Jureidini J. and Coulombe S. (2006) "Optimisation d'un réacteur à plasma hybride pour la dégradation directe de produits pharmaceutiques présents dans l'eau," 74ème Congrès de l'ACFAS-Colloque: Science et ingénierie des plasmas, Université McGill, 18-19 mai.

Appendix I. Rotameter calibration curves

A gilibrator (GILIAN Gilibrator-2 Calibration System from Sensodyne) was used to calibrate two rotameters with different flow ranges. These rotameters were each calibrated for both air and oxygen. The inlet pressure was 30 psig in all cases. Model 82B7920 from Megs only had one float made of black glass. Matheson 602 model had 2 floats, one made of glass (Black Ball) and the other of stainless steel (Silver Ball). Each point was replicated three times. The averages are presented on the calibration curves.

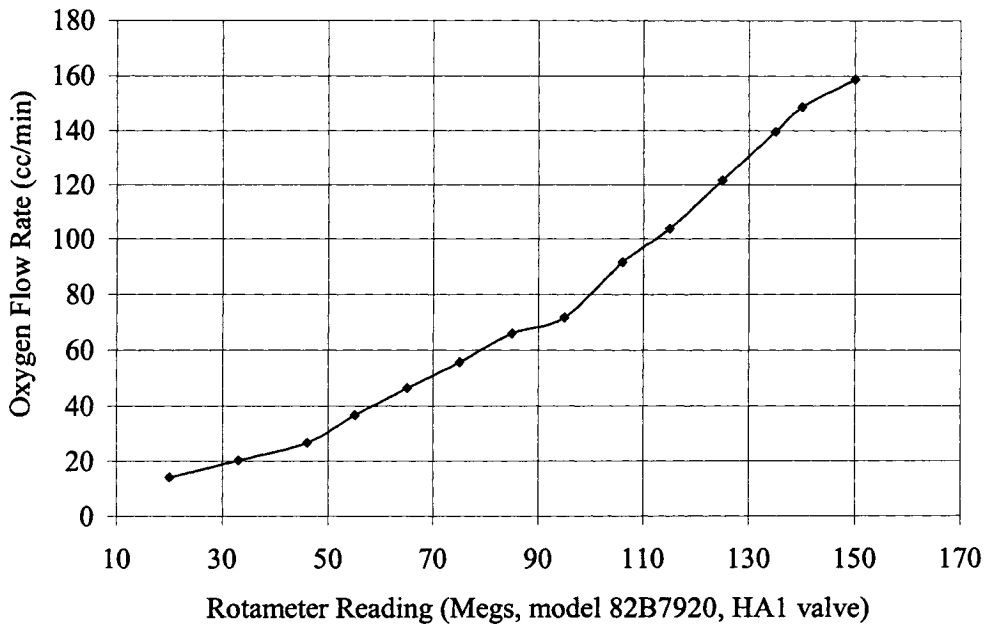

Figure I.1 Rotameter calibration curve for oxygen at 30 psig (Megs, model 82B7920, HA1 valve)

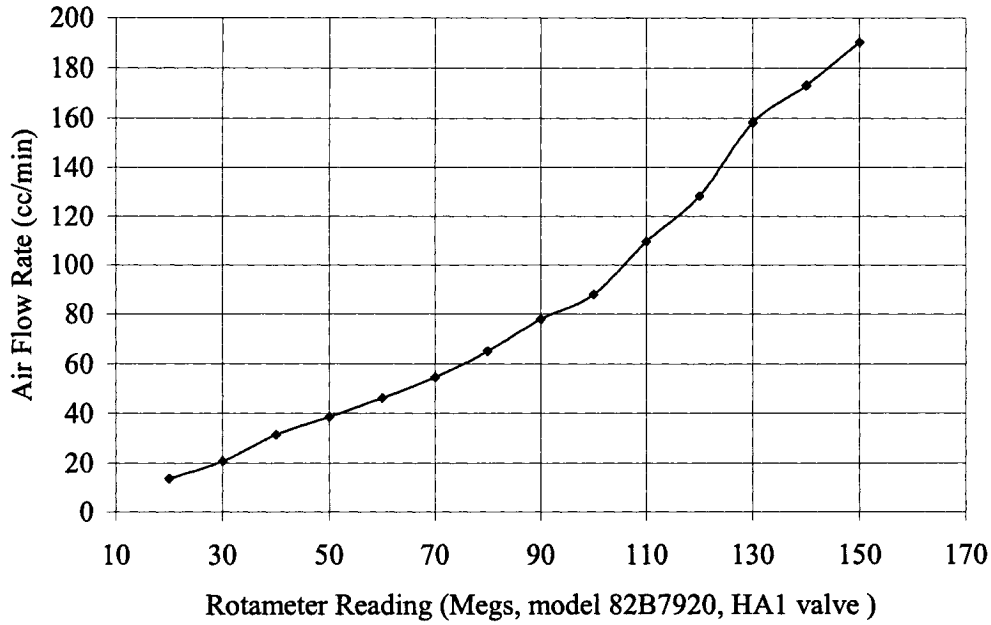

Figure I.2 Rotameter calibration curve for air at 30 psig (Megs, model 82B7920, HA1 valve)

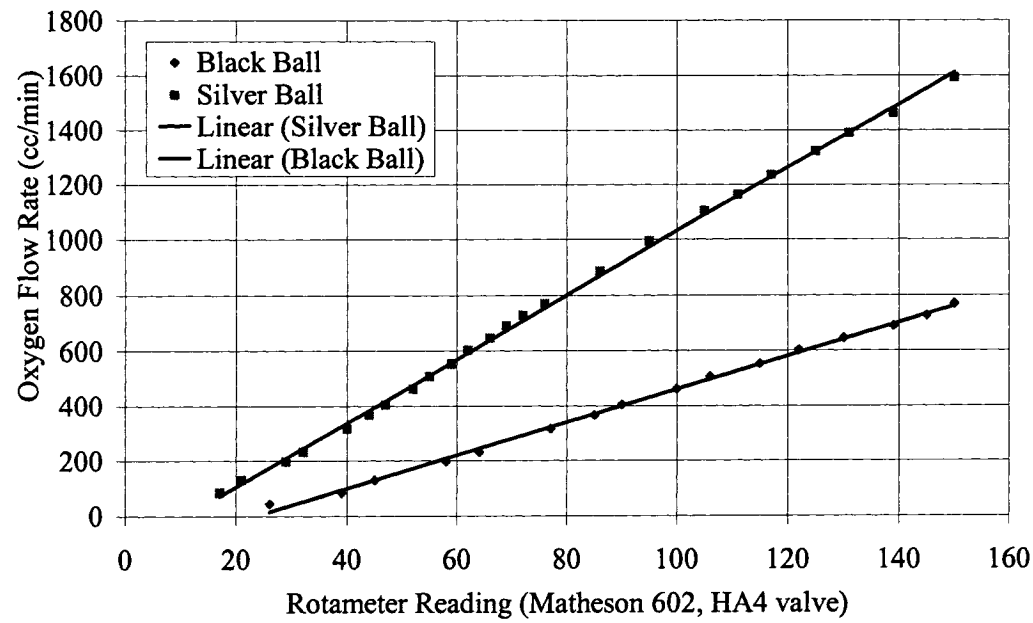

Figure I.3 Rotameter calibration curve for oxygen at 30 psig (Matheson 602, HA4 valve)

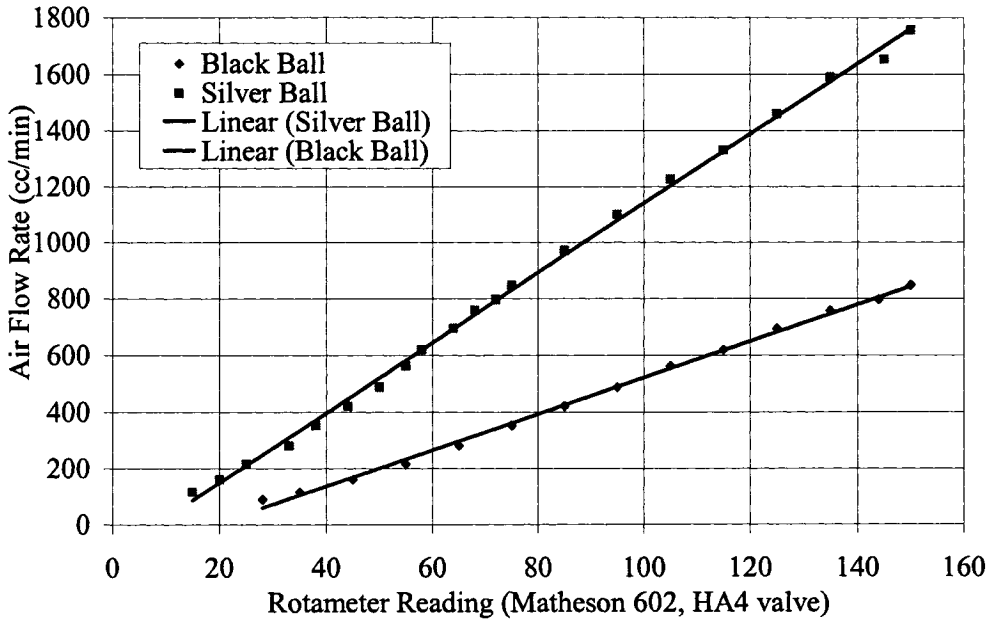

Figure I.4 Rotameter calibration curve for air at 30 psig (Matheson 602, HA4 valve)

Appendix II. Problems encountered and modifications of the method for the reactor optimization

It was determined that semi-batch experiments with the DBD reactor would allow the optimization of the parameters. It was initially decided to optimize those parameters by determining ozone concentration in the liquid phase with the indigo colorimetric method [99]. The indigo trisulfonate batch method or colorimetric method was developed by H. Bader and J. Hoigné in Switzerland [63]. The method consists in adding to an ozonated sample, a specific volume of a solution that contains a known composition of the indigo dye. The decrease in absorbance of the mixture is followed by spectrophotometry and a correlation links the absorbance to the ozone concentration in the sample. More details about the method, with the DBD reactor, were written in a project report submitted to Professor Sylvain Coulombe [100].

The first step was to choose the type of water that would be used to perform the experiments. Experiments worked well with tap water but streamer propagation would not take place with distilled water. It seemed that conductivity affected considerably their propagation. With distilled water, only one microdischarge would form and its tip would produce white fumes in the liquid, which were probably due to hydrogen peroxide formation. A more conductive solution had to be used. In order to obtain accurate results, the type of water used to perform all the experiments had to meet three conditions. It should have the same composition with time, should not interfere with the indigo method, and should not consume ozone.

Deionized water, distilled water and tap water were tested by IC (Ion Chromatography, used for negative ions identification) and ICP (Inductively

Coupled Plasma, used for positive ions identification): The results of the analyses are reported in the tables below.

Table II.1 IC Results for deionized, distilled and tap waters

	Elements Concentrations (PPB)		
IC Results	***Deionized H_2O***	***Distilled H_2O***	***Tap H_2O***
Fluoride	0.00	35.14	1730.74
Chloride	39.29	46.27	34528.00
Nitrate	0.00	14.98	2736.16
Phosphate	11.83	1.60	477.83
Sulphate	1.99	33.66	50360.00
Total	**53.11**	**131.65**	**89832.73**

Table II.2 ICP Results for deionized, distilled and tap waters

	Elements Concentrations (PPB)		
ICP Results	***Deionized H_2O***	***Distilled H_2O***	***Tap H_2O***
Ca	-	-	24630.00
Cu	1.32	2.64	225.20
Fe	-	-	1.93
Mg	-	-	6644.00
Mn	-	-	-
Ni	-	-	2.48
Pb	-	3.99	2.72
K	4.50	9.10	819.10
Na	-	-	6855.00
Zn	-	-	22.28
Cd	-	-	-
Cr	-	-	5.09
Co	-	-	-
Total	**5.82**	**15.73**	**39207.80**

These results show that there is a great difference in ions concentration between distilled and tap waters. Furthermore, tap water compounds could vary with time due to the changes in the city of Montréal water supply. Therefore,

ozone might be consumed differently and the results could be inaccurate. Furthermore, chlorides could be oxidized and that would interfere with the indigo colorimetric method [63]. There was relatively not much of a great difference between deionized and distilled water concentrations in ions and since distilled water had been used with the standard indigo method for ozone measurements in the liquid phase, it was used in the present study.

Since the DBD reactor proved to function properly only with tap water, which has an average conductivity of 300 μS, a compound had to be added to distilled water to make up for the difference in conductivity. Adding sulphuric acid (H_2SO_4) to distilled water had a double effect: it would increase the conductivity and decrease the pH. Decreasing the pH would decrease the ozone degradation rate and increase its lifetime. A concentration of 0.4695 mMol/L of H_2SO_4 in distilled water was found to increase the conductivity of distilled water from 2.2 μS at 22.5 °C to 300 μS (close to the value of tap water) and with a pH of 3.

A temporal decrease in absorbance of the treated samples reflected that other oxidative species were reacting with the indigo solution, but at lower rates. This phenomenon was not seen when ozonated samples, prepared by collaborators using an ozone generator, were tested with the method. Therefore, when using the DBD reactor, ozone concentrations had to be calculated after an exact amount of time for the results to be comparable.

The parameters were not yet optimized but approximately the same very low ozone concentrations were obtained when comparing the results with different parameters. Varying the type of water, the flow of oxygen and the treatment time did not significantly change ozone concentration in the liquid phase when using the DBD reactor.

Different thicknesses for the reactor were tested (0.797 cm, 0.434 cm and 0.655 cm). It was first changed from 0.797 cm to 0.434 cm for the area of surface to volume ratio to be increased therefore improving the reactor efficiency. Since short-circuiting problems would occur frequently with that thickness of reactor, a thickness of 0.655 cm was found optimal. When using the optimal thickness of reactor (0.655 cm) and introducing a very dilute indigo solution added to the synthetic solution, the discoloration of the solution was complete after a few seconds only of discharge. It was deduced that oxidizing species had induced the discoloration and that the reactor could be optimized based on the decrease in absorption obtained. Since the discoloration was complete after only a few seconds, it was decided to use a solution with a much higher indigo dye concentration to study the decrease in absorbance. A greater decrease in absorbance would show that a greater amount of oxidizing species was produced. Finally, a much more concentrated indigo solution was prepared by diluting by half one of the indigo solutions that had been used for the indigo colorimetric method.

For the reactor to work properly, it was necessary to purge it in advance at high flow rate to dry completely the alumina plate. Otherwise, a microdischarge would form at the spot where the discharge gap was the smallest. It would short-circuit the electrical circuit by inducing the solution to reach the alumina plate. Another option was to turn on and off consecutively the LabVIEW™ interface, customized to control the voltage of the power supply. This was performed at the start up for approximately one minute with a small volume of the solution. With a small volume, only one streamer would form and would travel inside the reactor, building up charges on the dielectric and drying it. When the liquid was added, the streamers would form readily. It was realized that at the high concentration of indigo, the exposure to one streamer for one minute or the

exposure to a high flow of oxygen did not affect its absorbance. This debugging phase could therefore be neglected. Finally, the reactor was always purged to avoid as much as possible the debugging phase.

Based on the problems encountered, a procedure was written to obtain accurate and comparable results. It is presented in Appendix III.

Appendix III. Procedure used for experiments with the indigo solution

A table was used to keep tract of the different parameters used from one experiment to the other.

Table III.1 Experiments data sheet

	Value	Time	Time on Chronometer
Indigo absorbance			
pH			
Conductivity (µS)			
Temperature (°C)			
Volume initially added (mL)			
Before the treatment time:			
O_2 Purging flow rate (cc/min)	70		
Starting time (of purging with O_2)			0
Ending time (of purging with O_2)			30
Time on watch (beg. of experiment)			0
Experiment parameters:			
Water temp beg (°C)			
Black ball reading			
Oxygen flow rate (cc/min)			
Total volume (mL)			
Treatment time (min)			
Voltage applied (KV)			
After the treatment time:			
Water Temperature (°C)			
Level of stirrer			
Time when sample added to stirrer			
Time when sample removed from stirrer			
In the analytical Laboratory:			
Time (for 1rst measurement)			
Absorbance at 600 nm (1rst meas.)			
Absorbance at 600 nm after 15 min			
Absorbance at 600 nm after 30 min			

In the analytical laboratory:

1) Check indigo stock solution properties:
   Conductivity/ pH/ Absorbance (QS 10.00 mm Hellma Vial)
   Compare to previous values
2) Prepare a 50%/50% indigo solution and distilled water using volumetric flasks
3) Check solution Properties:
   Conductivity/ pH/ Temperature/Absorbance
   Compare to previous values
4) Using the spectrophotometer, prepare:
   A Scan interface (600 nm, zero)
   A Kinetic interface (600 nm, zero, 180 min)

Material and equipment needed

- 100 mL flask with cap
- Magnetic stirrer and magnet
- 200 mL beaker
- Pipette pump and 2 x 10 mL pipettes
- Spectrophotometer cell
- Chronometer
- Thermometer
- Funnel
- 25 mL pipette (in case have to remove liquid from the reactor if short-circuits)

In the plasma laboratory

1) Connect the reactor to the power supply
2) Wear gloves + mask+ chemical safety glasses
3) Add the initial volume with the funnel ,10 mL by 10 mL without liquid touching alumina (shake the reactor so that the solution is dispersed inside the reactor)
4) Connect inlets of gas and close well the fumehood
5) Open the oxygen supply and purge the reactor for 25 minutes at a rate of 70 cc/min (Change to the required flow value at 25 minutes)
6) Close the doors and put warnings
7) Open the LabVIEW™ interface
8) Open the three switches for power supply
9) Close the light of the fumehood

10) Restart the chronometer: 0
11) Perform an experiment noting some of the parameters shown in TableIII.1. Mainly: Oxygen flow rate, voltage applied, treatment time, and total volume of solution.
12) After the experiment, make sure to put a value of 0 for the voltage on the LabVIEW™ interface to turn off the plasma. Turn off the LabVIEW™ interface. Turn on light and close all power supply switches. Unplug the electrical connections.
13) Join both electrodes, starting with the ground electrode and with one hand, to discharge the capacitor and disconnect the reactor
14) Let purge with O_2 for 1 min, close oxygen supply and disconnect all gas connections
15) Collect the treated sample in the fumehood using the 100 mL flask containing the magnet
16) Add the thermometer to measure temperature
17) Mix the treated solution on the magnetic stirrer for one minute
18) Wash the reactor with distilled water to prepare for next experiment and let it dry

In the analytical laboratory

Introduce the treated sample to be analyzed, in the spectrophotometer, and measure its absorbance at 600 nm after 15 and 30 minutes from the beginning of the experiment (replicates)

Appendix IV. CCD images of microdischarges in oxygen and in air

Approximately 200 images were collected for both oxygen and air using the same operating parameters (initial SMX concentration: 40 ppm, volume of solution: 48 mL, gas flow rate: 25 cc/min, V_M: 10 kV), same probe arrangement, and for a focus on a width of 5.25 cm along one side of the reactor. Twenty representative images have been inserted in this appendix to illustrate the microdischarges shape and number. The number attributed to each image represents the order in which the image was collected when a set of 200 images were taken consecutively in each of the gases. The X and Y axes are proportional but the aspect ratio was unlocked so that the data units were not the same in both directions. The light emitted by the microdischarges in air was much more intense than in oxygen. The images obtained in oxygen were intensified to be able to count the number of microdischarges.

In oxygen

IMAGE 26 in O_2

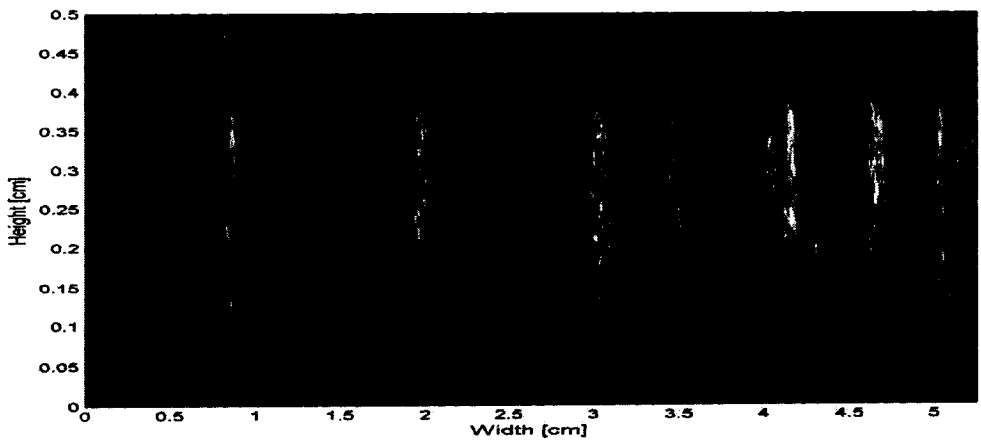

IMAGE 50 in O_2

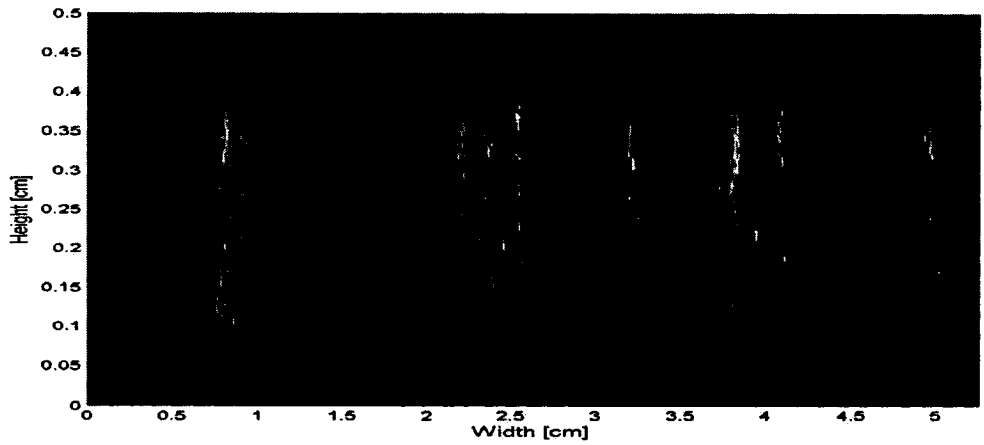

IMAGE 55 in O_2

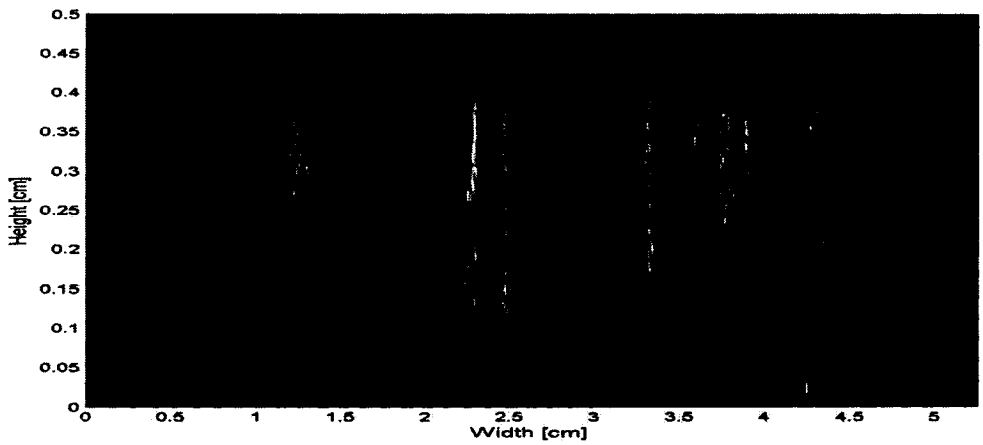

IMAGE 69 in O_2

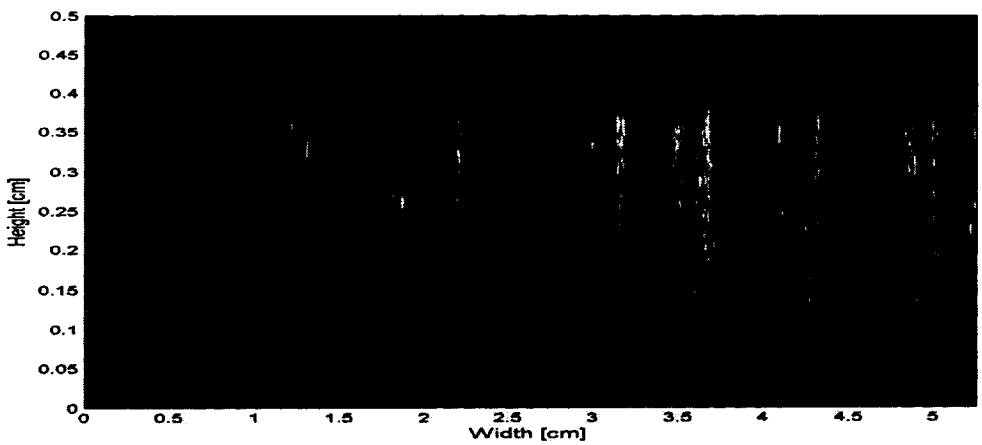

IMAGE 89 in O_2

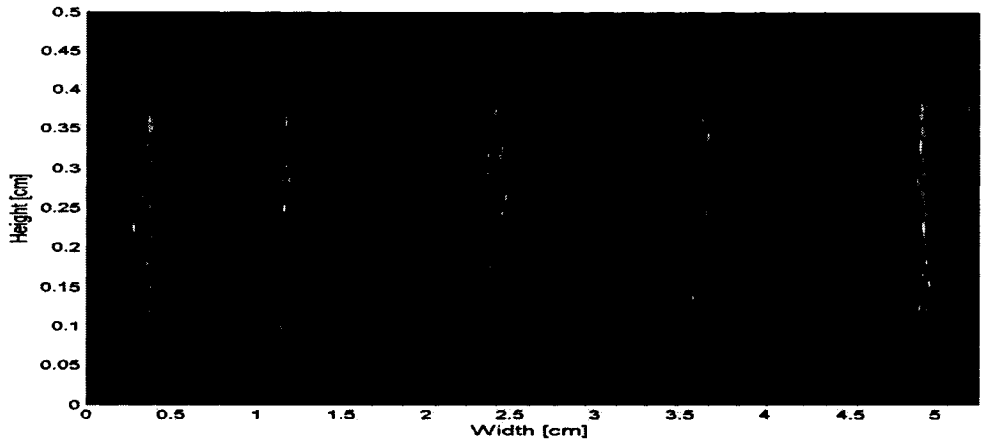

IMAGE 99 in O_2

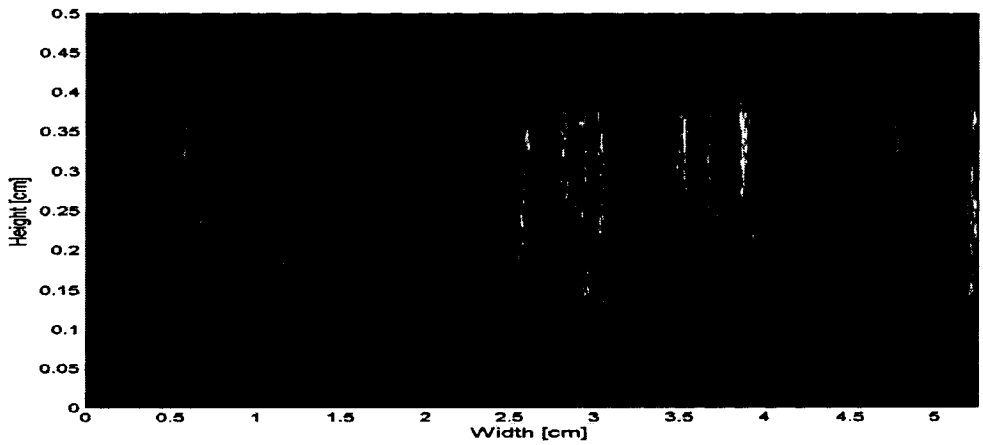

IMAGE 100 in O_2

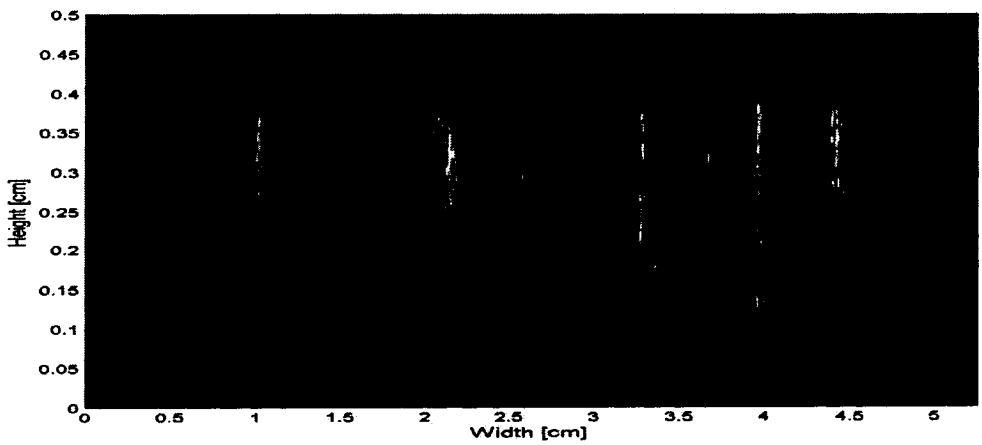

IMAGE 101 in O_2

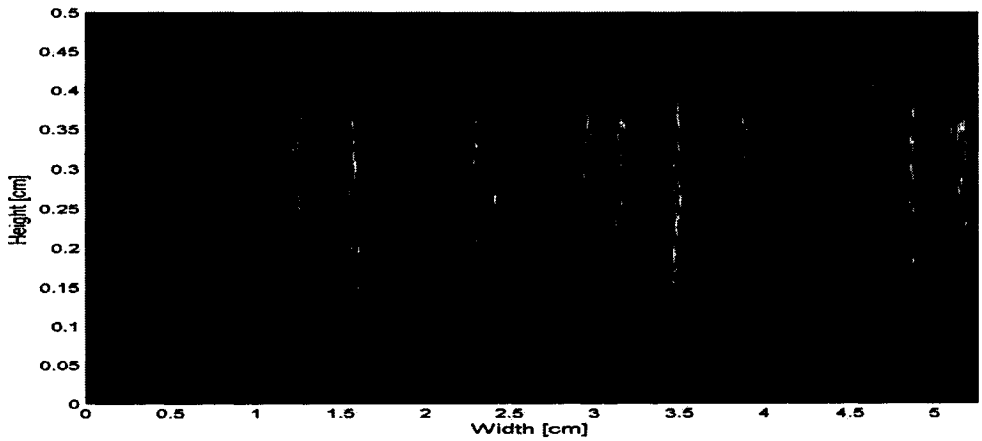

IMAGE 135 in O_2

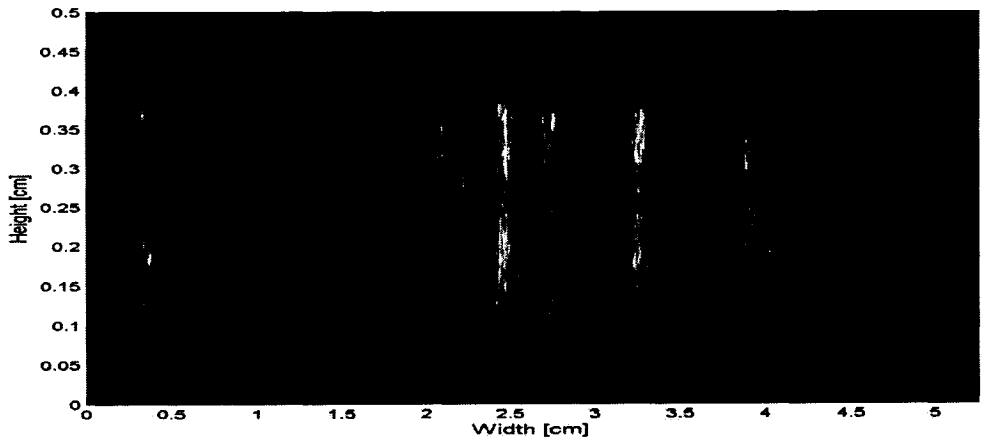

IMAGE 142 in O_2

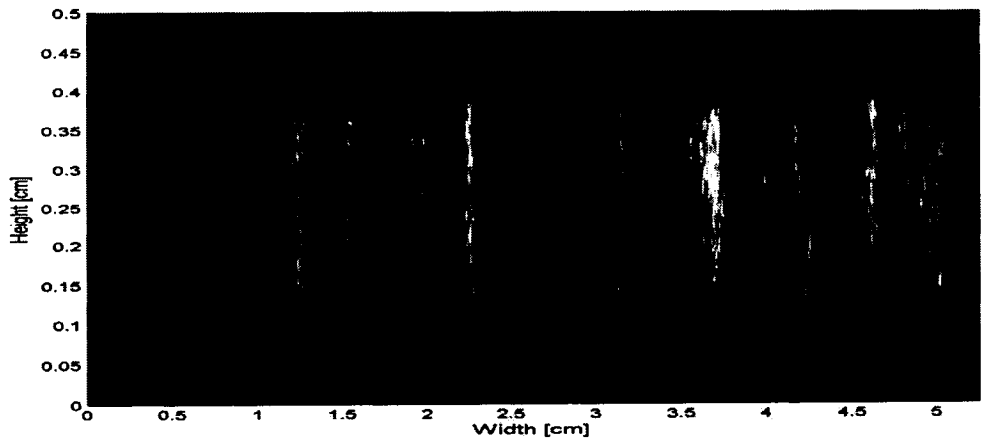

In Air

IMAGE 22 in Air

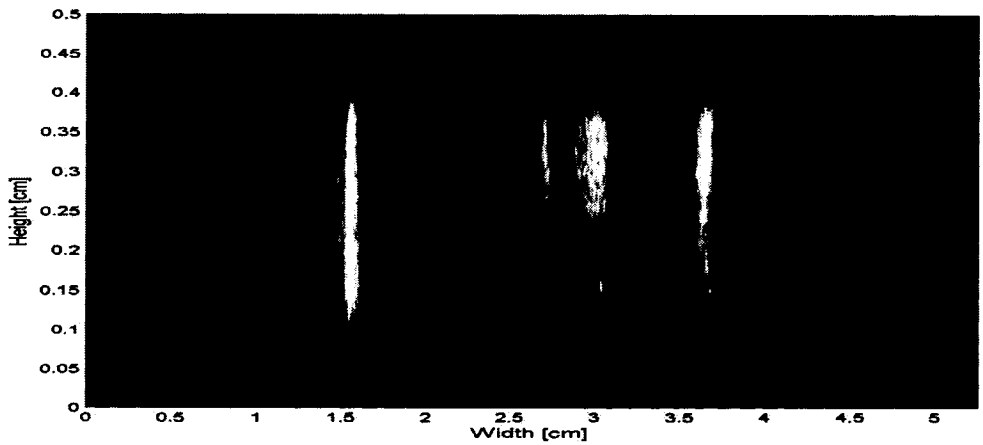

IMAGE 31 in Air

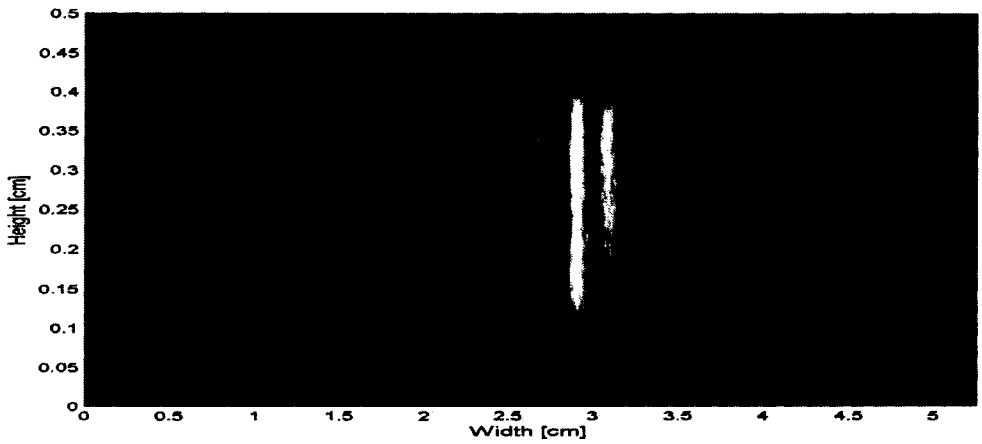

IMAGE 62 in Air

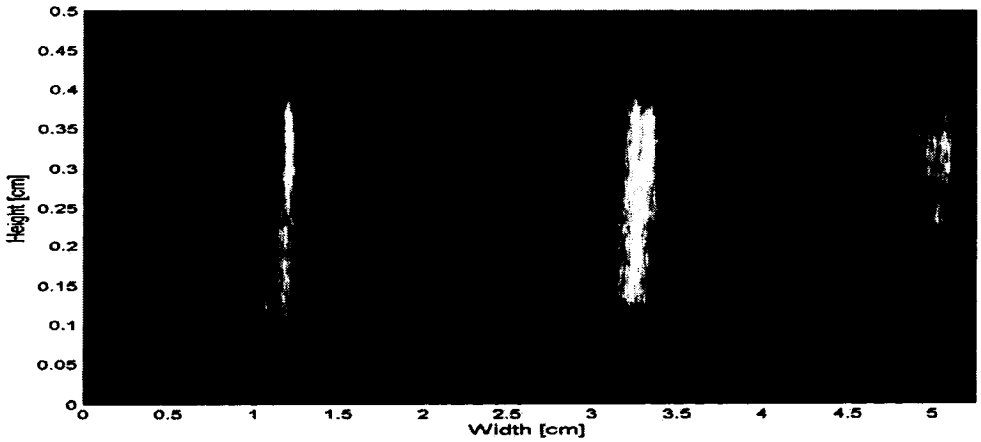

IMAGE 75 in Air

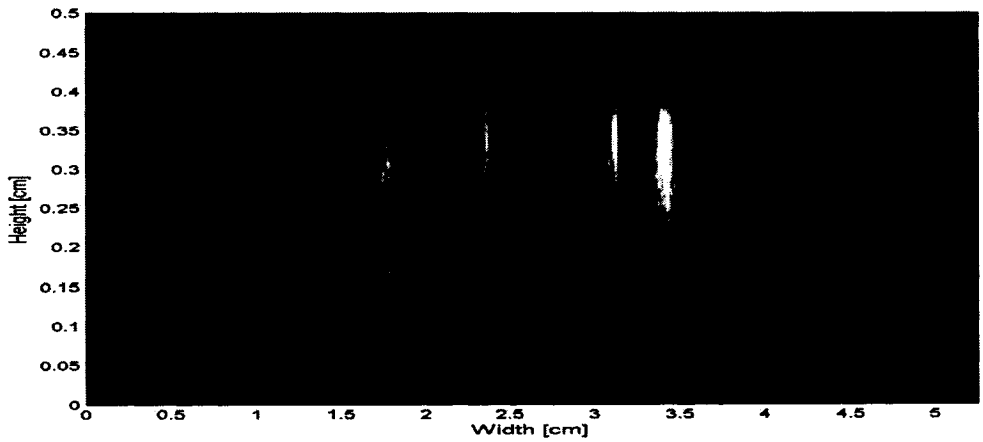

IMAGE 80 in Air

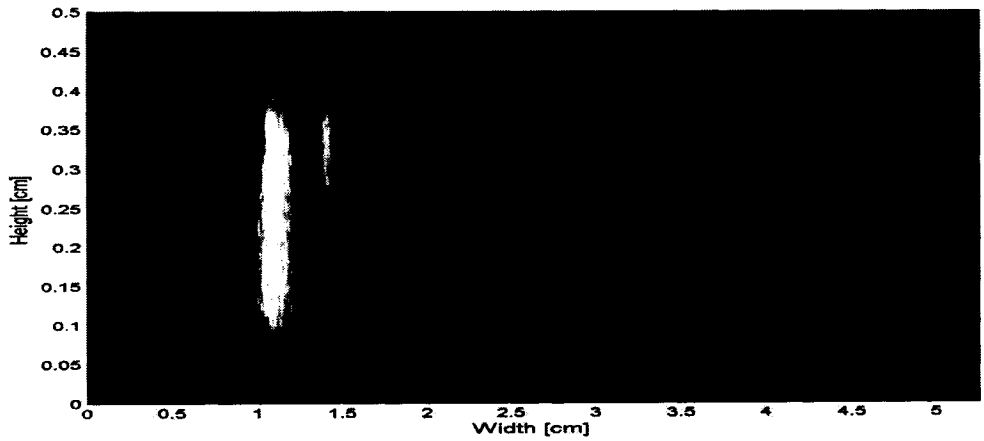

IMAGE 102 in Air

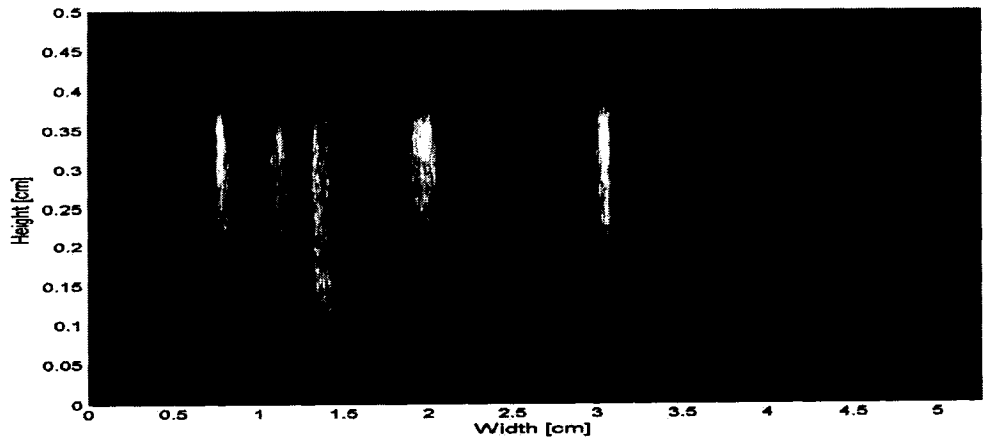

IMAGE 103 in Air

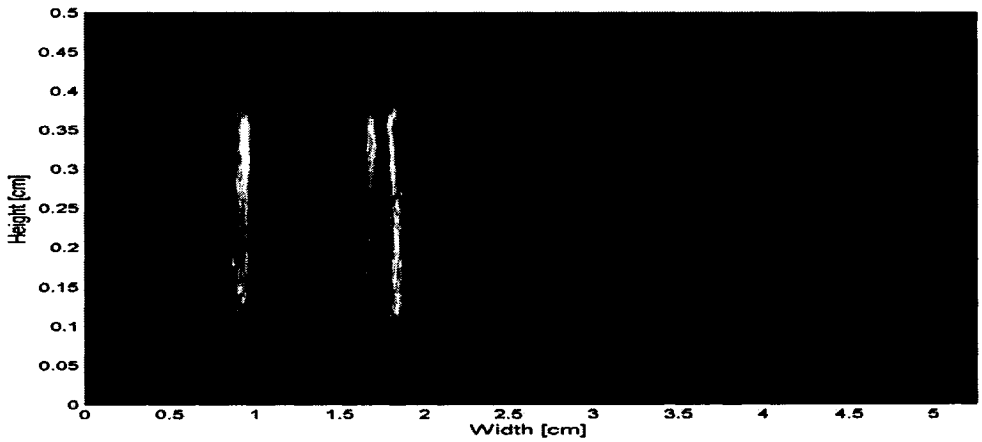

IMAGE 129 in Air

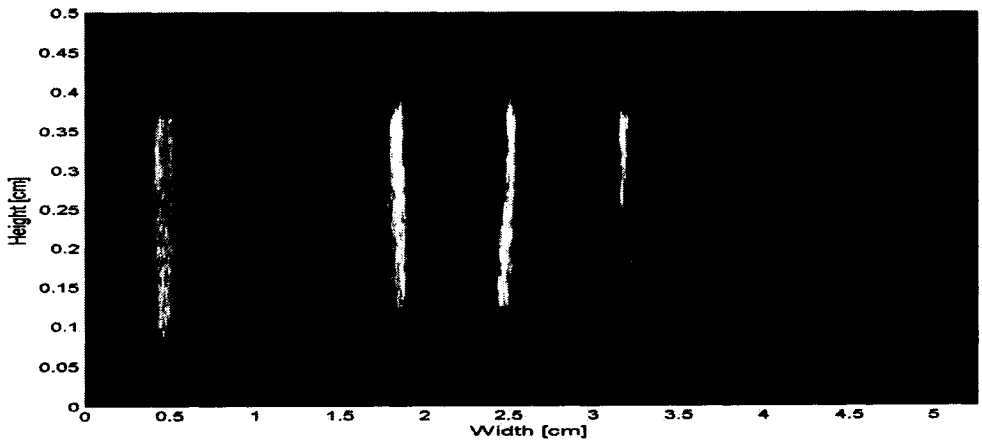

IMAGE 135 in Air

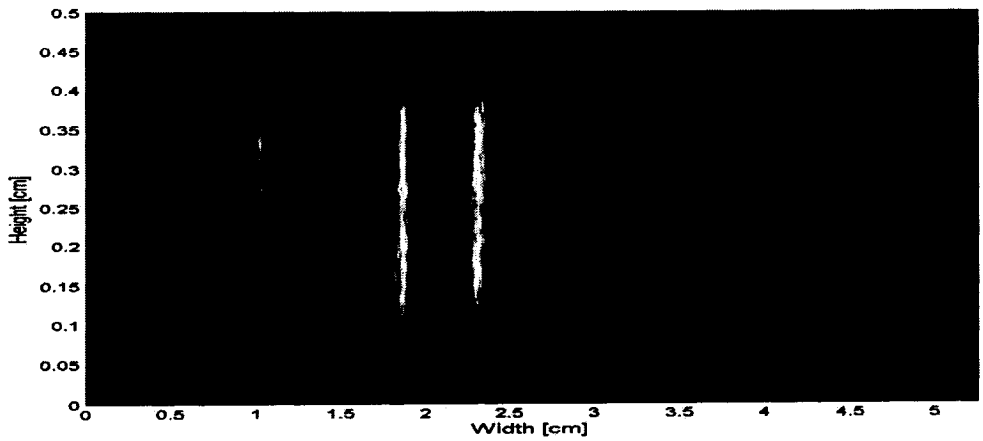

IMAGE 144 in Air